

# **Characterisation of Rhodopsin Retinitis Pigmentosa mutants located in Intradiscal Loop 1**



**Luke Christopher Neaves**

A thesis submitted for the degree of  
Masters by Dissertation (MSD)

School of Life Sciences  
University of Essex

April 2020

## **Acknowledgements**

I would like to thank my supervisor Dr Phil Reeves for his clear guidance and patience that has allowed me to understand and complete this project. I would also like to thank Lynwen James, technician for Lab 4.25, for helping me get to grips with techniques and procedures that I was unfamiliar with. Fellow masters student Hannah Hargreaves deserves thanking as well for her helpful discussions, advice and friendship throughout the project. Lastly, but by no means the least, I would like to thank my parents and friends for their constant support during this project. To all of you, a massive thank you.

## **Abstract**

Retinitis Pigmentosa (RP) is a genetic condition that results in blindness. There are several hundred RP mutations associated with rhodopsin, a photosensitive GPCR pigment found within rod cells of the retina. Previous studies have shown that many rhodopsin RP mutants fold incorrectly or affect protein stability. This study investigates the effect of three RP mutants located in Extracellular loop 1 of bovine rhodopsin. Expression levels and protein folding have been examined using HEK 293 GnTI<sup>-</sup> cells and two methods have been used in an attempt to correct protein folding. The effects of these two correction methods on three mutations have been analysed by investigating their UV-visible absorption spectral properties, photobleaching properties, active light-activated state stability kinetics and pigment thermal stability. Pharmacological chaperone rescue with 9-*cis*-retinal was found to enhance expression levels and folding in two of the three mutant pigments. However, these rescued pigments were unstable at high temperatures (55 °C) when purified. The second approach involved the insertion of a disulphide bridge linking the N-terminal cap to ECL 3 and is known to increase the thermostability of WT rhodopsin. The N2C/D282C bond was found to repair two of the three mutant pigments and enhance stability, signal transduction, photobleaching and Meta-II stability to near WT levels. These two methods, when deployed together, had little additive effect. The main conclusion is that the N-terminal cap of rhodopsin is prevented from either folding correctly or docking correctly to ECL 3 due to the mutations located in ECL 1. However, when the N-terminal cap of rhodopsin is tethered in place by a disulphide bridge or when the retinal binding pocket is occupied, thermal stability and active state properties are restored in some rhodopsin RP mutants.

## Abbreviations

**(ad/ar)RP**- (autosomal dominant/autosomal recessive) Retinitis Pigmentosa  
**AMD**- Age-related Macular Degeneration  
**ANOVA**- Analysis of Variance  
**bp**- base pairs  
**Cas 9**- Caspase 9 (Cysteine Aspar<sup>t</sup>ic protease)  
**(c)GMP**- (cyclic) Guanosine Monophosphate  
**CL**- (Intracellular) Cytoplasmic Loop  
**C-opsins**- Ciliary Opsins  
**CRISPR**- Clustered Regular Interspaced Short Palindromic Repeats  
**DDM**- n-Dodecyl  $\beta$ -D-maltoside  
**DMD**- Duchenne Muscular Dystrophy  
**DSB**- Double Strand Break  
**ECL**- Extracellular Loop  
***E. coli***- *Escherichia coli*  
**ER**- Endoplasmic Reticulum  
**ERAD**- ER associated protein degradation  
**GDP**- Guanosine Diphosphate  
**GnTI**- N-Acetylglucosaminyltransferase I  
**GPCR**- G Protein-Coupled Receptor  
**GRK**- G Protein-Coupled Receptor Kinase  
**gRNA**- guide Ribonucleic Acid  
**GTP**- Guanosine Triphosphate

**HDR**- Homology Directed Repair  
**HEK**- Human Embryonic Kidney cells  
**hESC**- human Embryonic Stem Cells  
**iPSC**- induced Pluripotent Stem Cells  
**Meta-II**- Metarhodopsin II  
**NAD(H)**- Nicotinamide Adenine Dinucleotide  
**NHEJ**- Non Homologous End Joining  
**PAGE**- Polyacrylamide Gel Electrophoresis  
**PSB**- Protonated Schiff Base  
**PTM**- Post Translational Modification  
**PVD**- Posterior Vitreous Detachment  
**REP1**- Rab Escort Protein 1  
**RGS**- Regulator of G protein Signaling  
**RK**- Rhodopsin Kinase  
**RMM**- Relative Molecular Mass  
**ROS**- Rod Outer Segment  
**RPGR**- Retinitis Pigmentosa GTPase Regulator  
**sgRNA**- single guide Ribonucleic Acid  
**UV**- Ultra Violet  
**VEGF**- Vascular Endothelial Growth Factor  
**VPU**- Video Processing Unit  
**WT**- Wildtype  
  
 **$\gamma$ PDE**- Gamma Phosphodiesterase

## Units

**g**- Grams  
**mg**- Milligrams  
 **$\mu$ g**- Micrograms  
**ng**- Nanograms

**L**- Litres  
**ml**- Millilitres  
 **$\mu$ l**- Microlitres

**$\mu$ m**- Micrometres  
**nm**- Nanometres

**M**- Molar  
 **$\mu$ M**- Micromolar  
**nM**- Nanomolar

**kDa**- Kilodaltons

**AU**- Arbitrary Units

## Contents

Acknowledgments.....	ii
Abstract.....	iii
Abbreviations & Units.....	iv
<b>1. Introduction.....</b>	<b>7</b>
1.1 Anatomy of the Eye.....	7
1.2 Rod and Cone Photoreceptor Cells.....	9
1.3 Retinitis Pigmentosa and Retinal Dystrophies.....	10
1.4 Rhodopsin protein and Signal Transduction pathway.....	13
1.5 Rhodopsin Mutation Classes.....	17
1.6 Potential Treatments and Therapies.....	19
1.7 Techniques and Rationale.....	21
1.8 Investigative Aims and Hypotheses.....	26
<b>2. Methodology and Materials.....</b>	<b>28</b>
2.1 General Methods.....	30
2.1.1 Preparation of growth media.....	30
2.1.2 Culturing Techniques.....	30
2.2 Molecular Biology Methods.....	31
2.2.1 Sample Sequencing.....	31
2.2.2 Agarose Gel Electrophoresis.....	32
2.2.3 DNA Extraction.....	32
2.2.4 Tissue Culture.....	34
2.2.5 Transfection Protocols.....	35
2.3 Purification of rhodopsin Biochemical and Spectroscopic Analysis.....	37
2.3.1 Immunoaffinity Purification.....	37
2.3.2 UV-visible absorption Spectroscopy.....	38
2.3.3 SDS-PAGE and Western Blots.....	39
2.3.4 Rhodopsin Photobleaching.....	41
2.3.5 Rhodopsin Active State (Meta-II) Decay.....	41
2.3.6 Rhodopsin Thermal Stability.....	41
<b>3. Results.....</b>	<b>42</b>
3.1 Verification of the DNA sequence for Retinitis Pigmentosa mutation in the rhodopsin gene.....	42
3.2 Medium and Large-scale plasmid DNA preparation.....	48
3.3 Expression levels of ADRP rhodopsin mutants examined using UV-visible absorbance spectroscopy-Disulphide Bridge mediated Repair and Pharmacological Chaperone Rescue.....	49
3.4 Analysis of RP mutant rhodopsin biochemical properties and spectral characteristics.....	53
3.4.1 Examination of protein profiles rhodopsin ADRP mutants as judged by SDS-PAGE.....	53
3.4.2 Purification of RP mutant pigments.....	55
3.4.3 Photobleaching properties of the immunoaffinity purified rhodopsin mutants.....	57
3.4.4 Photoactivation of purified ADRP pigments by observation of Meta-II Decay.....	59
3.4.5 Thermal Stability of Rhodopsin RP mutant pigments.....	62
<b>4. Discussion.....</b>	<b>65</b>
4.1 Recombinant expression of rhodopsin mutants located in Extracellular Loop 1 (ECL 1).....	66
4.2 Thermal Stability of rhodopsin mutants in ECL 1.....	67

4.3 Dark state spectral properties of mutants pigments and their photoconversion to the active state (Metarhodopsin II).....	68
4.4 Stability of the active state of RP mutants located in ECL 1.....	69
4.5 Use of PyMol to investigate the basic structural perturbations in these mutants.....	69
4.6 Explanatory model for the role of ECL 1 in structure and pathology.....	73
<b>5. References.....</b>	<b>79</b>
<b>6. Appendices.....</b>	<b>85</b>
6.1 Rhodopsin sequence homology.....	85
6.2 MidiPrep yield and UV absorbance properties of purified samples.....	86
6.3 Rhodopsin pigment expression levels using disulphide bridge mediated repair or pharmacological chaperone rescue with 9- <i>cis</i> -retinal.....	87
6.4 ANOVA Statistics.....	89
6.5 PyMol RP rhodopsin structure perturbations.....	92

## **1. Introduction**

### **1.1- Anatomy of the Eye**

The eye is one of the most important organs of the human body, and vision is one of the most valuable senses that humans possess. Blindness is considered to be when an individual has visual field of less than 3/60 (perfect visual field is 20/20) and cannot read, write or manoeuvre as instructed to do so, whilst not having any other reason in which this may be the case (i.e. meaning they are not illiterate, dyslexic, dyspraxic or have any mobility issue restricting said individual from moving freely) (Genensky and Science, 1971, Thylefors *et al.*, 1992). As of 2017, it has been reported that well over two million people in the UK are living with a form of blindness and over 360 million people worldwide (Bourne *et al.*, 2017). With 19 million of those affected being children, and 1.4 million of those are irreversibly blind. As somewhat expected, 81% of all moderate to severe cases of visual impairment are attributed to those over the age of 50 years, this is most likely due to the ageing population (Bourne *et al.*, 2017). This is expected to increase to 38.5 million by 2020 and then to over 115 million by 2050, according to a recent study (Flaxman *et al.*, 2017). Some are born without the ability to see, whilst others lose it over time, yet 80% of all recorded visual impairment cases are either curable or preventable.

The eye is composed of several different parts, some of which are shown in Figure 1.1. The cornea is the outermost covering layer of the eye. It is slightly dome shaped and protects all the inner eye structures from elemental damage (for example dust). Also, like skin, the cornea is made up of many layers. These layers can regenerate faster than other tissue types and help heal the eye (Bailey, 1987). Next, the sclera is the smooth white fibrous outer wall of the eye (the 'whites' of our eyes), but underneath is a pale brown layer with tendons that attach the eye to the eye socket. The sclera provides structural support for the eye but is flexible enough to allow the eye to move and see in a different direction to the position of the face and head (Kivelä *et al.*, 1998). The pupil is the central black dot in the middle of the eye. It is actually a hole so that light can be focused onto the retina and objects can be clearly distinguished (Walsh and Charman, 1988). The iris is the pigmented area of the

eye surrounding the pupil (the part that determines what colour eyes someone has). The iris uses muscles to either dilate or contract the pupil depending on the amount of light that is present, allowing us to focus more easily.

There are mucus excreting glands on the outside of the eye known as the conjunctiva glands, which help keep the eye moist/wet and prevent itching (Kobayashi and Kohshima, 2001). There are also lacrimal glands which are commonly known as the tear ducts. They too help keep the eye moist and remove particles of dust or dirt that could irritate the eye. The lens is located behind the pupil and is held *in situ* by the ciliary muscles. It is a clear layer that can change shape to focus light onto the retina (Delaye and Tardieu, 1983). The retina is composed of two photoreceptor cell types; rod cells and cone cells. These are layered across the back of the eye and transmit the light into electrochemical signals via the optic nerve. The back of the retina is called the macula and helps interpret the details of what is being viewed. The central region of the macula is the fovea, which heightens the resolution of the image sent to the brain (Kobayashi and Kohshima, 2001). The ciliary body muscles hold and control the eye lens movement. Whilst, the choroid resides between the retina and the sclera, providing a blood and nutrient supply to the eye via a capillary network (Kivelä *et al.*, 1998).

At the back of the eye, there is a gel which transports nutrients from the blood vessels to the internal eye structures called the vitreous humor. If debris becomes trapped in the vitreous humor then these appear as floaters in our vision (Bailey, 1987). The debris is caused by a condition known as posterior vitreous detachment (PVD), where the vitreous cavity shrinks and pulls away from the retina, resulting in debris being seen when stimulated. Once the vitreous cavity has become fully detached, the debris disappears. This is a very common condition affecting almost everyone over time, but rarely causes any problems (Sebag, 2004). The aqueous humor is the liquid that fills the front of eye and gives some form of structural support to the lens and cornea. It is separated into two chambers within the eye, the anterior and posterior chambers. The aqueous humor is drained through the Schlemm canal to

prevent any build-up of pressure, if this does not occur then glaucoma can develop (Kobayashi and Kohshima, 2001).

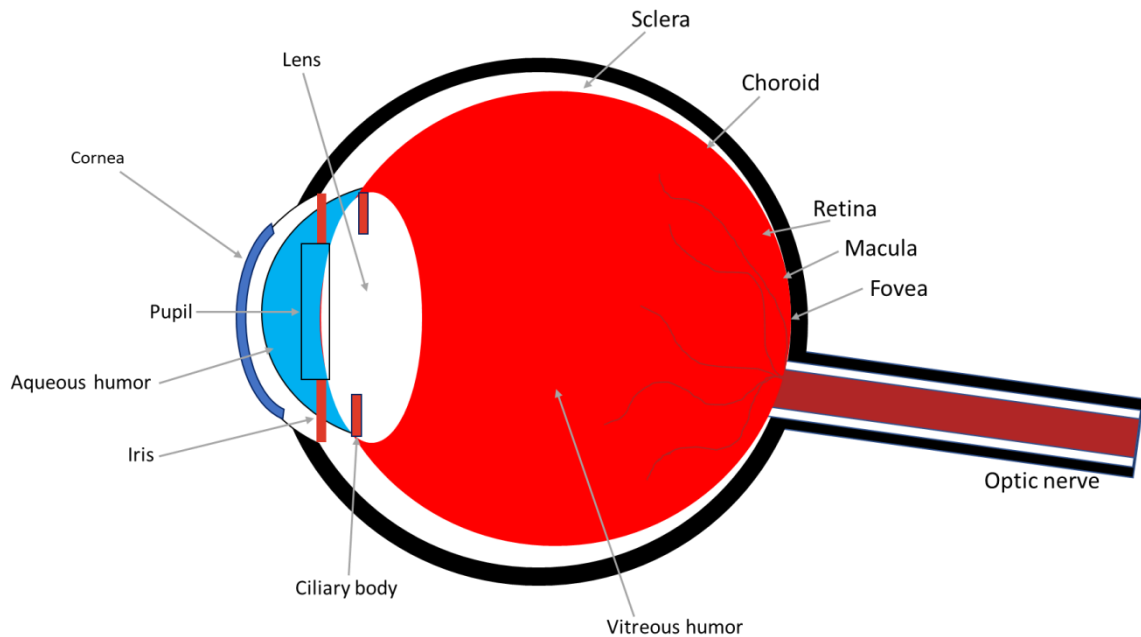


**Figure 1.1- Cross section of the eye.** Labelled diagram of the eye, showing the relative position of the main structures both internal and external, from the cornea and pupil at the front to the optic nerve at the back. Adapted from Willoughby *et al.*, 2010.

### 1.2- Rod and Cone Photoreceptor Cells

There are two different types of photoreceptor cells within the eye; rod and cone cells. Cone photoreceptor cells are responsible for our colour vision and work optimally in bright light conditions. In humans there are three types of cone cells; S (small), M (medium) and L (long). Each type of cone cell responds to a different wavelength of light. S cone cells absorb short light wavelengths, peaking at 420 nm (detects the colour purple). M cone cells absorb medium length light wavelengths, with a peak near 530 nm (detects the colour green). Finally, L cone cells respond to the longer wavelengths of light, peaking at 560 nm and allowing us to see the colour yellow. Using all three cone cells types in unison, we are able to visualise most colours of the visible light spectrum. Cone cells are approximately 40-50  $\mu\text{m}$  long and 0.5-40  $\mu\text{m}$  in diameter, with one end being slightly pointed or cone shaped (hence their name, see both Figures 1.2 and 1.3) and are mainly focused around the fovea. Cone cells can be separated into three sections; synaptic terminal, inner segment and outer segment. The synaptic terminal forms a synapse with a neuron from the optic nerve, the inner segment houses

all of the cell's organelles (such as the nucleus and many mitochondria), whilst the outer segment contains the photopigment. The inner and outer segments are joined together by a connecting cilium (also known as primary cilium, and houses most of the protein molecules involved in the phototransduction cascade-see Figure 1.3) (Jin *et al.*, 1994; Khanna, 2015). On the other hand, rod photoreceptor cells function in low light conditions and are responsible for night vision. Rod cells are more concentrated in the outer areas of the retina and less so near the macula. Rod cells are significantly longer than cone cells at 100  $\mu\text{m}$  long and 2  $\mu\text{m}$  in diameter. There are also far more rod cells than cone cells, with 100 million compared to 7 million, respectively. Rod cells are separated into the same three sections as the cone cells, but slightly differ in shape (Merino *et al.*, 2011).

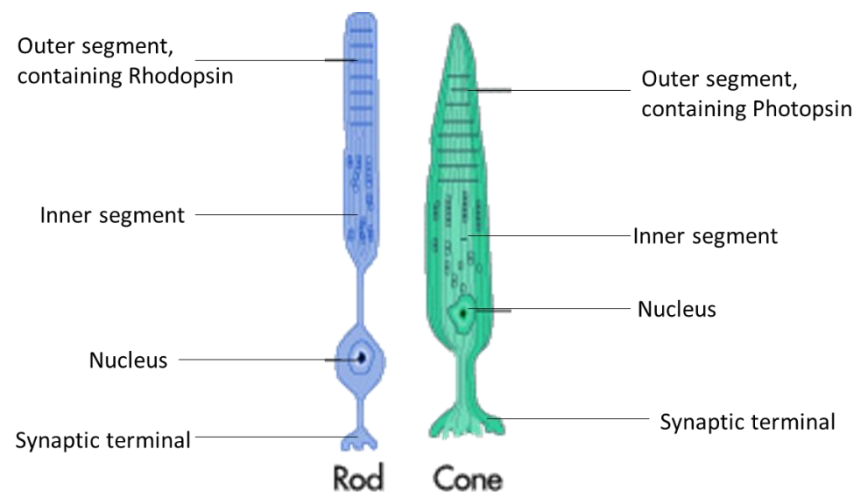


**Figure 1.2- Rod and Cone cell structure.** Labelled diagram showing the overall shape of both types of photoreceptor cells along with the main sections and position of the nucleus.

### 1.3- Retinitis Pigmentosa and Retinal Dystrophies

Each one of the structures of the eye conveys a particular role, but each one also has the possibility to go wrong and cause a number of differing visual impairments or blindness. If the aqueous humor is not drained correctly then glaucoma can develop. Glaucoma is a condition where the optic nerve becomes damaged due to a build-up in pressure of the aqueous humor in the front of the eye (Quigley, 1996). In contrast, a breakdown of the choroid will lead to choroideremia. Choroideremia is an X-linked recessive disease which results in blindness because of mutations to the CHM gene encoding for Rab escort protein 1 (REP1). It currently has no cure and affects roughly one in 50,000

males worldwide (MaLaren *et al.*, 2014). Choroideremia is a subtype of blindness referred to as retinal dystrophies. Retinal dystrophies are the most common form of blindness, aside from colour blindness. The two main types of retinal dystrophies are Age-related Macular Degeneration and Retinitis Pigmentosa (similar to choroideremia) (Gregory-Evans and Bhattacharya, 1998).

Age-related Macular Degeneration (AMD) is a constant destruction of the central retinal region, known as the macula, resulting in the irreversible loss of central vision and leaving only peripheral vision, mainly for those who are aged 50 years or older (Klein *et al.*, 2005). AMD has two different forms; wet and dry. Dry AMD is the slow degenerative onset and is caused by the deposition of metabolites (mainly lipofuscin) underneath the retinal pigment epithelium (drusen), whereas wet AMD has a quick onset caused by leaking blood vessels and can be treated with Lucentis or Avastin (Rosenfeld *et al.*, 2006; Brown *et al.*, 2019). Lucentis (or non-tradename Ranibizumab) is an antibody fragment used due to its anti-angiogenic properties (it prevents the growth of new blood vessels by targeting Vascular Endothelial Growth Factors, VEGF). Whereas Avastin (non-tradename Bevacizumab) is the ancestor antibody to Lucentis and is also used to treat various types of cancer (Fung *et al.*, 2007, Avery *et al.*, 2006).

Retinitis Pigmentosa (RP) refers to a group of hereditary conditions affecting many genes and their subsequent proteins, very often via point mutations. One particular gene (RHO, chromosome position 3q22.1) encodes for a protein called Rhodopsin and is located within the rod photoreceptor cells of the eye. The mutation (or sometimes mutations) will eventually lead to the death of the rod photoreceptor cells and cause the individual to turn blind (Campochiaro *et al.*, 2017). The first stage of RP is night blindness (or nyctalopia), this is when rod photoreceptor cells in the eye have begun to die. Over time, large scale rod cell death will lead to the loss of peripheral vision and create tunnel vision, roughly by the time of adulthood. Finally, central vision will be lost as the remaining cone photoreceptor cells die (Hartong *et al.*, 2006). Rod photoreceptor cells give us monochromatic vision, meaning they allow us to see in dim light conditions and most things appear to be black and white.

Whereas cone photoreceptor cells allow us to see in colour and detail. It is these different cells, and their corresponding pigments, that mediate our vision. There are three main types of RP: autosomal dominant Retinitis Pigmentosa, autosomal recessive Retinitis Pigmentosa and X-linked Retinitis Pigmentosa (Daiger *et al.*, 2013). Autosomal dominant Retinitis Pigmentosa (adRP) is when a single faulty gene has been inherited from one parent, and this type of RP tends to be present throughout the family history (Sung *et al.*, 1993). Autosomal recessive Retinitis Pigmentosa (arRP) is when two faulty genes have been inherited and the gene will be passed on to any offspring conceived. X-linked RP tends to only affect men and the faulty gene passed on is located on the X chromosome (Daiger *et al.*, 2007) mainly the RPGR gene (Xp11.4) and the RP2 gene (Xp11.23) (Buraczynska *et al.*, 1997; Sandberg *et al.*, 2007). X-linked inheritance is when the mother has a faulty gene within one of her X chromosomes, resulting in her offspring having a 50% chance of inheriting it. This tends to affect males more than females as males only have one X chromosome, so will develop the condition if the X chromosome contains the faulty gene. For females, they can develop the condition if their father also has it, if not then they will become a carrier for the disease. This type of inheritance is also associated with Duchenne Muscular Dystrophy (DMD) and Haemophilia (Dobyns, 2006).

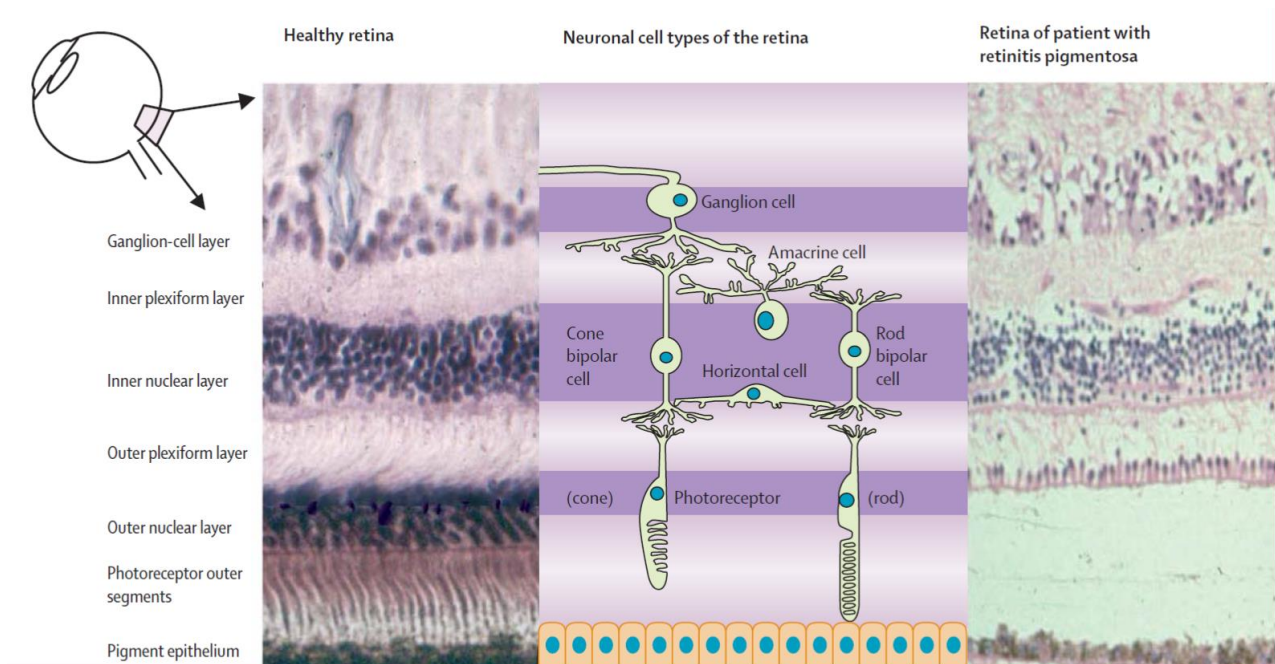


**Figure 1.3- Phenotypical appearance of both healthy and RP affected retinal layers.** Microscope image showing the phenotypic appearance of a healthy human retina (left) compared with a retina of a patient suffering from Retinitis Pigmentosa (RP) (right). In the centre is a diagram of the photoreceptor cells present within the retina. Far left shows a basic cross section of the eye and the different retinal layers (Hartong *et al.*, 2006).

#### 1.4- Rhodopsin protein and Signal Transduction pathway

Rhodopsin is a photosensitive G protein-coupled receptor (GPCR) located in the disc membranes of rod cell outer segments and is involved in the visual transduction pathway (sometimes referred to as the phototransduction cascade) (Chabre and Deterre, 1989). GPCRs are a superfamily of signal transduction proteins that can transmit communication signals across cellular membranes, rhodopsin is a Class A GPCR (defined as rhodopsin-like GPCRs based on function and sequence homology), there are six GPCR classes in total from A to F (Cherezov *et al.*, 2007). The rhodopsin molecule consists of seven transmembrane  $\alpha$ -helices connected together by three intracellular cytoplasmic loops (CL) and three extracellular loops (ECL) (Figure 1.4) (Sakmar, 2002). Along with this, rhodopsin can be divided into two distinctive parts; a protein called opsin and a derivative of Vitamin A known as 11-*cis*-retinaldehyde (or 11-*cis*-retinal for short) (Palczewski *et al.*, 2000). Both of these sections are covalently bound together. Retinal is the light sensitive molecule that mediates converting photons into a signal. Rhodopsin (or Rod Opsin, referring to opsins within the rod cells) is a type of vertebrate

visual opsin, which itself is a sub set of ciliary opsins (C-opsins), which are Type II opsins or animal opsins (Type I opsins are microbial opsins) (Shichida and Matsuyama, 2009, Feuda *et al.*, 2012). 11-*cis*-retinal, also called a chromophore, is bound by a Schiff base (covalent bond) to a lysine residue at position 296 in the seventh transmembrane helix (Zhukovsky *et al.*, 1991). 11-*cis*-retinal, once bound, occupies the binding pocket of opsin.

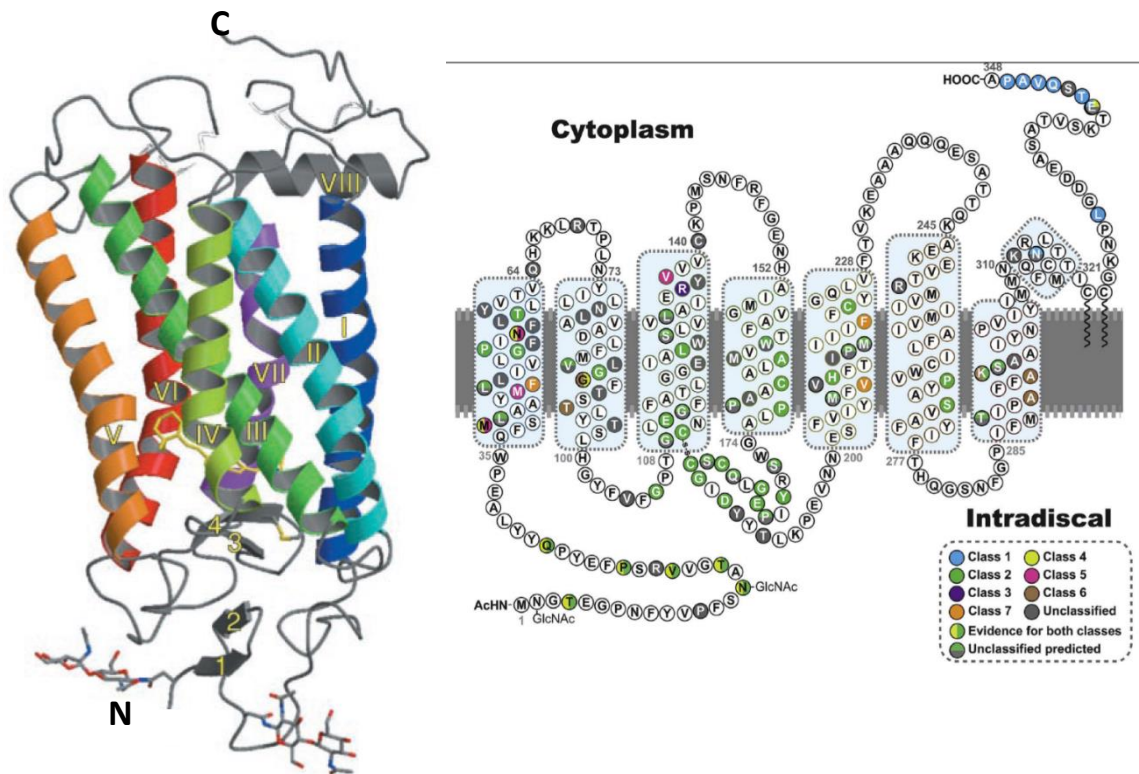


**Figure 1.4- Three-dimensional ribbon diagram of rhodopsin and a two-dimensional model of bovine rhodopsin's secondary structure showing the positions of most mutations from Class I-VII.** Both show the seven  $\alpha$ -helices along with connecting loops, as well as the carboxyl and amino terminals (Palczewski *et al.*, 2000, Athanasiou *et al.*, 2017).

When a photon of light is absorbed by the rhodopsin pigment within the rod cell, a change in shape occurs. In dark conditions the retinal exists in the 11-*cis*-retinal state, but exposure to light stimulates a conformational change to the all-*trans* retinal state (it is now referred to a Metarhodopsin II - Meta II). This conformational change causes an increased affinity for a regulatory protein called transducin (a G protein) (Chabre and Deterre, 1989). Once transducin has bound to the Meta-II molecule (R\*G in Figure 1.5), the alpha G protein subunit exchanges Guanosine Diphosphate (GDP) with Guanosine Triphosphate (GTP). This in turn causes the G protein alpha subunit to dissociate from the G protein

beta and gamma subunits, activating the molecule. The now free alpha subunit ( $G^*$ ) binds to a cyclic Guanosine Monophosphate (cGMP) phosphodiesterase effector protein and an inhibitory gamma phosphodiesterase molecule ( $\gamma$  PDE), to prevent the G protein beta and gamma subunits from being blocked and inactivated. This then activates the cGMP phosphodiesterase and converts cGMP to 5'-GMP, via hydrolysis. The reduction in cGMP concentration causes cGMP regulated sodium and calcium ion channels to close, changing the rod cell from a depolarised to a hyperpolarised state, by changing the cell's potential. In the hyperpolarised state, the glutamate neurotransmitter is not released into the synaptic cleft for recognition by ganglion and bipolar cells. This is the visual transduction pathway or the phototransduction cascade in Figure 1.5 (Rosenbaum *et al.*, 2009).

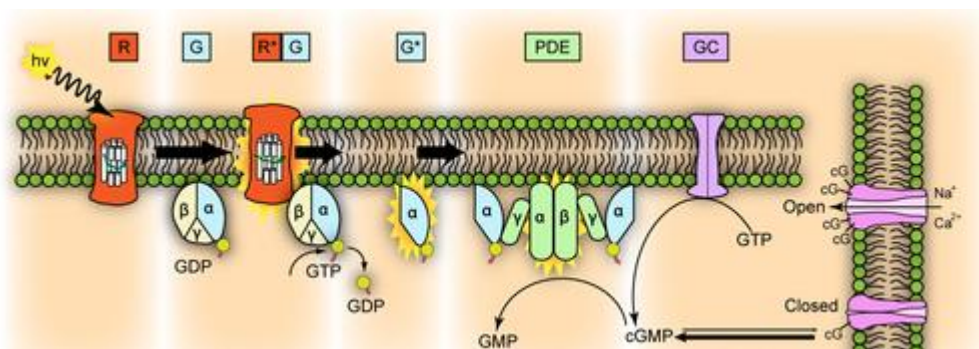


**Figure 1.5- Simplified diagram of the phototransduction signal pathway.** Main stages of the phototransduction pathway, from the absorbance of a photon to the activation of Transducin to hyperpolarisation of the rod cell. R is rhodopsin, G is transducin, R+ is Meta II, GC is guanylyl cyclase (Leskov *et al.*, 2000).

Once this pathway has terminated, the rod cell must return to a resting depolarised state, and rhodopsin must be deactivated. A protein called rhodopsin kinase (RK) phosphorylates several serine residues in the cytosolic tail region, inhibiting the transducin binding. At the same time, arrestin (a G protein-coupled receptor regulatory molecule) binds to the phosphorylated rhodopsin molecule. As the activity of the rhodopsin molecule reduces, an RGS protein (regulator of G protein signalling) reverts the transducin bound GTP back to GDP, deactivating the G protein. Whilst cGMP concentrations return to normal, so does the calcium ion influx. As calcium ion concentrations decrease, guanylyl cyclase enzymes become activated and replenishes the cGMP stocks. Altogether, this causes the rod cell to become depolarised again (Muradov and Artemyev, 2000).

The activation and deactivation pathways of rhodopsin (or rod cells) only occur in low light conditions. During the day, when rod cells are exposed to excessive amounts of light, they become desensitised. As the rhodopsin molecules are phosphorylated by RK, arrestin becomes bound. Arrestin limits the interactions between transducin and Meta-II, as well as helping clathrin dependent endocytosis machinery to begin receptor mediated endocytosis (Okawa and Sampath, 2007).

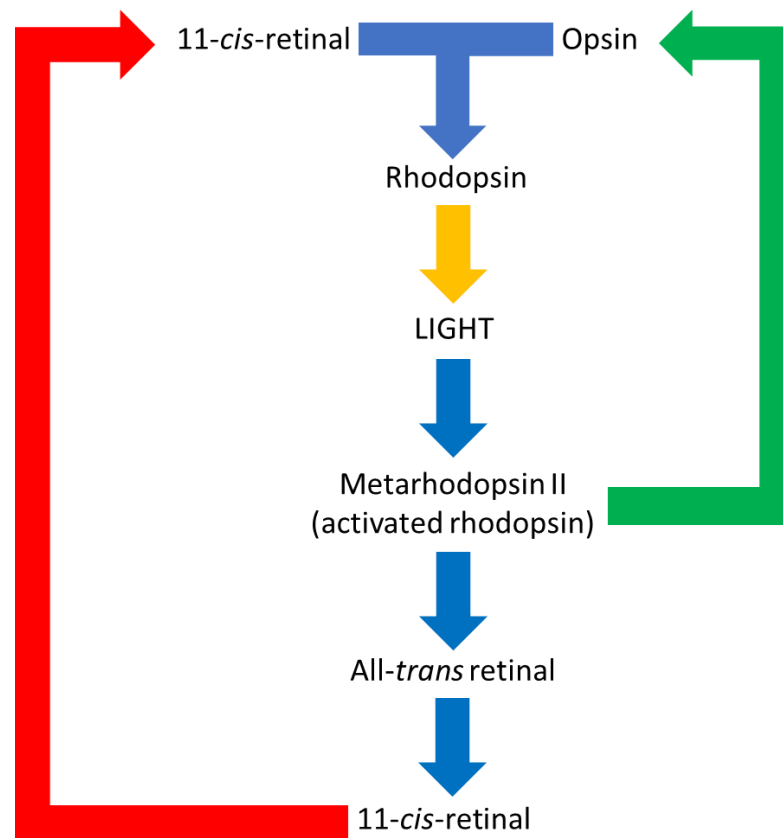


**Figure 1.6- Rhodopsin activation and deactivation cycle.** Flow chart displaying each step of the cycle from the inactivated stable-state Rhodopsin to the Meta-II activated state, along with retinal state change and reformation (Leskov *et al.*, 2000).

To regenerate 11-*cis*-retinal, all-*trans* retinal binds with NADH to form all-*trans* retinol. All-*trans* retinol combines with a fatty acid and forms all-*trans* retinyl ester (Moiseyev *et al.*, 2005). This retinyl ester can bind with water and NAD<sup>+</sup> to reform 11-*cis*-retinal (Jin *et al.*, 2007). The regeneration cycle is shown in more detail in Figure 1.7.

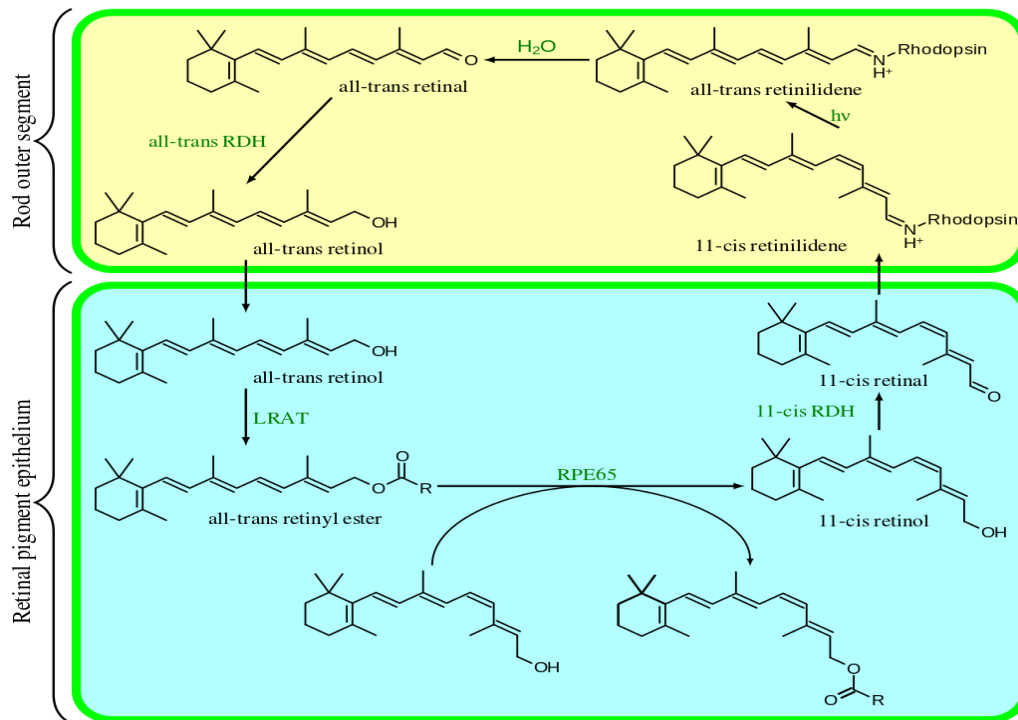


**Figure 1.7- Enzymatic pathway showing the visual cycle of retinal.** 11-*cis*-retinal is converted to all-*trans* retinal following the activation of bound rhodopsin by exposure to light in the ROS. All-*trans* retinal is converted back to 11-*cis*-retinal in the retinal pigment epithelium by binding to NADH to form all-*trans* retinol, a fatty acid to form all-*trans* retinyl ester and water to regenerate 11-*cis*-retinal (Moiseyev *et al.*, 2005).

### 1.5- Rhodopsin Mutation Classes

Along with the different types of RP there are seven different classes of mutations to the rhodopsin protein, each of which has its own characteristics. Class I mutations are when the mutant rhodopsin protein folds correctly or normally but is not transported out of the Endoplasmic Reticulum (ER) and Golgi apparatus, to the outer segments of the rod cell. Class II mutations involve misfolded proteins that are unable to leave the ER and Golgi to be transported to the cell outer segments. Class III mutations interfere with endocytosis and class IV mutations affect rhodopsin stability and post translational modifications (PTM), but do not tend to influence protein folding as such. Class V mutations show an increased amount of transducin activation (Mendes *et al.*, 2005). And finally, class VI and VII mutations refer to constitutive activation (mutated protein causes constant activation) and dimerization deficiency (remain as monomers and unable to form quaternary protein structures), respectively (Athanasίου *et al.*, 2017; Ploier *et al.*, 2016).

**Table 1.1- Classifications of rhodopsin mutations.** Describes the basic characteristics of each of the seven mutations classes along with whether the mutant protein formed is misfolded and some examples.

Mutation Class	Characteristics	Mutation examples	Misfolded
<b>Class I</b>	Normal folding, not transported to outer segments	T342M, P347S	No
<b>Class II</b>	Misfolded, contained within ER	P23H, G106R, K296E	Yes
<b>Class III</b>	Affects endocytosis	R135G	No
<b>Class IV</b>	Affects stability and PTM	T4K	Not always
<b>Class V</b>	Increased activation of transducin	M44T, V137M	No
<b>Class VI</b>	Constitutive activation	T94I, A295V	No
<b>Class VII</b>	Dimerisation deficiency	F45L, F220C	No

Therefore, theoretically, every rhodopsin mutation can be categorised into one or possibly more than one of the classes above. However, this is incredibly difficult to prove as there are over 150 distinct rhodopsin mutations that have been clinically diagnosed for adRP alone, and it is likely that some mutations remain either unclassified or undiscovered (Reeves *et al.*, 2002). Yet some of these mutations seem to occur more frequently than others. The most common rhodopsin mutation is P23H, this is where the amino acid Proline has been replaced by the amino acid Histidine at residue number 23 (refer to Figure 1.4). P23H is a missense mutation that causes a mild adRP phenotype in patients, as well as having the characteristics of both class II and class IV mutations (it both prevents protein movement from the ER and affects overall stability) (Tam *et al.*, 2010). Similarly, T17M (Threonine is replaced by Methionine at residue 17) is another common missense mutation but does not result in such a severe adRP phenotype. Other common rhodopsin mutations include; Q64ter, G106R, A269G, and P347S. Q64ter is where Glutamine has been replaced by a stop codon/termination sequence at residue 64, giving a nonsense mutation. Although this mutation is currently unclassified, it has been shown to cause advanced retinal degradation (John *et al.*, 2000). G106R, Glycine to Arginine at residue 106, is a well-studied common class II mutation that also causes advanced degradation of the retina. P347S, Proline to Serine at residue 347, is a well-studied class I mutation despite being less common than the previously mentioned two. Being a class I mutation the protein formed does not

reach the outer cell segments, so increasing the concentration of the retinal chromophore available has virtually zero effect (Li *et al.*, 1998). In a slightly different aspect A269G, where Alanine is substituted by Glycine at residue 269, is a polymorphism. A polymorphism is a Mendelian trait that is present in the wild population of a species in a minimum of two individuals (both phenotypically and genotypically) with an occurrence frequency more than 2% (Meyer and Genomics, 1991). This particular polymorphism results in a phenotypically silent mutation as the DNA and protein code have been altered, but the individual with the mutation does not exhibit RP to any degree (Sung *et al.*, 1991).

### **1.6- Potential Treatments and Therapies**

Over the years vast amounts of research have been undertaken to try and understand RP, albeit to no avail as of yet. However, there are some techniques that do have the potential to one day be developed into a treatment and/or a cure. The four main categories of treatments for RP are; gene therapy, cell transplantation, neurological-retinal prosthetics and pharmacologic therapeutics (Shintani *et al.*, 2009).

Gene therapy refers to altering or correcting the current genetic sequence, potentially by inserting a site-specific mutation or by inserting a transgene with the aid of a virus. Gene augmentation therapy using adenovirus-associated 2/5 vector human RPGR gene along with GRK1 promoters, injected into the retina, has shown some positive results for X-linked RP, but not so much for adRP (Beltran *et al.*, 2012). The findings of this investigation showed that the therapy must influence both photoreceptor cell types, due to the shared promoter region for the opsins (Beltran *et al.*, 2012). This technique is very popular as many other studies also insert a human transgene to mitigate rod cell degeneration (Cideciyan *et al.*, 2018). An alternative to inserting a gene would be to create a site-specific mutation which corrects the faulty genetic code. A way to achieve this is to use CRISPR/Cas9. Clustered Regularly Interspaced Short Palindromic Repeats with Caspase 9 is a bacterial immune response in order to protect its genetic integrity and was discovered by the Japanese molecular biologist

Yoshizumi Ishino in 1987 from *Escherichia coli* (Zakeri *et al.*, 2012). CRISPR/Cas9 works by creating multiple small targeted sequences in DNA, where the genetic code can alter a genes function, either by knocking out (reducing the gene function to zero) or knocking in (increasing or altering gene function) (Housden and Perrimon, 2016).

Cell transplantation involves the insertion of stem cells into the retina in order to alleviate the symptoms of RP by the 'donated' cells introducing the correct genetic sequence or protein. The most logical form of this would be to use induced pluripotent stem cells (iPSCs). However, the autologous cells would need to be repaired using a technique like CRISPR/Cas9 as the patient's cells would still contain the mutations (Bassuk *et al.*, 2016). This means that human embryonic stem cells (hESCs) or allogenic cells from a donor may be a more suitable option. The hESCs will contain the correct genetic sequence and will not have a risk of being rejected by the recipient, the allotransplanted cells (compatible cells from a genetically different individual of the same species) may be rejected. The cells would be surgically implanted into the macular region of the retina and monitored over several years to observe any improvements in eyesight or RP progression (Kaplan *et al.*, 1997). But most of these studies have proved either unsuccessful or inconclusive.

Along with cell transplants, there have also been prosthetic retinal implants. An example of this is the surgical insertion of a Retina Implant Alpha AMS, a device which sits on the retina and stimulates the inner retina to respond normally to incoming light. Essentially, restoring an individual's sight to normal without interfering with the rhodopsin gene (Edwards *et al.*, 2018). Or an artificial silicon retina microchip could be implanted into the same region to give a similar effect (Chow *et al.*, 2004). Studies like this, such as the Argus<sup>®</sup> II Retinal Prosthesis System, have shown some improvement to the visual fields of some individuals, but the rates of success are far from being significant. The Argus II system is made up of a 200  $\mu\text{m}$  60-electrode microarray (implanted onto the back of the retina and optic nerve) connected via a coiled link to an external video processing unit (VPU) and a miniature camera attached

to a pair of glasses. The cameras work in real time and transmit the images as stimulating pulses to the optic nerve, which can then be interpreted by the brain in the same way as viewing something normally. In essence, the idea is for the cameras to take over the role of the eyes and allow the individual to 'see' via an unconventional route (Ahuja *et al.*, 2011). 27 subjects were used for this study, so more investigations are needed to confirm whether this system is accurate, reliable and should be used more widely. But of these 27 subjects, 26 showed a significant improvement in identifying a given point and touching it when using the system compared to without (Ahuja *et al.*, 2011).



**Figure 1.8- Argus® II Retinal Prosthesis System.** Illustrations showing the position of the electrode implant (left), external video processing unit-VPU (centre) and cameras mounted to a pair of glasses (right) (Ahuja *et al.*, 2011).

Pharmacological treatments involve using small molecules, such as retinal, to alter the mutant rhodopsin pigment instead of interfering with its genetic sequence. Pharmacological chaperones do this by acting as scaffolding proteins and allow the misfolded proteins to reach their native conformation (Morello *et al.*, 2000). These small molecules can be used to stabilise the mutant rhodopsin pigment and help stop the progression of RP (Chen *et al.*, 2018). This is one of the main focuses of this project and will be discussed later.

### **1.7- Techniques and Rationale**

The focus of this project is to investigate what effect three particular rhodopsin mutations have and infer this onto the mechanism that RP seems to follow, as well as its severity. Alongside this, a secondary background mutation will also be investigated to see whether this has any mitigating rescue properties when present with the other primary mutations (meaning does the secondary mutation help 'fix' the rhodopsin molecule). Objectives that will also be looked at include: what role the

chromophore has and whether changing this can yield any beneficial results and the effect of mutating the docking region for the cap.

The three mutations that will be investigated are G101V, V104F and G106W. For the mutation at residue 101 Glycine has been replaced by Valine, for residue 104 Valine is substituted by Phenylalanine and at residue 106 Tryptophan replaces Glycine (Figure 1.9). Each of these mutations has been created within separate bovine rhodopsin genes and DNA extracted. Along with these mutants, there is also a bovine wild type rhodopsin for comparison at each stage (please note, bovine rhodopsin has a slightly different genetic code to human rhodopsin, resulting in a different order of amino acids-see Appendix). Very few studies have been conducted on the G101V and V104F mutations, but some similar mutations have been investigated. One study has shown that at residue 104, Valine has been replaced by Isoleucine. The result of this study was that this residual substitution did not result in a RP phenotype, meaning that the mutation has a phenotypically silent effect, therefore V104F may have the same effect (Macke *et al.*, 1993). Whereas the G106W mutation has been investigated to some extent and is believed to interfere with the Schiff base (overall protein folding, stability and chromophore association as well), preventing the formation of the rhodopsin molecule, but does not reduce the levels to zero (Kaushal and Khorana, 1994). All of these mutations are located on Extracellular loop 1 (ECL 1) and are either Class II mutations (G106W) or unclassified (Figure 1.4).

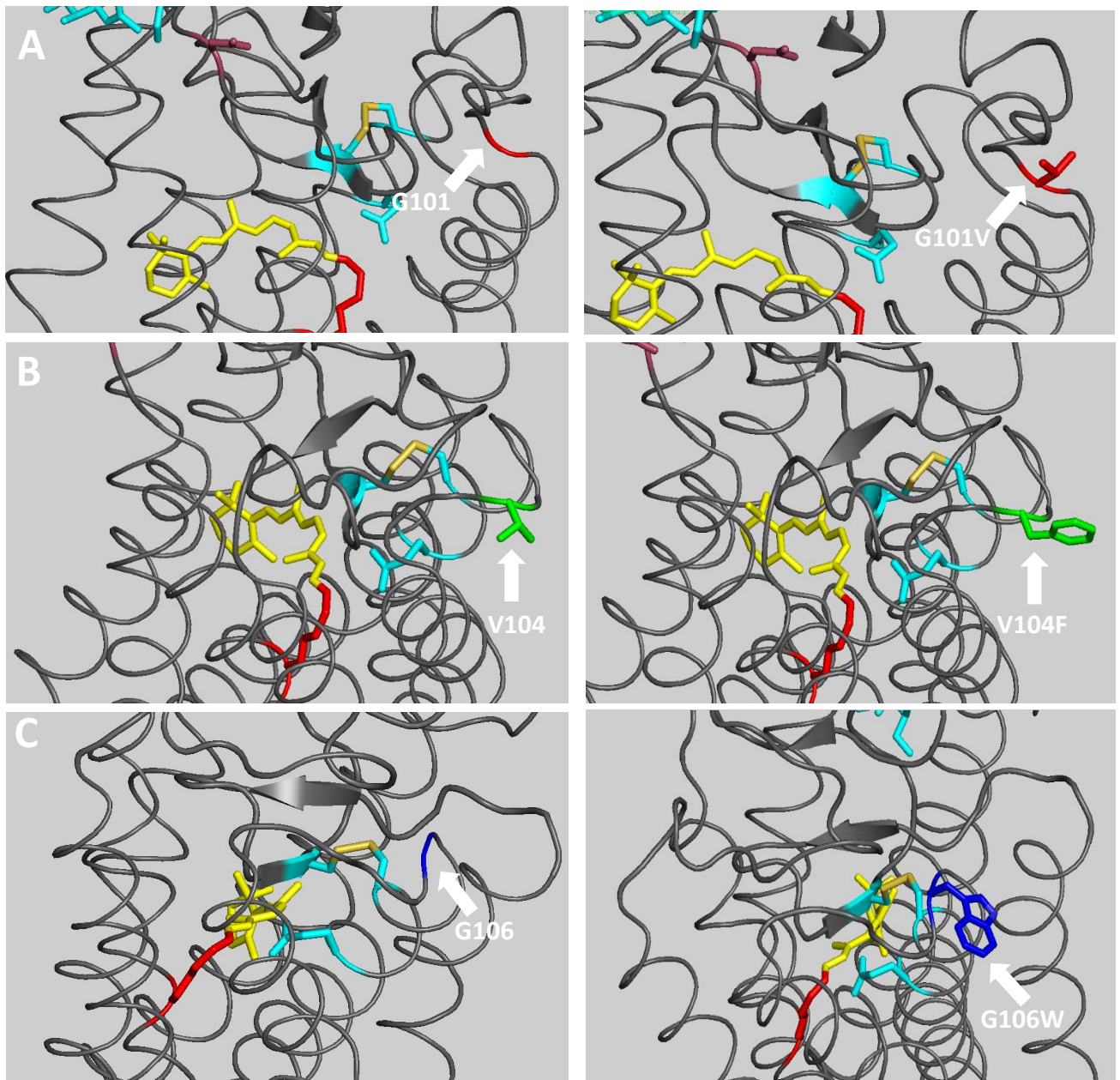


**Figure 1.9- PyMol images of the mutations G101V, V104F and G106W.** PyMol diagrams showing the original residue at their corresponding base locations with their mutated versions to the right. A) Highlighted in red is Glycine at position 101 with the mutated Valine next to it, B) Highlighted in green at position 104 are Valine and Phenylalanine, C) Highlighted in dark blue are Glycine and Tryptophan at position 106. 11-*cis*-retinal is shown in yellow bound to Lysine 296 (K296).

The secondary background mutation will replace Asparagine and Aspartic Acid with Cysteine at residues 2 and 282, respectively (N2C/D282C). This mutation results in a disulphide bridge forming between the two new cysteine residues, giving the intracellular N-terminus and ECL 3 a more stable configuration. The disulphide bridge replaces the weaker hydrogen bond between the two previous amino acids (Asparagine and Aspartic Acid) (Standfuss *et al.*, 2007). The replacement of

Asparagine with Cysteine also results in the removal of a glycosylation site at residue 2, leading to a reduction in protein size (shown in Figure 3.9, Reeves *et al.*, 2002).

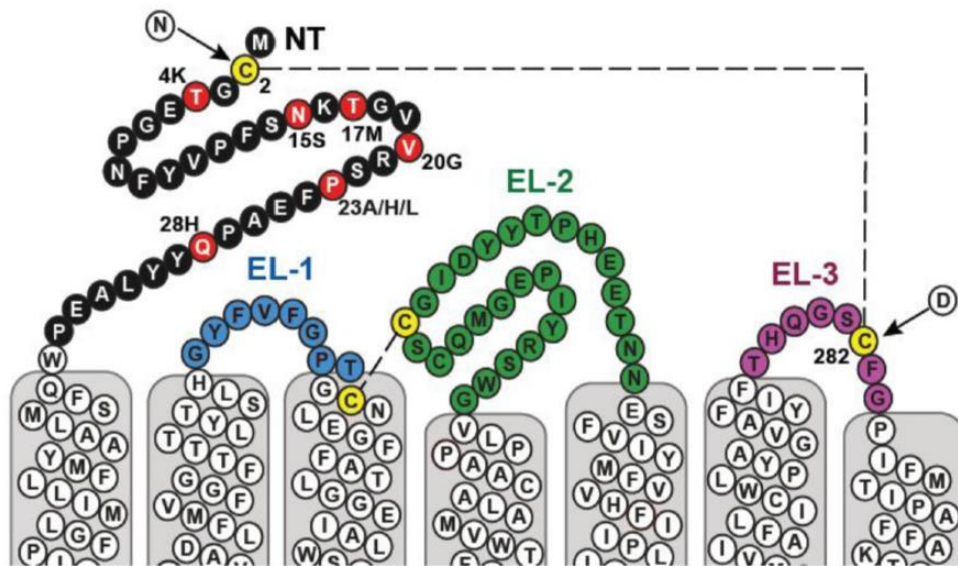


**Figure 1.10- Secondary structure of the N-terminal cap for rhodopsin.** Showing where the disulphide bridge (indicated by the dotted lines) will form between inserted cysteine residues (in yellow) at positions 2 and 282 (Opefi *et al.*, 2013).

Some preliminary results have shown that the presence of this background mutation (N2C/D282C), whether other mutations are present or not, does increase the thermostability of rhodopsin (Deupi *et al.*, 2012; Opefi *et al.*, 2013).

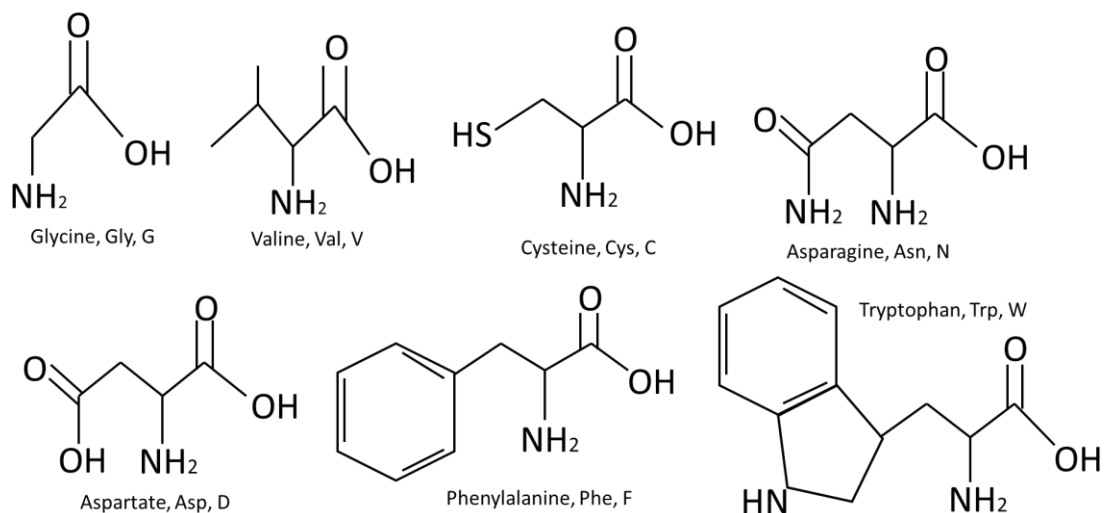


**Figure 1.11- Skeletal diagrams of the main seven amino acids involved in the rhodopsin mutations in this project, along with their appropriate functional groups.** Diagrams start with the most basic amino acid Glycine and become more complex through to Tryptophan. The structure of each can be used to theorise any additional (or reduced) interaction when one amino acid is replaced by another at positions 101, 104 and 106 in the rhodopsin protein.

This project will also include investigating pharmacological chaperone rescue. As stated earlier, this involves using small molecules to bind and stabilise the rhodopsin structure rather than changing its genetic code. A simple way to do this is to use the natural ligand retinal itself. 11-*cis*-retinal is the natural derivative but it can be replaced by 9-*cis*-retinal, a variant that is believed to have some rescue properties (the term *cis* refers to the functional groups being on the same side of the carbon chain whilst *trans* means on opposite sides). This is because 9-*cis*-retinal has a very similar structure to 11-*cis*-retinal, meaning that it behaves in an almost identical way. The main difference, apart from structure, is that 9-*cis*-retinal exists in a slightly higher energy state, giving it the potential to increase stability when bound to a mutated rhodopsin molecule (Sekharan and Morokuma, 2011) and 9-*cis*-retinal is readily available.

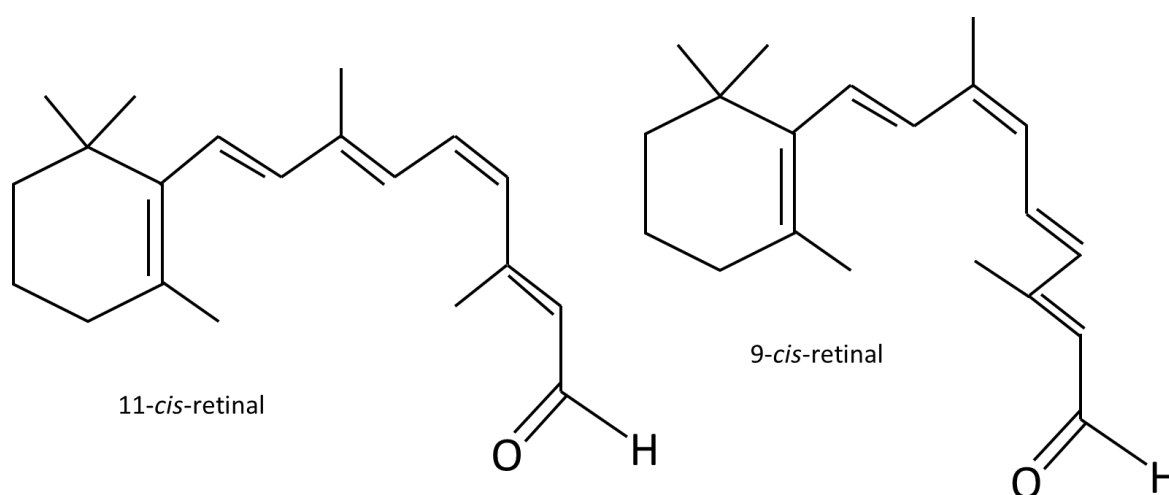


**Figure 1.12- 11-*cis*-retinal and 9-*cis*-retinal skeletal diagrams.** Diagrams showing the two different version of natural retinal.

A breakdown of the techniques that will be used in this project are: bacterial transformations, gel electrophoresis (agarose and SDS-PAGE), cell tissue culture, calcium chloride transfections, pharmacological chaperone rescue with 9-*cis*-retinal, disulphide bridge mediated repair, immunoaffinity purification, UV-visible absorbance spectroscopy, Metarhodopsin-II decays and thermal decays. At least three repeats of each data set will be carried out to gain concordant results and exclude any outliers. All of these techniques will be explained in more detail in the methodology chapter.

The cells being used are HEK 293 GnT1<sup>-</sup> cells (Human embryonic kidney) (n-acetylglucosaminyl transferase I knockout). HEK 293 cells are an extensively used cell line of epithelial origin that was first established by transformation with sheared Adenovirus type 5 DNA in 1973 by Alex van der Eb and Frank Graham (Graham *et al.*, 1977). This transfection with adenovirus DNA allows the cells to grow and be cultured with a much higher efficiency, but the DNA had to be sheared (made to correct fragment size) in order to prevent the HEK cells from lysing (Graham *et al.*, 1978). The reasons that this particular cell line is being used are because they are ideal for expressing transgenes from both mammalian and non-mammalian sources and are especially good for the study and isolation of particular receptor channels (Thomas *et al.*, 2005). GnT1 is a type II protein located in the Golgi apparatus membrane and, because of its name, it has an important role in the initiation of complex N-glycan formation in both plants and animals (Burke *et al.*, 1994, Schoberer *et al.*, 2009). These N-glycans (complex carbohydrates bound to Asparagine residues via glycosidic bonds) are essential at particular sites and are believed to have some role in aiding stabilise the tertiary and quaternary structures of rhodopsin (Reeves *et al.*, 2002; Stanley *et al.*, 2017). Although HEK cells can function without GnT1 present (termed GnT1<sup>-</sup>), the formation of complex N-glycans can be interrupted.

### **1.8- Investigative Aims and Hypotheses**

The main hypotheses are:

- The use of either disulphide bridge mediated repair or pharmacological chaperone rescue will result in a more stable mutant rhodopsin protein being formed, when compared to its non-repaired or non-rescued counterpart.
- The use of both rescue and repair methods together will result in an added stability effect in comparison to each method being used individually.

The overall hypothesis for this project is: The rhodopsin RP mutations G101V, V104F and G106W alter ECL 1 structure which prevents the N-terminal cap either from folding correctly or from docking to ECL

3. But the use of pharmacological chaperone rescue and/or disulphide bridge mediated repair restores native rhodopsin function and stability.

The findings of this project may have much larger implications than just research, they may develop into ideas for a treatment for RP. If the stated hypotheses are proved correct, then initiating a disulphide bridge (not practical to carry out in humans at the moment) or supplementing 11-*cis*-retinal with 9-*cis*-retinal could prevent the progression of rod cell death and possibly stop RP. But other techniques like CRISPR/Cas9 or stem cell transplants could yield better results, be safer for the individual and are far better understood.

## 2. Methodology and Materials

Chemicals/Reagents	Provider	Reference number
9-cis-Retinal	Sigma	R5754
Agar Granules	Melford Biolaboratories Ltd	GM1002
Agarose-gel Ladder Sequence	Thermo Scientific	SM0313
Ammonium Phosphate (APS)	Melford Biolaboratories Ltd	A1512
Bes	Sigma	B6420
Bis-acrylamide	Sigma	A3574
Bis-Tris Propane (BTP)	Melford Biolaboratories Ltd	64431
Calcium Chloride (CaCl <sub>2</sub> )	Sigma	C5670
Dimethyl Sulphoxide (DMSO)	Sigma	67685
Disodium Phosphate (Na <sub>2</sub> HPO <sub>4</sub> )	Sigma	71643
DMEM and F12 (Dulbecco's Modified Eagle Medium)	Lonza, Bio-Whittaker	BE12-719D
FastDigest Green Buffer (10x)	Thermo Scientific	B72
Gel Red Nucleic Acid Stain in water (10,000x)	Sigma	SCT123
Glycerol	Fisher Chemical	G0650
Glycine	Fisher Chemical	G0800
Heat-Inactive Foetal Bovine Serum	Thermo Scientific (HyClone)	SV30180.03
Hydrochloric Acid (HCl)	Sigma	7647
L-Glutamine	Lonza, Bio-Whittaker	BE17-605F
Monopotassium Phosphate (KH <sub>2</sub> PO <sub>4</sub> )	Melford Biolaboratories Ltd	P0574
<i>n</i> -Dodecyl β-D-maltoside (DDM)	Sigma	D4641
PenStrep (Penicillin-Streptomycin)	Lonza, Bio-Whittaker	DE17-602E
pMT4 plasmid	Massachusetts Institute of Technology (Franke <i>et al.</i> , 1988)	N/A
Potassium Chloride (KCl)	Sigma	P9541
Skim powdered Milk	Marvel	N/A
Sodium Azide (NaN <sub>3</sub> )	Sigma	S8032
Sodium Chloride (NaCl)	Fisher Chemical	S3160
Sodium Dodecyl Sulphate (SDS)	Melford Biolaboratories Ltd	B2008
Sodium Hydroxide (NaOH, pellets)	Fisher Chemical	54920
Tetramethylethylenediamine (TEMED)	Melford Biolaboratories Ltd	T3100
Triton X-100	Sigma	T9284
Trizma base	Sigma	T1503
Trypsin	Lonza, Bio-Whittaker	BE02-007E
Tryptone	Melford Biolaboratories Ltd	T1332
Tween 20	Melford Biolaboratories Ltd	P1362
Yeast Extract Powder	Melford Biolaboratories Ltd	Y1333

Equipment
Heraeus Multifuge 3 S-R Centrifuge
Hoefer PS600 600-volt Power Supply (with Bio-Rad Centurion range)
Marshall Scientific Eppendorf 5417R Centrifuge
New Brunswick Scientific Innova 43 & 4300 Incubated floor Shakers
Perkin-Elmer Lambda 35 UV-vis Spectrophotometer
Perkin-Elmer LS 50B Fluorometer
Schott KL 1500 compact light source
Sorvall Discovery 90SE Ultra-Centrifuge
Thermo Scientific Nanodrop (ND) 1000 Spectrophotometer
Vilber Fusion FX Fluorescence Imager

Buffer	Reagents
2x YT Broth (2x YT with Agar)-1 L	5 g NaCl, 10 g Yeast Extract, 16 g Tryptone (3 g Agar per 200 ml Duran bottle) in MilliQ water
2x Bes Buffer- 100 ml	50 mM Bes, 250 mM NaCl, 1.5 mM NaHPO <sub>4</sub> [pH 7.02] with NaOH, in MilliQ water
10x CaCl <sub>2</sub>	2.5 M CaCl <sub>2</sub> dissolved in 100 ml distilled water
4x Running Gel Buffer	18.15 g Tris-HCl [pH 8.8] in 100 ml of MilliQ water
4x Stacking Gel Buffer	3 g Tris-HCl [pH 6.8] in 50 ml of MilliQ water
H <sub>2</sub> O saturated Iso-butanol	10 ml Iso-butanol mixed with 3 ml H <sub>2</sub> O
10x Tank Buffer- 500 ml	15.14 g Tris, 72.07 g Glycine, 5 g SDS, dissolved in MilliQ water
1x Tank Buffer	100 ml of 10x Tank buffer and 900 ml MQ H <sub>2</sub> O
1x Transfer Buffer	100 ml 10x Tank buffer, 200 ml Methanol, made up to 1 L with MQ H <sub>2</sub> O
4x Loading Buffer	0.125M Tris-HCl [pH 6.8], 4% SDS, 20% Glycerol, 0.2 M DTT, 0.02% Bromophenol Blue
10x PBS (Phosphate Buffered-Saline)- 800ml	64.05 g NaCl, 1.61 g KCl, 1.63 g KH <sub>2</sub> PO <sub>4</sub> , 11.39 g Na <sub>2</sub> PO <sub>4</sub> ·2H <sub>2</sub> O, dissolve in water and autoclave
Blocking Buffer	5 g Skim powdered milk, 50 µl Tween 20, few grains of NaN <sub>3</sub> , made up in 50 ml 1x PBS
Wash Buffer	2.75 g Skim powdered milk, 550 µl Triton X-100, made up in 550 ml of 1x PBS
Freezing Media Buffer	10% sterile HybriMax DMSO (WARNING: double glove and avoid all contact to the skin) and 90% DMEM-F12 media
Solution 1- 100 ml	5 ml 1 M Tris (pH 7.6), 2 ml 0.5 M EDTA and autoclaved. 100 µl 100 mg/ml Heat-treated RNase and stored at 4 °C
Solution 2- 10 ml	200 µl 10 M NaOH, 1 ml 1% SDS, 8.8 ml H <sub>2</sub> O
Solution 3- 100 ml	38.2 g 4 M Guanidine Hydrochloride, 4.9 g 0.5 M Potassium Acetate, pH to 4.2 with Glacial Acetic acid with stirring at 70 °C before autoclaving
Binding Buffer- 200 ml	95.53 g 5 M Guanidine Hydrochloride, 0.48 g Tris in 124 ml MQ water, autoclave, add 76 ml ethanol
Wash 1- 200 ml	2.34 g NaCl, 4 ml 1 M Tris (pH 7.5), 10 ml 1 M EDTA in 84 ml water (pH with Glacial Acetic acid, stirring, 70 °C) and autoclave. Add 116 ml ethanol
Wash 2- 100 ml	20 ml sterile MQ water and 80 ml ethanol
BTP (High-salt BTP)- 100 ml	2.82 g BTP to make 100 mM stock (with 140 mM NaCl, 0.82 g)

All medias and buffers listed above were mixed together in a beaker (size dependent upon the volume of the end solution) using a magnetic stirring flea (on a Fisher-Scientific Mixer) to ensure all reagents dissolved. Following this, the pH of the buffers were adjusted (if needed) with the stated chemicals and poured into appropriately sized Duran bottles and autoclaved (again, if needed).

## 2.1 General Methods

### 2.1.1 Preparation of growth media

2x YT Broth (200 ml, 20 x 10 ml universal tubes)- 1 g NaCl, 2 g Yeast extract, 3.2 g Tryptone.

The 200 ml solution was aliquoted into 10 ml amounts using a pipette aid and a 25 ml pipette.

Overnight culture broth (800 ml 2x YT, 100 ml x 8 L conical flasks)- 12.8 g Tryptone, 8 g Yeast extract, 4 g NaCl.

800 ml was made in total with 100 ml used per conical flask.

### 2.1.2 Culturing techniques

Ampicillin growth plate- Agar solution, 200  $\mu$ l Ampicillin.

The agar was melted in a microwave to a point of a rolling boil and was then allowed to cool to a touchable temperature (approximately 50 °C). 200  $\mu$ l of ampicillin (concentration 100 mg/ml, 1:1000 dilution) was then added and gently mixed in to the 200 ml of 2x YT broth. The broth was poured equally into eight sterile petri dishes near a lit Bunsen flame, once set the plates were inverted to prevent condensation build-up.

Transformation- Escherichia coli XL1 blue

1  $\mu$ l of each rhodopsin RP mutant glycerol stock was diluted with 9  $\mu$ l of MilliQ water in Eppendorf tubes and chilled on ice. 1  $\mu$ l of diluted sample was added to 40  $\mu$ l of competent *E. coli* cells and cooled on ice for 30 minutes, before being heat shocked in a water bath at 42 °C for 45 seconds and returned to ice for a further five minutes. 500  $\mu$ l of 2x YT broth was added before the tubes were placed on a shaker (250 rpm, 37 °C, 10 minutes). 50  $\mu$ l of each sample was added to the appropriate growth plate and incubated at 37 °C for roughly 16 hours.

### Day Culture- 3 ml 2x YT broth, 25 µl Ampicillin.

A single colony was picked using a sterile toothpick and gently dipped into 3 ml of broth solution with 3 µl of ampicillin in a 15 ml centrifuge tube, one tube for each mutant sample. The tubes were then placed onto a holding rack and incubated overnight on a shaking incubator (37 °C, 250 rpm).

### Glycerol mutant stocks

500 µl of each mutant sample (from original ampicillin growth plates) was added to 500 µl of 50% glycerol and stored at -80 °C in cryopreserve tubes.

### Streak plates

A pipette tip was used to apply glycerol stock sample to the ampicillin plate. Sterile toothpicks were used to streak the sample around the plate and isolate colony growth and incubated overnight at 37 °C.

### Overnight culture

A 100 µl amount of day culture was added to conical flasks (100 ml of 2x YT broth) with 100 µl of Ampicillin. Incubated overnight at 37 °C, 200 rpm on an Innova 43 or 4300 floor incubator. Samples were removed the following morning and centrifuged in 50 ml centrifuge tubes (4500 rpm, 10 minutes) and the pellets frozen at -20 °C for MidiPrep.

## **2.2 Molecular Biology Methods**

### 2.2.1 Sample Sequencing

Samples from agarose gel were sent to Eurofins for standard Sanger sequencing. Samples were diluted to 100 ng/µl in a volume of 15 µl. Both F1 and F2 primers were diluted to 10 pmol/µl in a volume of 55 µl. Each sample and primer was placed into a separate Eppendorf tube and sent for sequencing. Sample numbers were recorded and used to label sequencing results received three days later.

### 2.2.2 Agarose Gel Electrophoresis

Agarose gel (Midi gel, 20 wells)- 1.2 g Agarose, 1x TAE buffer, DNA ladder solution, mutant samples, restriction endonucleases NotI and EcoRI

1.2 g of Agarose was dissolved in 150 ml of 1x TAE buffer and heated to a boil before being allowed to cool. The gel mixture was then poured into the gel casing (assembled as per instructions) with well comb and left to set (30 minutes). Once set, the gel was placed into the gel tank and covered in 1x TAE buffer. 5 µl (0.1 µg) of ladder sequence, 10 µl 1x loading buffer and 5 µl gel red added to well number one, the following wells contained alternating undigested (2 µl mutant sample, 2 µl 10x Fast Digest Green buffer, 5 µl Gel red and 11 µl MilliQ water) and double digested (1 µl of both restriction enzymes, 2 µl mutant sample, 2 µl 10x Fast Digest Green buffer, 5 µl Gel red and 9 µl MilliQ water) samples. The midi gel was run for 75 minutes at 100 V, visualised and photographed using a UV transilluminator (302-312 nm).

### 2.2.3 DNA Extraction

Miniature DNA Preparation- MiniPrep

1 ml of day culture broth was centrifuged (two minutes, 20 °C, 14000 rpm) and the supernatant was removed. The pellet was resuspended in 250 µl resuspension solution and vortexed to mix. 250 µl of lysis solution was added and inverted five times, followed by 350 µl of neutralisation solution and inverted five times. The next step was centrifuging (five minutes, 20 °C, 14000 rpm) and the supernatant was transferred to a GeneJet column and centrifuged (one minute). 500 µl of wash solution was added, centrifuged and the flow through discarded (repeated twice). This was followed by another centrifugation (one minute) to remove any excess wash solution and ethanol. The GeneJet column was then transferred to an Eppendorf tube and 50 µl of MilliQ water (preheated to 65 °C) was added before being centrifuged for two minutes. The purified plasmids were then stored at -20 °C.

#### Medium scale DNA Preparation- MidiPrep (Kit)

The pelleted *E. coli* cells from the overnight culture were resuspended in 5 ml of SN1 solution and vortexed until no clumps were left. Next the cells were lysed with 5 ml of SN2 and inverted to mix. Following this, 5 ml of SN3 was used to neutralise the solution once inverted several times until there was no blue colour visible (only an off-white flocculate). The lysate was then transferred to a Nucleospin Plasmid Filter column and centrifuged for two minutes at 3700 rpm. Afterwards, the column was discarded and roughly 7 ml of SN4 was added to the filtered solution (approximately half the volume of the filtered solution), vortexed to mix for five seconds. The DNA solution was then filtered using a NucleoSnap Plasmid column on a vacuum manifold, set to -0.3 bar. The column filter was then washed with 2 ml of SN5 and then 4 ml SN6. Following on, the funnel was broken away from the spin column, which was placed into a collection tube and centrifuged at 1000 rpm for one minute. The column was then transferred to an Eppendorf tube and 500 µl of MilliQ water was added (preheated to 65 °C). This was again centrifuged and then frozen at -20 °C. All steps listed above are carried out for each individual pellet.

#### Medium scale plasmid DNA Preparation- MidiPrep (Celite)

The pelleted *E. coli* cells from the overnight culture were resuspended in 5 ml of Solution 1 and vortexed until no clumps were left. Following this, 5 ml of Solution 2 was added, and the tubes inverted several times to mix the solutions for less than four minutes. 5 ml of Solution 3 (on ice) was added before being mixed via inversions. The tubes were then centrifuged for 30 minutes, 4000 rpm at 4 °C (but room temperature is acceptable if there is no alternative). After the centrifugation, the supernatant was poured through a tea bag into a separate 50 ml tube and the flocculate discarded (a new glove is advised for each sample to avoid cross contamination of the plasmids). The plasmid solution was then added to 0.4 g of Celite in 10 ml Binding buffer and mixed by rotation for 10 minutes. The 25 ml solution was then poured into a 5 ml Pierce column with funnel extender and allowed to pack under pressure on a vacuum manifold. Once the solution had run through, 10 ml of Wash 1 followed by 3 ml of Wash 2 were added and run through. The resin was left on the manifold

until it turned white in colour and the column no longer felt cold. However to save water, the column was centrifuged at 4000 rpm for 5 minutes after both washes before being returning to the manifold. The DNA was eluted out using two separate additions of 500  $\mu$ l of 65 °C MQ water and centrifuged for 10 minutes at 4000 rpm. The DNA can then be measured and stored at -20 °C.

#### Nanodrop

Nanodrop spectroscope was used to measure the plasmid DNA concentration (in ng/ $\mu$ l). First, blanked with 1.5  $\mu$ l of MilliQ water before testing each DNA sample. Concentration (ng/ $\mu$ l), 260/280 and 260/230 ratios were recorded.

#### 2.2.4 Tissue Culture

##### Resuscitation of cells

1 ml of frozen HEK-293 GnTI<sup>-</sup> cells were thawed rapidly at 37 °C and added to 9 ml of complete DMEM-F12 media (500 ml DMEM-F12, 50 ml Heat Inactivated FBS, 5 ml PenStrep, 5 ml L-Glutamine) in a 15 ml centrifuge tube. Cells were then centrifuged at 1000 rpm for four minutes. The supernatant was then removed, and the cells resuspended in 10 ml of DMEM-F12 media before being added to a 10 cm culture plate and placed into an incubator at 37 °C and 5% CO<sub>2</sub> to grow.

##### Sub culturing- DMEM-F12 media and trypsin.

Two sterile cell culture plates were labelled and prepared with the appropriate amount of media for the dilution factor. The DMEM-F12 media from the original plate was aspirated off and the plate was washed with 5-10 ml of 1x PBS (to ensure all media had been removed). The PBS was then aspirated off and 1 ml of trypsin (preheated to 37 °C) was added to the plate (made sure to cover the entire plate) and incubated for one minute in the incubator (37 °C, 5% CO<sub>2</sub>). 9 ml of DMEM-F12 media (preheated to 37 °C) was then added to neutralise the effect of trypsin. Using a 10 ml pipette and pipette aid, the cells were reverse pipetted 10 times to achieve a cell monolayer. After this, the correct amount of cells (and media) were added to the new plates.

### Freezing cells

Freezing media was comprised of 10% sterile HybriMax DMSO and 90% DMEM-F12 media (amounts depend on total volume of freezing media created).

Cells were split via the normal subculture technique, transferred to a 15 ml centrifuge tube and centrifuged at 1000 rpm for four minutes. The supernatant was removed via aspiration and replaced by the freezing media for resuspension. This was then aliquoted into 1 ml per cryovial (total volume used was equal to the volume placed into the cryovials) and stored in Styrofoam boxes at -70 °C before being moved to liquid nitrogen.

### 2.2.5 Transfection Protocols

All conditions and reagent concentrations stated have been optimised for the transfection protocols.

#### Buffer Solutions

2x Bes Buffer (100 ml, for transfections)- 50 mM Bes, 250 mM NaCl, 1.5 mM NaHPO<sub>4</sub> [pH 7.02] with

#### NaOH

The correct amount of each component was mixed together in a glass beaker using a magnetic mixing flea. NaOH was then added dropwise to the solution until the pH reached 7.02 (measured using a calibrated pH meter). This was then filter sterilised and stored as 20 ml aliquots at -20 °C.

#### 10x CaCl<sub>2</sub> (100 ml)

36.7 g CaCl<sub>2</sub> (2.5 M) was dissolved in 100 ml distilled water. The solution was then filter sterilised and stored as 20 ml aliquots at -20 °C.

#### Scaling up

On the Friday before beginning the transfections, the small 10 cm cell culture dishes were scaled up to the larger 15 cm cell culture dishes. The process was exactly the same as the subculture technique, with the only difference being that more media was used to cover the larger plate (therefore accommodating a greater number of cells).

### Transfection Stage 1 (Dish preparation) Monday

The media was removed from one of the 15 cm plates and washed with 20 ml of 1x PBS. The PBS was then aspirated off and 2 ml of trypsin was added before incubating for two minutes (in incubator 37 °C, 5% CO<sub>2</sub>). 8 ml of complete DMEM media was added and the cells evenly suspended by pipetting up and down multiple times. 10 ml of the plate's media was then added to 82 ml of complete DMEM media in a sterile 250 ml Duran bottle and gently swirled to mix. 9 ml was then added to each cell culture plate and then incubated at 37 °C and 5% CO<sub>2</sub> for 24 hours. NOTE: This is for creating 10 plates, each with 9 ml of media and cells. Amounts would need to be adjusted for different plate numbers and different cell confluencies.

### Transfection Stage 2 (Seeding cells) Tuesday

After 24 hours, the cells were transfected with the mutant DNA. The transfection cocktails contained; 27 µg of DNA, 3 µg of pRSV T-ag and 450 µl of MilliQ water (this is for a single plate, so amounts would have to be adjusted to accommodate for more). To each cocktail mixture, 50 µl of 10x CaCl<sub>2</sub> was added whilst vortexing, followed by 500 µl of 2x Bes buffer whilst vortexing over 45 seconds (again, amounts equate to a single plate). 1 ml of the transfection cocktail was then added to the plate and incubated at 37 °C, 1% CO<sub>2</sub> for 24 hours. Fine black precipitates were visible soon after transfection. 1% CO<sub>2</sub> was used to slow down precipitate formation for maximum DNA uptake. Additional pRSV T-ag was added to increase pMT4 plasmid replication (as the plasmid contains a SV40 promoter region).

### Transfection Stage 3 (Washing cells) Wednesday

Complete DMEM media was aspirated off (this was done very carefully as to not disturb the cells), and the cells were washed with unsupplemented DMEM media. This media was added slowly to keep the cells attached to the plate (marked the spot of addition). The unsupplemented DMEM media was removed and replaced by complete DMEM before being placed into the incubator again (37 °C, 5% CO<sub>2</sub>, 48 hours).

#### Transfection Stage 4 (Harvesting) Friday

All transfected plates were removed from the incubator and a scraper was used to detach the cells from the bottom of the culture plate and a pipette with pipette aid was used to suspend the cells in the media. The media and cells were then transferred to a 15 ml centrifuge tube and centrifuged at 4500 rpm, 4 °C for five minutes. The DMEM media was then removed and replaced by 10 ml PBS and the cells resuspended, before centrifugation. Once centrifuged, the PBS was removed, and the cells suspended in 450 µl of PBS with 1 µl of PMSF.

#### In the dark room (use safe red lights only)

1 µl of 10 mM 11-*cis*-retinal in ethanol was added to the suspended cells and incubated at 4 °C for two hours with constant nutator mixing before being snap frozen in liquid nitrogen and stored at -80 °C.

#### Rescue Transfections

The process of these transfections was exactly the same as mentioned before, except after the wash stage 9-*cis*-retinal was added to the cell plates and then wrapped in foil to prevent any exposure to light. 20 µM 9-*cis*-retinal in 0.9 ml ethanol was evaporated under argon before being dissolved in 95 µl of filter sterilised DMSO to give a final concentration of 10 µM. 10 µl of 9-*cis*-retinal dissolved in DMSO was added to each plate, wrapped in foil and returned to 37 °C, 5% CO<sub>2</sub> incubator as normal.

#### Stable Cell-line

A stable cell-line (HEK 293S-GnTI-Rho) was used to create large amounts of WT Rhodopsin protein via the same conditions as stated above for passaging, along with the antibiotic Geneticin (200 µg/ml). Cells were induced using Tetracycline (20 µl of 2 µg/ml) and Sodium Butyrate (50 µl of 5 mM) before being left for three days and harvested in the same way as transfected cells.

### **2.3 Purification of rhodopsin Biochemical and Spectroscopic Analysis**

#### 2.3.1 Immunoaffinity Purification

Once the cells had been harvested following transfection (usually 9 x 10 cm plates or 4 x 15 cm plates per protein sample and suspended in 5 ml 1x PBS) a 500 µl aliquot (solubilised with 50 µl 10% DDM

and mixed for an hour) was taken and photobleached to determine the total amount of protein produced (normalised bleached spectra was taken away from normalised dark spectra to give rough estimate of protein concentration). The remaining 4.5 ml sample (or relative amount needed to contain approximately 100 µg of protein) was solubilised with 1% DDM and mixed in the dark at 4 °C for an hour. This was followed by a centrifugation for 20 minutes at 4000 rpm, before the supernatant was removed and added to 200 µl of 1D4-sepharose bead slurry (50:50 beads to slurry, binds to the TETSQVAPA sequence in C terminus of the rhodopsin protein) and mixed for two hours. After mixing, the sample was poured into a 2 ml polystyrene filter column (with frit) and allowed to filter through. The column was then washed by 1x PBS/0.1% DDM overnight and 10 mM BTP/0.1% DDM the following day. For rescued samples; 100 ml of 1x PBS wash, 150 ml low salt BTP wash and 30 ml high salt BTP wash were used. After the washes, the samples were eluted using 10 mM BTP/0.1% DDM/1% Rho 9mer Elution peptide (200 µl instantly for the first elution and 500 µl after 50 minutes for the other four elutions). High salt elutions can also be taken to elute misfolded proteins (the same as above except containing 140 mM NaCl). All respective samples taken were centrifuged (4 °C, 14000 rpm, 25 minutes) and then tested with the spectrophotometer to record how much protein had been eluted and whether the elution was pure.

### 2.3.2 UV-visible absorption Spectroscopy

Once the cells had been thawed (in darkness) 50 µl of 10% DDM was added and the sample nutator mixed for an hour at 4 °C. Following this, the samples were transferred to non-autoclaved Eppendorf tubes and centrifuged for 30 minutes at 14000 rpm, 4 °C (pre-cooled microcentrifuge beforehand). Blanks were created using 500 µl 1x PBS and 50 µl 10% DDM. The spectrophotometer was loaded correctly with a water bath circulator set to 19 °C (checked with a thermocouple) and setup with data collection between 250 and 650 nm. The cuvettes were cleaned via vacuum suction with 1% SDS, then RO water and finally absolute ethanol. Both cuvettes were filled with the blank solution and the spectrophotometer autozeroed (checked reading and repeated until zero baseline was achieved). Each sample was then run with a blank comparison (in darkness) and then photobleached with light

for 45 seconds. Each sample was then returned to its Eppendorf tube and frozen again for use in SDS-PAGE and western blots.

### 2.3.3 SDS-PAGE and Western Blot

Making the gel:

The gel rig apparatus and glassware (with 10 well comb) were washed with 1% SDS, absolute ethanol and RO water before being dried with Kimtech tissues and assembled. Resolving gel was made up of; 2.65 ml Acrylamide, 2 ml 4x Running buffer, 80  $\mu$ l 10% SDS, 3.2 ml MilliQ water, 80  $\mu$ l APS, 4  $\mu$ l TEMED and inverted to mix. 3 ml was then added to each gel rig and overlaid with 0.5 ml iso-butanol and left to polymerise. Once polymerised, the gels were rinsed with RO water and dried with blotting paper. The gel rig was then overflowed with the stacking gel (0.7 ml Acrylamide, 1.13 ml 4x stacking buffer, 60  $\mu$ l 10% SDS, 2.7 ml MilliQ water, 60  $\mu$ l APS and 4  $\mu$ l TEMED) and the comb inserted.

Running the gel:

The electrode assembly was set up (as per the manufactures' instructions) and placed into the running tank. The upper chamber filled with 1x Tank buffer and left for a few minutes to check that there were no leaks. A syringe and lancet were used to clear out the wells formed of any non-polymerised gel. The samples were loaded from right to left; 6  $\mu$ l of Ladder sample (5  $\mu$ l ladder sequence and 1  $\mu$ l 1x Loading buffer) and then 6  $\mu$ l of each sample (12  $\mu$ l of sample and 4  $\mu$ l 4x Loading buffer) were added to the appropriate wells. The lower chamber was then filled with 1x Tank buffer and run for an hour at 200 V.

Coomassie blue staining:

One gel was removed and rinsed with RO water before being incubated in instant blue staining solution for an hour at room temperature with constant rotator mixing or until the bands became visible. The gel was then left overnight in the staining before being placed on a light box and photographed.

#### Western blot:

Cold transfer buffer was used to soak the other gel, cassette, blotting paper (4 pieces), nitrocellulose and sponges. They were then assembled as follows: black cassette side, sponge, two pieces of blotting paper, nitrocellulose, gel, two pieces of blotting paper, sponge, and all air was removed by using a roller before closing the array. Once closed, the black cassette side was placed facing the red positive transfer frame, an ice pack and magnetic stirrer were also placed into the tank and filled with the transfer buffer. The western blot was run at 100 V for an hour and the tank placed onto a stirring plate inside a bucket of ice. Afterwards, the blot was placed into a box and covered in blocking buffer, then incubated overnight at 4 °C with constant rotator mixing. The following morning, the membrane blot was washed with PBS and incubated for five hours in the primary antibody. After this, the blot was washed five times every five minutes with 50 ml of wash buffer. Once washed, the blot was incubated for an hour in the secondary antibody with rotator mixing. The blot was again washed five times with the wash buffer before incubating in 10 ml ECL reagents (10 ml 0.1 M Tris-HCl [pH 8.5], 50 µl 0.25 M Luminol, 22 µl 0.01 M Coumestrol, 3 µl 30% H<sub>2</sub>O<sub>2</sub>) for one minute. Excess ECL was blotted away and the blot wrapped in clingfilm with no air bubbles (tissues were used to remove and flatten) before being tapped to the radiographic cassette. IN THE DARK ROOM a piece of film was cut into four equally sized pieces and four trays were filled with photographic developer, photographic fixer or two with RO water. One piece of film was exposed to the blot in the cassette (time varied depending on the sample) before being placed in the developer until bands started to form. The film was then washed in RO water before being placed into the fixer. Once fixed, the film was washed again and left to air dry and repeated with other film pieces. **Alternatively**, once the ECL reagents had been added and the blot wrapped in clingfilm, a fluorescent imager was used to take digital photos of the blot. A chemiluminescence setting was used to highlight the protein bands and a blot marker setting to highlight the ladder sequence, before both images were merged together to create a whole western blot image.

#### 2.3.4 Rhodopsin Photobleaching

An aliquot of the sample, equal to an absorbance of 0.02 AU or 20 µg, was made up to 500 µl in 10 mM BTP/0.1% DDM and centrifuged for 20 minutes. The sample then underwent a standard photobleaching reaction for 30 seconds, at 20 °C from a water bath circulator, where both dark and bleached spectra were recorded. Following this, 3 µl of 2 M sulphuric acid (H<sub>2</sub>SO<sub>4</sub>) was added to the sample and blank. Then the acidified spectra were measured. All three spectra were then combined together on a single graph.

#### 2.3.5 Rhodopsin Active State (Meta-II) Decay

An aliquot of the sample, equal to 4 µg of protein, was made up to 600 µl in 10 mM BTP/0.1% DDM and centrifuged for 20 minutes. The sample was then placed in a fluorometer, with water bath circulator set at 20 °C, for two hours. The sample was exposed to light at a wavelength of 250 nm and emitted at an excitation wavelength of 380 nm. The data was then recorded and used in SigmaPlot to create a graph with a single component exponential decay curve and calculated the half-life.

#### 2.3.6 Rhodopsin Thermal Stability

An aliquot of the sample, equal to an absorbance of 0.02 AU or 20 µg, was made up to 500 µl in 10 mM BTP/0.1% DDM and centrifuged for 20 minutes. The UV-Visible spectrophotometer was blanked at room temperature before being heated to 55 °C using a water bath circulator (checked using a thermocouple). The sample, kept in darkness, was then placed in the spectrophotometer and the absorbance (between 250 and 650 nm) was measured every five minutes for the first hour and then every 30 minutes for the next 24 hours. The data was then recorded and used in SigmaPlot to create a decay graph with a single component exponential decay curve and calculated the half-life.

### **3. Results**

#### **3.1 Verification of the DNA sequence for Retinitis Pigmentosa mutation in the rhodopsin gene**

At the onset of this project it was necessary to confirm the identity of all rhodopsin mutants by DNA sequencing. For this *Escherichia coli* XL1-Blue strain was transformed with pMT4 plasmids that contained the following RP mutations: WT, WT N2C/D282C, G101V, G101V N2C/D282C, V104F, V104F N2C/D282C, G106W and G106W N2C/D282C. The pMT4 plasmid is the same as that used by Franke *et al.*, 1988 except the pMT2 vector now contains a rhodopsin gene sequence. This was completed and followed up by growing the bacterial colonies in small culture volumes (approximately 1 ml) and then small-scale preparation of the plasmids (see Methods- Culturing Techniques). Table 3.1 shows the yield and UV absorbance properties of the purified samples.

**Table 3.1- Initial DNA concentrations and spectral properties.** Data recorded using a Nanodrop 1000 Spectrophotometer to measure mutant DNA concentrations and give their respective spectral properties.

<b>Rhodopsin Mutant</b>	<b>DNA Concentration (ng/μl)</b>	<b>260 nm/280 nm</b>	<b>260 nm/230 nm</b>
WT	160.2	1.89	2.34
WT N2C/D282C	162.4	1.92	2.31
G101V	145.1	1.89	2.30
G101V N2C/D282C	150.4	1.89	2.28
V104F	180.5	1.91	2.32
V104F N2C/D282C	142.6	1.88	2.27
G106W	161.6	1.93	2.35
G106W N2C/D282C	157.6	1.91	2.38

These results show that all plasmids gave good DNA yields at a high purity (260 nm/280 nm ~1.8 ml). These plasmids were then subjected to restriction enzyme digestion followed by separation of the fragments by agarose gel electrophoresis (Methods- Agarose Gel Electrophoresis). Here the restriction digest was performed using *EcoRI* and *NotI* together. As a control the undigested plasmids were also loaded onto the agarose gel. The results are shown below in Figure 3.1. The largest band from the undigested samples is about 8000 bp (base pairs) in size, whilst the smaller band is about 4000 bp. The *EcoRI-NotI* digested plasmids result in two DNA fragments of roughly 5000 bp and 1000 bp. When the agarose gel is compared to the plasmid map in Figure 3.2 (created using SnapGene and SnapGene

Viewer), the estimated band sizes are comparable. The total size of the Bovine Rhodopsin gene is 1048 bp and, taking into account the locations of the *EcoRI* and *NotI* restriction sites, the small fragments shown on the agarose gel below are 1058 bp in size (the restriction sites sit either side of the rhodopsin gene). The *EcoRI* site is located between base pairs 1061 and 1066, whereas *NotI* restriction site is between base pairs 2117 and 2125. As the total plasmid size is 6186 bp, then the large fragment must be 5128 bp in size. These actual sizes are very similar to the estimations made from the agarose gel of 1000 bp for the small fragment and 6000 bp for the large fragment (even numbered lanes). The odd numbered lanes (undigested plasmids) show bands at 4000 bp and 8000 bp, in line with the various relaxation states of non-linearised plasmids.

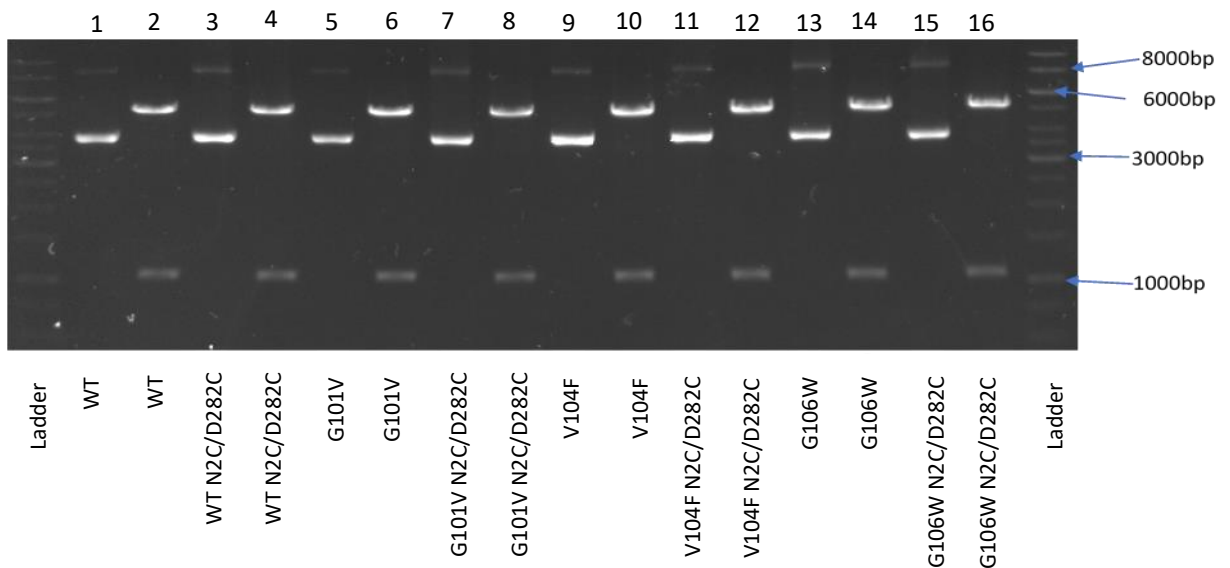


**Figure 3.1- Restriction digest pattern of pMT4 plasmids containing mutant rhodopsin genes.** Odd numbered lanes were loaded with undigested plasmids, whereas even numbered lanes were loaded with plasmids digested by *EcoRI* and *NotI* restriction endonucleases. DNA fragments were then separated by agarose gel electrophoresis (Methods- Agarose Gel Electrophoresis). Samples were then loaded as follows: 1-2 WT; 3-4 WT N2C/D282C; 5-6 G101V; 7-8 G101V N2C/D282C; 9-10 V104F; 11-12 V104F N2C/D282C; 13-14 G106W and 15-16 G106W N2C/D282C. The DNA ladder is loaded as indicated.

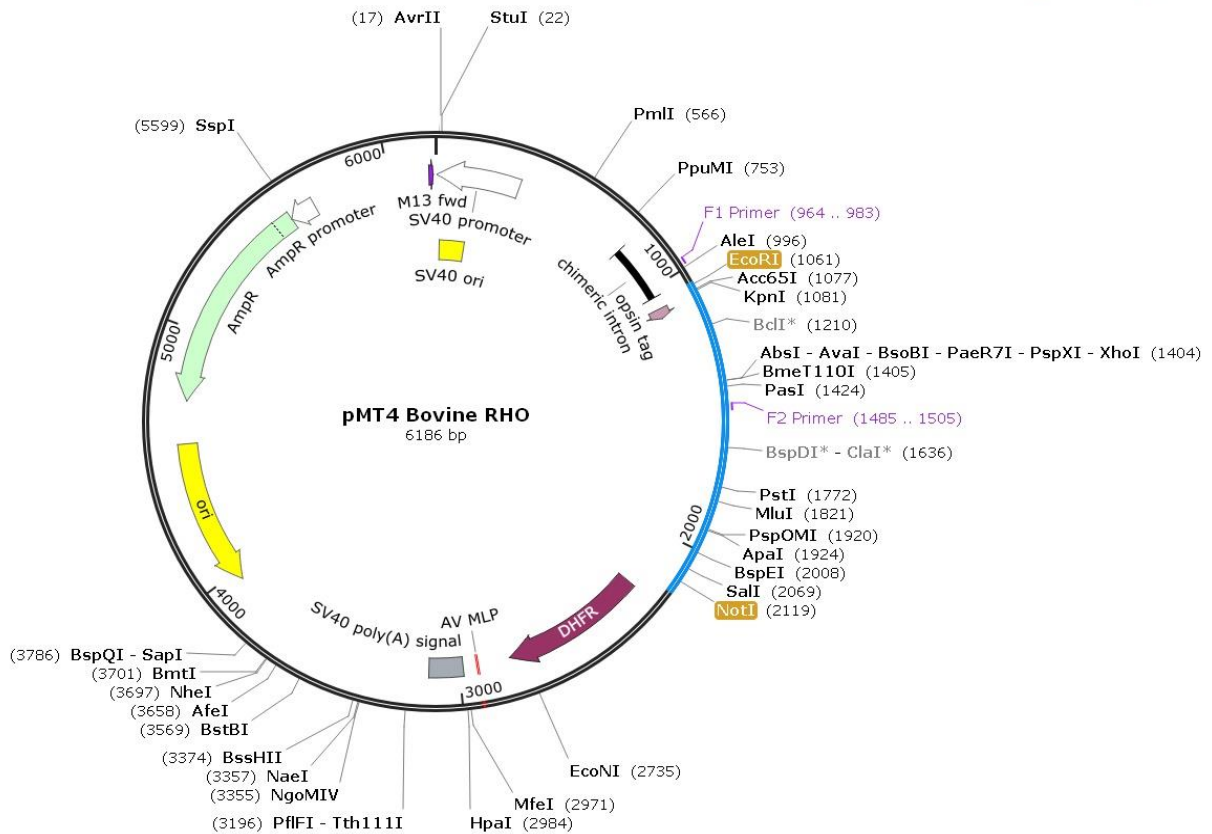


**Figure 3.2- pMT4 Bovine Rhodopsin Gene plasmid map.** Complete pMT4 plasmid map diagram showing the representative locations of the wildtype bovine rhodopsin gene (blue region between 1051 bp and 2171 bp) as well as the restriction endonuclease sites for *EcoRI* (at 1061 bp) and *NotI* (2119 bp), both highlighted in orange boxes. Other significant aspects are also shown including the origin of replication, ampicillin resistance gene and Adenovirus MLP. The total number of base pairs for the entire plasmid is also stated at 6186 bp. This diagram was created using SnapGene and visualised using SnapGene Viewer.

Following on from the confirmation that all plasmids had the correct restriction pattern mutants, the plasmids were subjected to Sanger sequencing. Sequencing reactions were performed with rhodopsin sequencing primers F1 and F2 labelled in purple (F1 sequence: 5' GGT GTG GCA GGC TTG AGA TC 3' and F2 sequence: 5' GTG TGC AAG CCC ATG AGC AAC 3').

1_F1	1	ACAA-CTTGAAGTGAATGACTCCCTTTGCCTTTCTCTCCACAGGTGTCCA	49
2_F1	1	--AAGCTTGAAGTGAATGACTCACTTTGCCTTTCTCTCCACAGGTGTCCA	48
1_F1	50	CTCCCAGGTCCAACCTGCAAGAATTCCACCATCAACGGTACCGAAGGCCCA	99
2_F1	49	CTCCCAGGTCCAACCTGCAAGAATTCCACCATCTGCGGTACCGAAGGCCCA	98
1_F1	100	AACTTCTACGTTCTTTCTCCAACAAGACGGGCGTGGTGCAGCCCGTT	149
2_F1	99	AACTTCTACGTTCTTTCTCCAACAAGACGGGCGTGGTGCAGCCCGTT	148

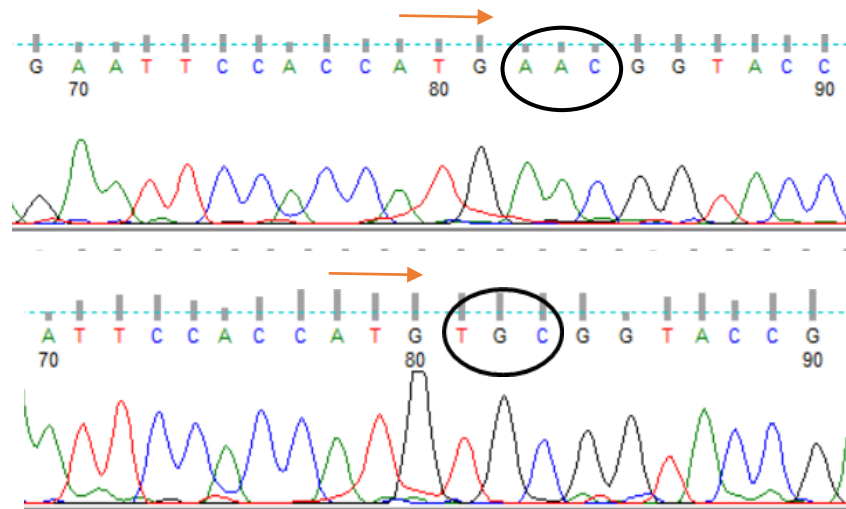


**Figure 3.3- Wildtype rhodopsin and N2C residue mutant sequence alignment.** Sequence alignments were created using the online EMBOSS needle website and the corresponding chromatograms were created using Finch TV. The sequence alignment displays a comparison between a wildtype rhodopsin sample (named as 1\_F1) and N2C mutation (named 2\_F1). Highlighted in black are the base differences at positions which correspond to amino acid 2. Amino acid 2, Asparagine (N) has been replaced by Cysteine (C). The chromatogram on top shows the sequences for the wildtype rhodopsin, whereas the chromatogram underneath shows the sequence of N2C variant. Orange arrows highlight the Methionine start codon (ATG) and the direction of translation.



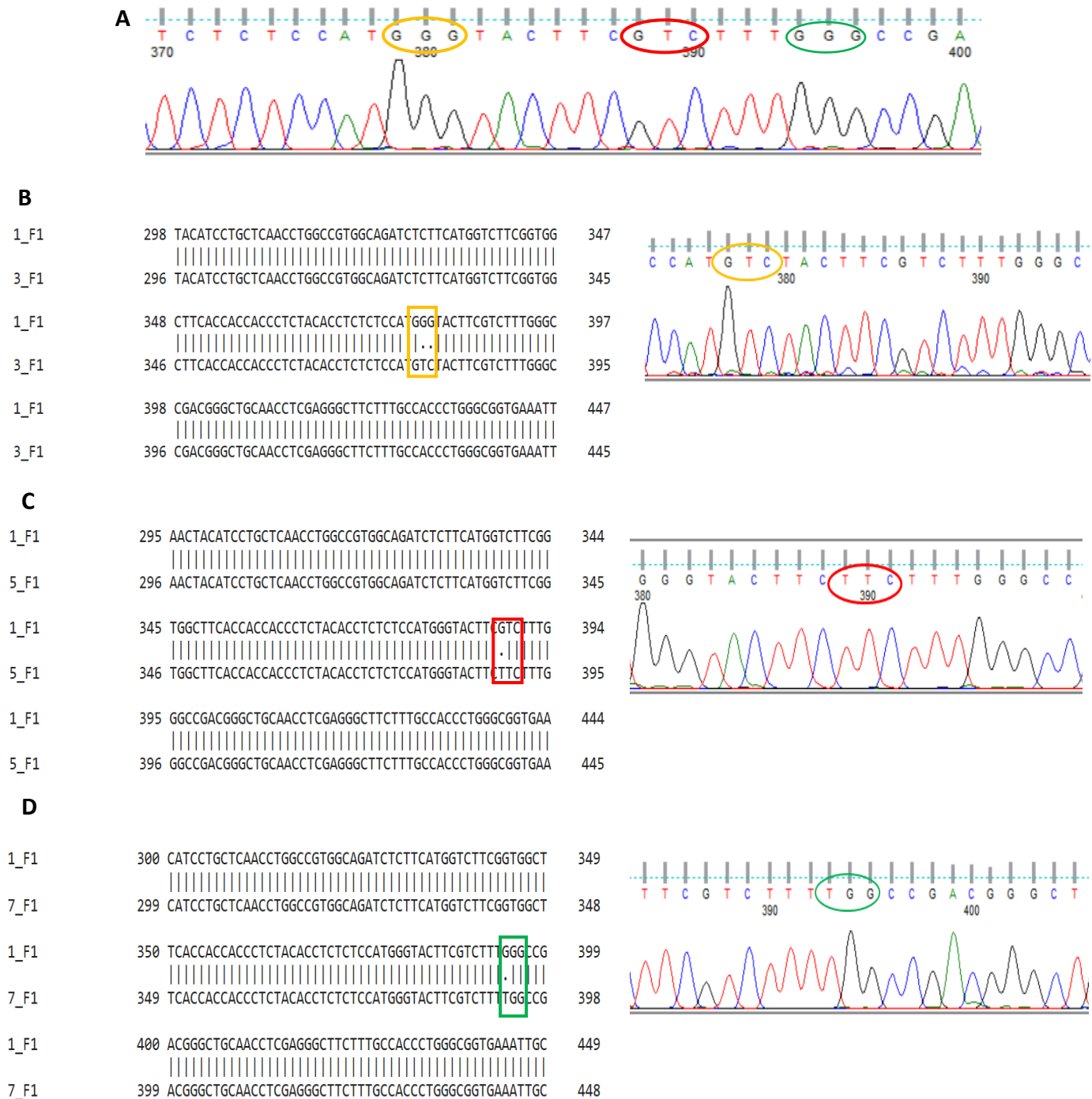


**Figure 3.5- Wildtype rhodopsin and RP rhodopsin mutant sequence alignment comparisons.** Sequence alignments were created using the online EMBOSS needle website and the corresponding chromatograms were created using Finch TV. Part A shows a magnified area of the WT rhodopsin sequence showing the original codons that make up residues 101 (yellow), 104 (red) and 106 (green). Part B shows a sequence comparison for WT rhodopsin (1\_F1) against G101V (3\_F1) and the chromatogram shows the codon for G101V. Part C shows a sequence comparison for WT rhodopsin (1\_F1) against V104F (5\_F1) and the chromatogram shows the codon for V104F. Part D shows a sequence comparison for WT rhodopsin (1\_F1) against G106W (7\_F1) and the chromatogram shows the codon for G106W.

Figures 3.3 through 3.5 have been created using the online sequence alignment website EMBOSS needle ([https://www.ebi.ac.uk/Tools/psa/emboss\\_needle/nucleotide.html](https://www.ebi.ac.uk/Tools/psa/emboss_needle/nucleotide.html)) and the chromatograms using the software program Finch TV. Figures 3.3 and 3.4 show the sequence alignments between a wildtype rhodopsin sample (labelled as 1\_F1) and the rhodopsin N2C/D282C mutant (labelled as 2\_F1) (see Introduction- Aims and Hypotheses). These differences are highlighted in black and blue. The black ovals and rectangle in Figure 3.3 show the differences for the mutation at amino acid codon 2, where Asparagine has been replaced by Cysteine (genetic sequence has changed from AAC to TGC, shown in the chromatograms from top to bottom). The blue ovals and rectangle in Figure 3.4 show the same but for mutations at amino acid 282, where Aspartic Acid has been replaced by Cysteine (genetic sequence has changed from GAC to TGC, shown in the chromatograms from top to bottom). Figure 3.5 shows similar comparisons between the wildtype rhodopsin (labelled 1\_F1) and the three single mutations being examined in this project. Figure 3.5 part A is a magnified area which shows the non-mutated WT rhodopsin codons for the mutations: G101V, V104F and G106W highlighted in their respective colours. Figure 3.5 part B shows a sequence alignment between the wildtype and G101V mutant (labelled 3\_F1) with the base differences highlighted in yellow. The amino acid Glycine has been replaced by Valine and the codon has changed from GGG to GTC. Figure 3.5 parts C and D show the same but for V104F (labelled 5\_F1) in red and G106W (labelled 7\_F1) in green. For the V104F mutant, Valine has been replaced by Phenylalanine with the codon changing from GTC to TTC. Whereas for the G106W mutant, Glycine has been replaced by Tryptophan with the codon changing from GGG to TGG.

### **3.2 Medium and Large-scale plasmid DNA preparation**

Plasmids containing the correct rhodopsin mutations were used for medium scale DNA preparation for use in mammalian cell transfections. Tens of microgram amounts of DNA were needed to transfect mammalian cells ( $1 \times 10^7$  cells on a 10 cm dish) on multiple occasions to generate results with biological replicates.

Large volume *E. coli* XL1 Blue cultures (100 ml) were grown (Methods- Culturing techniques) and used for large scale (MidiPrep) plasmid purifications to create larger amounts of DNA (~1 mg) to be used for transfection of mammalian cells (see Methods- DNA Extractions and Transfections).

Plasmids were prepared in 500 µg to 1 mg amounts with acceptable spectral properties indicating high purity.

### **3.3 Expression levels of ADRP rhodopsin mutants examined using UV-visible absorbance spectroscopy**

#### Disulphide Bridge mediated Repair and Pharmacological Chaperone Rescue

RP mutations in the extracellular region of rhodopsin often lead to misfolding and/or instability (Athanasίου *et al.*, 2018). Here we designed experiments to determine whether this set of mutants misfold upon expression in HEK 293S GnT1<sup>-</sup> cells and, if so, if the misfolding could be reversed or reduced by applying a N2C/D282C disulphide bridge bond repair strategy or by pharmacological chaperone rescue treatment with the ligand 9-*cis*-retinal *during expression* (Introduction- Figure 1.10). In all rescue transfection experiments, the cells were treated after harvest with 9-*cis*-retinal (non-transfected treated with 11-*cis*-retinal) in order to convert the rod opsin apoprotein to the rhodopsin pigment ( $\lambda$  max vis = 500 nm) formation.

The first set of experiments were designed to measure rhodopsin pigment expression levels for each RP mutant in the rhodopsin background or the N2C/D282C background (see Methods- UV-visible absorption Spectroscopy).

These experiments were repeated three times using HEK 293 GnT1<sup>-</sup> cells grown on 10 cm cell culture dishes (Methods- Tissue Culture). Similar experiments were also conducted to observe whether pharmacological chaperone rescue makes any difference in the amount of protein produced by the presence of a mutation (with a WT control). For this to occur, 9-*cis*-retinal is added to the cell plates during the transfection stages and wrapped in foil to prevent them being exposed to light (see

Methods- Rescue Transfection). Both experiments were also performed together to see whether 9-*cis*-retinal treatment can have an additive effect when in the N2C/D282C background.

The expression level of each mutant pigment was determined using detergent solubilised clarified cell extracts spectroscopy. The expression levels are presented in Figures 3.6 and 3.7.

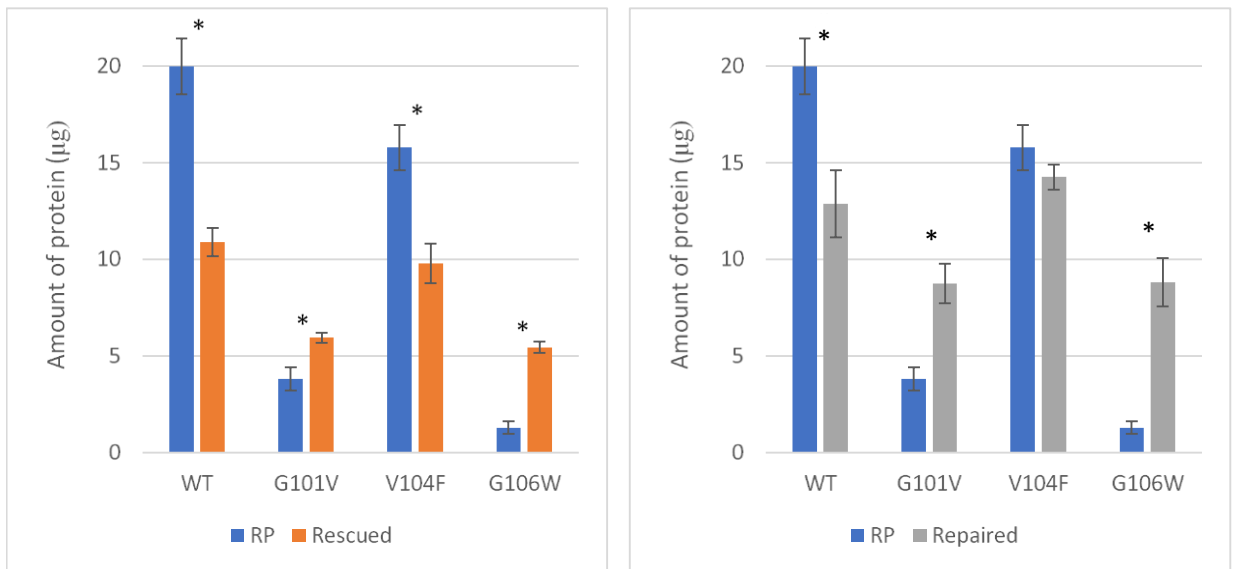


**Figure 3.6- RP mutant rhodopsin protein production after pharmacological rescue or N2C/D282C mediated repair.** Graphs showing the average amount of protein produced by RP mutant rhodopsin proteins compared with either the rhodopsin protein rescued by 9-*cis*-retinal treatment or in the N2C/D282C background, with WT controls (n=3). Blue columns represent untreated RP mutants, orange columns represent 9-*cis*-retinal rescued RP mutants and grey columns represent N2C/D282C repaired RP mutants. Each pair has a calculated p-value from a two tailed t-test to show any significant difference. \*- p<0.05 for RP vs rescued or repaired counterpart (e.g. WT rhodopsin vs. Rescued WT or WT N2C/D282C).

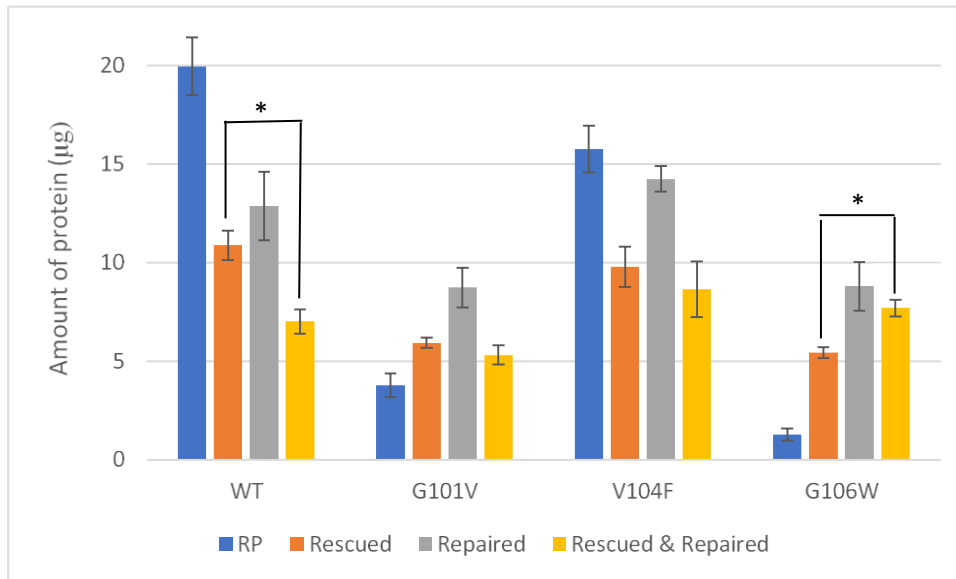


**Figure 3.7- RP mutant rhodopsin protein production after pharmacological rescue or N2C/D282C mediated repair.** Graphs showing the average amount of protein produced by RP mutant rhodopsin proteins compared with either the rhodopsin protein rescued by 9-*cis*-retinal treatment or in the N2C/D282C background, including N2C/D282C rescued mutants and WT controls (n=3). Blue columns represent untreated RP mutants, orange columns represent 9-*cis*-retinal rescued RP mutants, grey columns represent N2C/D282C repaired RP mutants and yellow columns represent rescued & repaired mutants. Each pair has a calculated p-value from a two tailed t-test to show any significant difference. \*- p<0.05 for rescued RP vs rescued N2C/D282C.

From the first graph shown in Figure 3.6, we can see that the RP mutant (blue columns) pairs have produced statistically different amounts of rhodopsin pigment when 9-*cis*-retinal is present during expression (orange columns). Non-rescued WT produces around 20 µg of protein but once rescued this drops to nearly 11 µg. A similar pattern can be seen with V104F which drops from 16 µg when non-rescued to less than 10 µg once rescued. On the other hand, both G101V and G106W show increased rhodopsin pigment formation once rescued, from 4 µg to 6 µg for G101V and 2 µg to about 6 µg for G106W. Each mutant pair was compared using a two tailed t-test and all were found to be statistically different with a p-value less than 0.05 (5%).

From the second graph in Figure 3.6, we can see the difference between RP mutants (blue columns) and in the context of the N2C/D282C rhodopsin background (grey columns). WT and V104F both show a decrease in protein production from 20 µg to 13 µg for WT to WT N2C/D282C and 16 µg to 14 µg for V104F to V104F N2C/D282C. G101V shows an increase in rhodopsin pigment formation from 4 µg to approximately 8 µg for G101V N2C/D282C, which is similar to G106W increasing from 2 µg to 8 µg

when repaired. A comparison using a two tailed t-test shows that WT - WT N2C/D282C, G101V - G101V N2C/D282C and G106W - G106W N2C/D282C are statistically different with a p-value of less than 0.05 (5%). Whereas V104F - V104F N2C/D282C has a p-value of greater than 0.05 (5%) indicating that this RP mutant pair is statistically similar.

Using all of the data in Figures 3.6 and 3.7, both rescue with 9-*cis*-retinal treatment and repair with a N2C/D282C disulphide bridge increase protein expression for G101V and G106W but reduce pigment production for WT and V104F. However in each case, more rhodopsin pigment is produced by the repaired N2C/D282C mutants than those rescued by 9-*cis*-retinal treatment. In Figure 3.7 the yellow columns denote RP mutants that have been subjected to simultaneous pharmacological chaperone rescue and disulphide bond repair. Each rescued-repaired mutant produces less pigment than solely repaired mutants (grey columns) and solely rescued mutants (orange columns) except for G106W. The only instance where rescue and repair methods have an additive effect is for G106W at 7 µg, but this is still lower than G106W N2C/D282C at 8 µg. Overall; WT rhodopsin production is hindered by both rescue and repair, G101V is enhanced by both rescue and repair but has no additive effect, V104F is hindered by both rescue and repair and finally G106W is enhanced by both rescue and repair with a slight additive effect.

### 3.4 Analysis of RP mutant rhodopsin biochemical properties and spectral characteristics

#### 3.4.1 Examination of protein profiles rhodopsin ADRP mutants as judged by SDS-PAGE

Solubilised cell lysates containing the rhodopsin mutants were loaded onto SDS-PAGE gels. Total protein content was visualised by staining the gels with Coomassie blue while western blotting uses the Rho-1D4 monoclonal antibody (Methods- SDS-PAGE and Western Blots). The Coomassie blue dye binds to and stains all proteins present in the sample and is used as a loading control only. Western blotting with Rho-1D4 recognises and binds to the TETSQVAPA sequence which corresponds to amino acids 340 to 348 in rhodopsin's C-terminal (see Introduction- Figure 1.4). From the western blots, the most vivid protein bands are estimated to be between 35 and 40 kDa (kilo-Daltons), which is consistent with the size of rhodopsin solubilised in DDM.

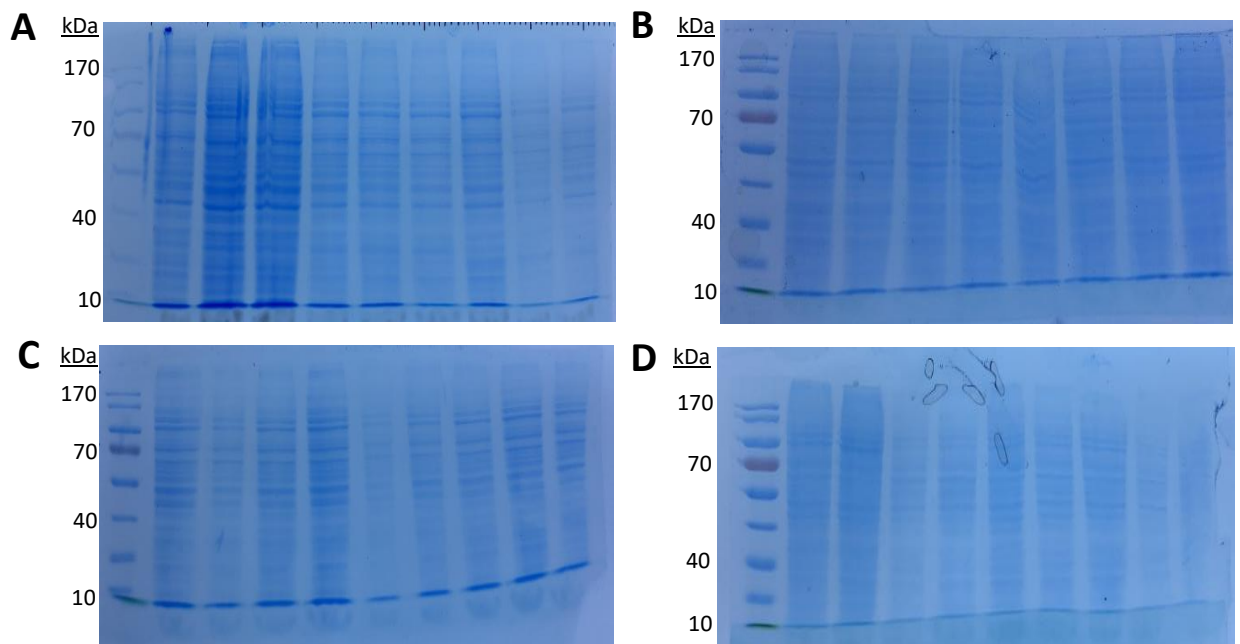


**Figure 3.8- Coomassie Instant Blue stained polyacrylamide gels of various mutant rhodopsin proteins.** Photos of polyacrylamide gels stained with Coomassie blue dye. All gels show three repeats of three different samples (post photobleaching) and a prestained ladder sequence in the first lane. Gel A shows Untransfected cell proteins, WT proteins and unstable WT proteins (from left to right). Gel B shows WT, G101V and G101V N2C/D282C. Gel C shows WT, V104F and V104F N2C/D282C. Gel D shows WT, G106W and G106W N2C/D282C.

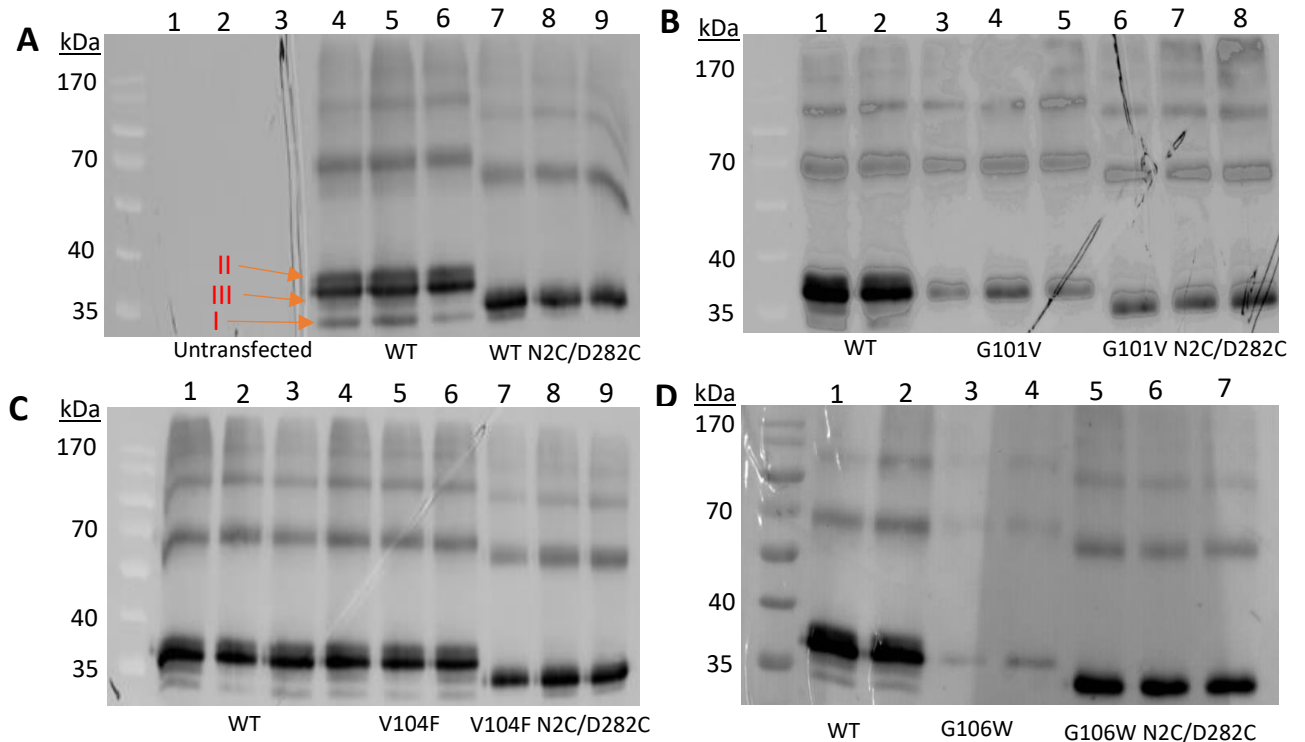


**Figure 3.9- ECL fluorescent image western blot images of various mutant rhodopsin proteins.** Images of western blot membrane treated with Enhanced Chemiluminescence reagents. All of the membranes show three repeats of three different samples (post photobleaching) and a prestained ladder sequence in the first lane. Blot A shows Untransfected cell proteins, WT rhodopsin and WT rhodopsin in N2C/D282C background (from left to right). Blot B shows WT rhodopsin, Rho G101V and G101V N2C/D282C. Blot C shows WT rhodopsin, Rho V104F and V104F N2C/D282C. Blot D shows WT rhodopsin, Rho G106W and G106W N2C/D282C. WT and RP mutants show glycoforms of rhodopsin; I- nonglycosylated species, II- major species containing initial N-glycan (GlcNAc<sub>3</sub>Man<sub>3</sub>GlcNAc<sub>2</sub>), III- trimming intermediate (Reeves *et al.*, 2002).

There is very little difference between the lowest bands displayed in each western blot in the figure above, however the three lanes that contain the relevant RP rhodopsin mutants in the N2C/D282C background are noticeably, albeit slightly, lower than the lanes containing WT rhodopsin or RP rhodopsin mutants (G101V, V104F and G106W). The size of the native rhodopsin protein, estimated from the western blots, appears to be in the region of 35 to 40 kDa, most likely sitting in the middle at about 37 kDa. This is for the WT and non-repaired RP mutant samples only as all of the repaired RP mutant sample bands are lower sitting at around 35 kDa, along with dimer (species II) and trimer (species III) rhodopsin glycoforms highlighted in Figure 3.9 part A. The trimming intermediate refers to the conversion of Man<sub>9</sub>GlcNAc<sub>2</sub> to Man<sub>5</sub>GlcNAc<sub>2</sub> (Reeves *et al.*, 2002). This drop in protein size is due to the substituted Asn2 residues that create said bridge removing a site for glycosylation. The true

molecular mass of rhodopsin when glycosylated and bound retinal is 42 kDa (Takeda and Haga, 2005), however runs through a PAGE gel faster with SDS bound so appears smaller.

#### 3.4.2 Purification of RP mutant pigments

The western blots below in Figure 3.10 show rhodopsin samples that have been purified by Rho-1D4 immunoaffinity chromatography (Methods- Immunoaffinity Purification). Both the PBS and BTP washing steps contain virtually no rhodopsin signal. The photobleached mutant samples look no different to those shown in Figure 3.8. All of the following lanes representing elutions, both low and high salt, contain rhodopsin. The largest amount of rhodopsin can be seen in low salt elution 2 (red arrow), each of which was considered to be pure with a 280 nm to 500 nm ratio of 1.6:1.

The larger transfections and purification process have been repeated when necessary to produce enough protein to perform experiments in replicate (see Methods- Transfections).

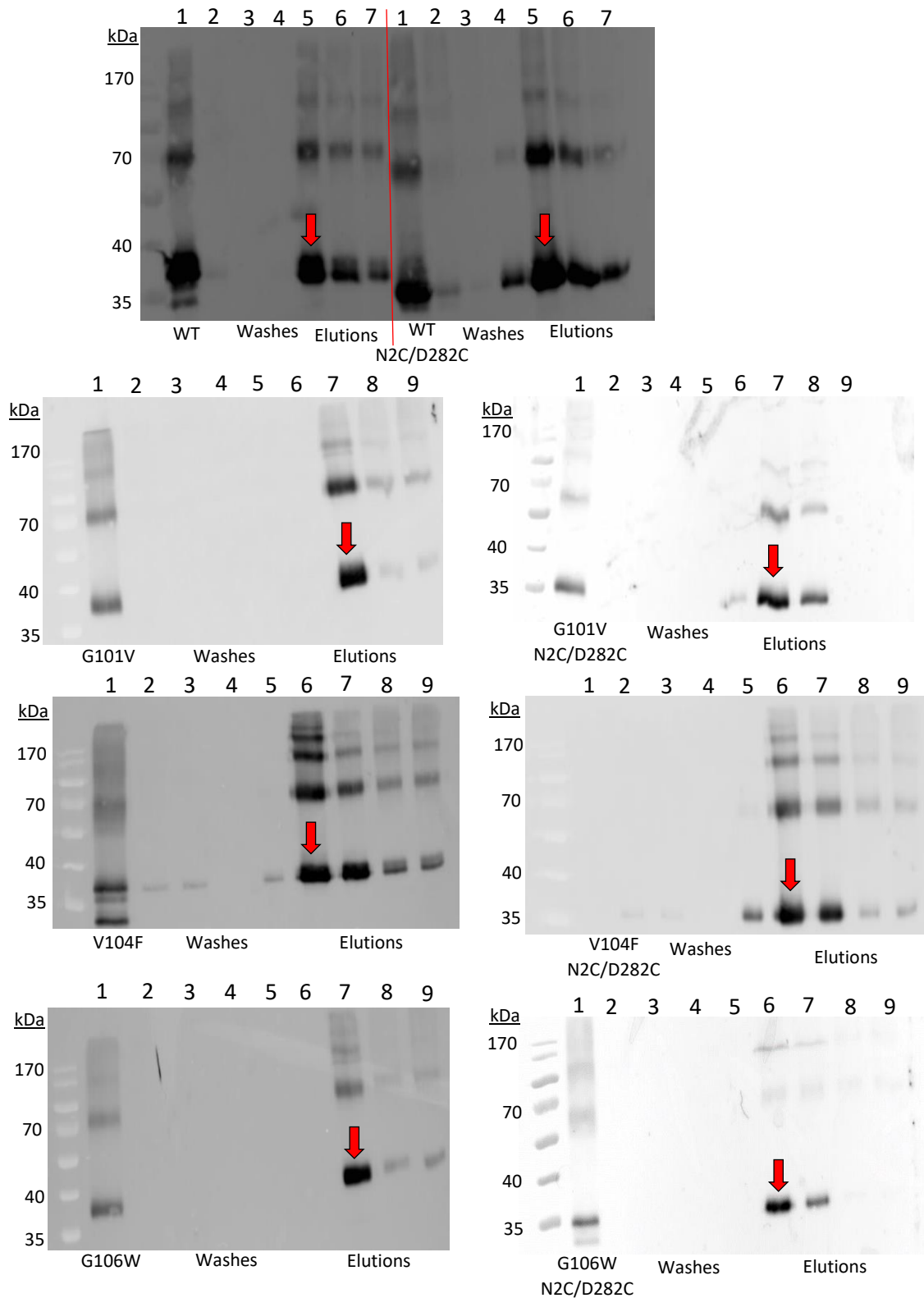


**Figure 3.10- Western blot images of purified RP mutant rhodopsin proteins.** Images of western blot membranes treated with Enhanced Chemiluminescence reagents. Membranes show a prestained ladder sequence in the first lane, followed by a rhodopsin sample. Moving towards the right, the lanes contain the protein flow-through, PBS and BTP washes followed by both low and high salt elutions. The second low salt elutions (highlighted by a red arrow) are considered pure.

### 3.4.3 Photobleaching properties of the immunoaffinity purified rhodopsin mutants

The non-photobleached rhodopsin sample (blue line) has a peak visible absorbance at 500 nm that upon exposure to light (30 seconds, >495 nm as described in Methods- Rhodopsin Photobleaching) is converted to a 380 nm form (orange line). Following the addition of sulphuric acid this peak then moves to about 440 nm (grey line), consistent with the Retinylidene-Schiff base at Lysine residue 296 becoming protonated. All of the spectra in Figure 3.11 below show a similar photobleaching profile. There is little difference between the non-repaired mutant proteins (WT, G101V, V104F and G106W) and their repaired counterparts (with the N2C/D282C background mutation). The only two that do not fit this trend are G101V and G106W, as these two were rescued with 9-*cis*-retinal to obtain a usable amount of pure protein (refer back to Figure 3.6 to see how rescuing increased G101V and G106W protein expression) and unbound retinal has remained within the eluted solution after washing. G101V and G106W show a partial 440 nm peak, whereas G101V N2C/D282C and G106W N2C/D282C have photobleached correctly. The clearly visible absorbance peak at 440 nm shows that the retinal molecules present are attached to the rhodopsin protein via a protonated Schiff base.

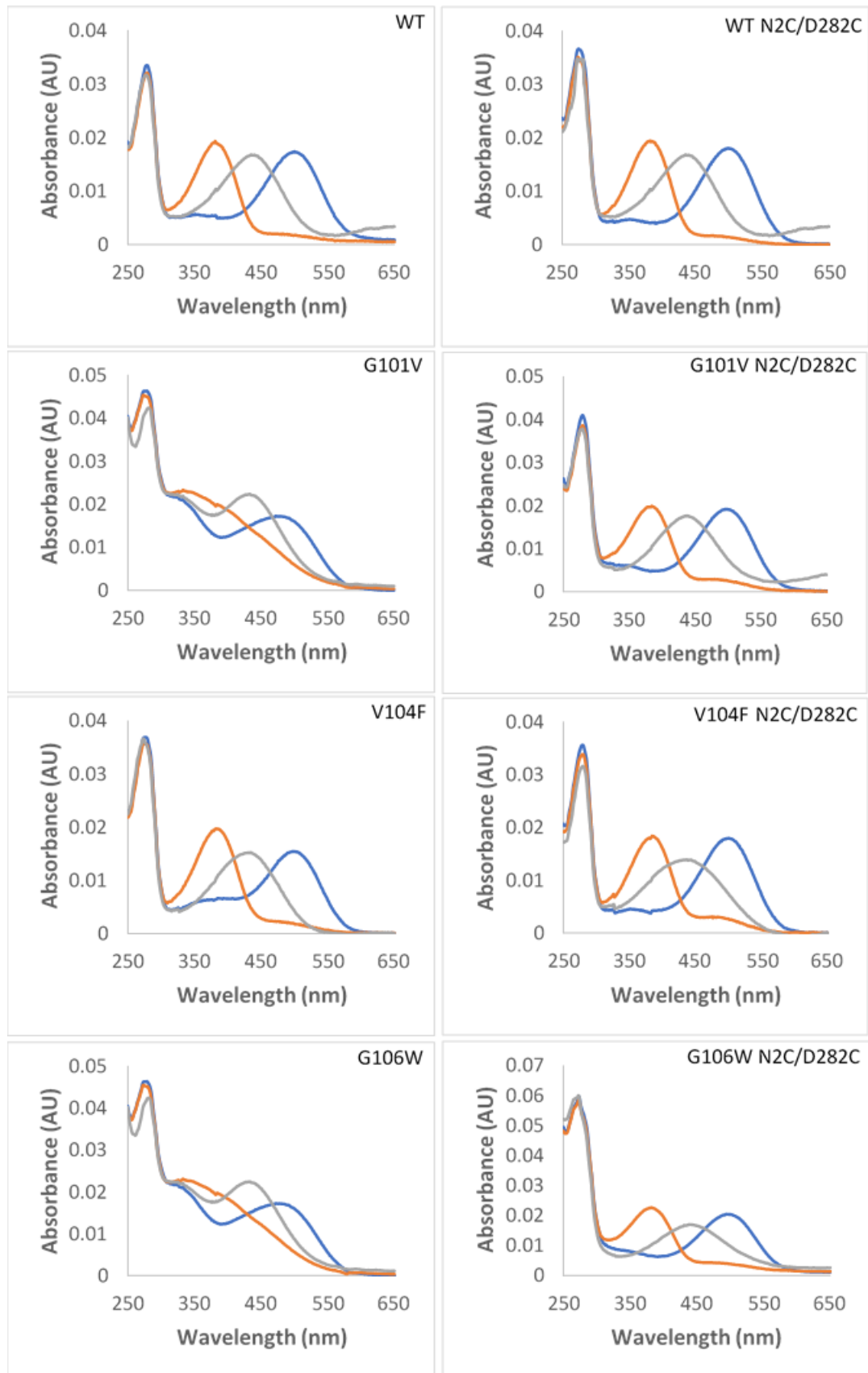


**Figure 3.11- UV-visible absorbance spectrographs for dark state, photobleached and acidified RP mutant pigments.** Purified pigments (blue line) were exposed to light for 30 seconds (orange line) before being acidified using  $H_2SO_4$  (grey line), all measured using a UV-visible spectrophotometer.

#### 3.4.4 Photoactivation of purified ADRP pigments followed by observation of Meta-II Decay

Active State Decay (or Meta-II Decay) experiments were carried out in order to monitor the stability of the active Meta-II form of rhodopsin (Methods- Rhodopsin Meta-II Decay). Exposure to light results in the isomerisation of 9-*cis*-retinal to all-*trans* retinal and activates rhodopsin to the Meta-II state. The protonated Schiff base releases the unstable all-*trans* retinal from the Meta-II rhodopsin, and the resulting energy excites nearby tryptophan molecules and increases their fluorescence. This increase in fluorescence rises to a plateau where the Meta-II rhodopsin molecules have fully decayed. The data was fitted with a single component exponential decay curve, which was used to calculate the half-life of the protein sample.

From Figure 3.12 it is observed that the Meta-II decay kinetics fit well to a single component. Upon photoactivation the rhodopsin Meta-II species decays with a half-life of 13.4 minutes. WT N2C/D282C Meta-II decays similarly to WT Meta-II with a half-life of 13.6 minutes. WT and WT N2C/D282C decay curves reach a plateau after about 60 minutes under these conditions. G101V and G101V N2C/D282C Meta-II species have average half-lives of 4.7 minutes and 9.3 minutes respectively. V104F and V104F N2C/D282C Meta-II species are similar to WT (and to each other) at 8.3 minutes and 9.7 minutes respectively. G106W and G106W N2C/D282C Meta-II products have half-lives of 8.7 minutes and 11.3 minutes, respectively. WT Meta-II is the most stable, with both V104F and G106W being less stable and G101V being the least stable.

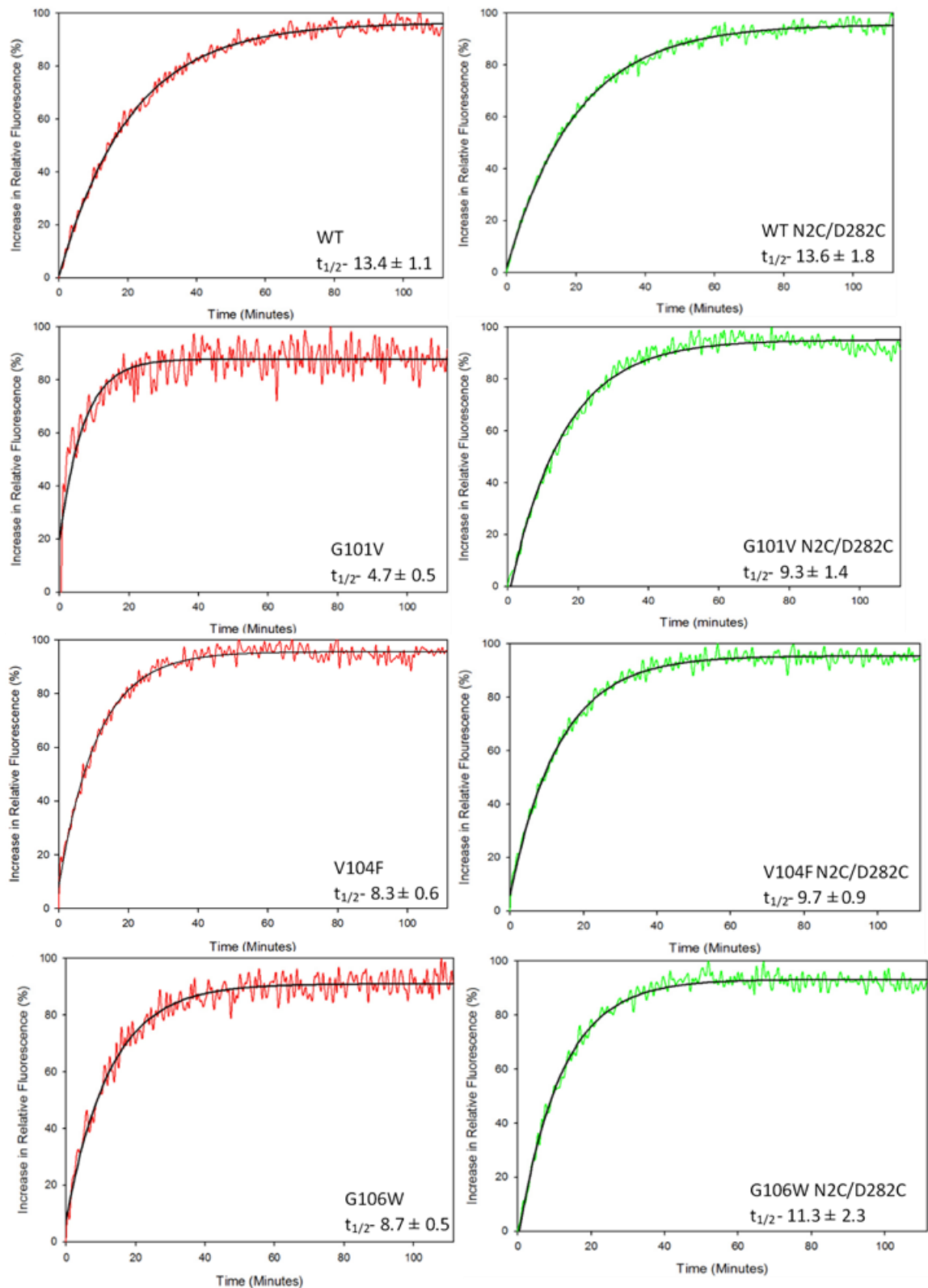


**Figure 3.12- Active State/Meta-II Decay curves.** Single component Meta-II decay curves of WT rhodopsin, RP mutant rhodopsin and RP mutant rhodopsin in the N2C/D282C background. Decay curves ( $n=3$ ) fluorescence increase measured over the course of two hours, emission wavelength 250 nm and excitation wavelength 380 nm. Half-lives (minutes) calculated using SigmaPlot software. Non-repaired rhodopsin sample are shown in red whilst repaired rhodopsin samples are green.

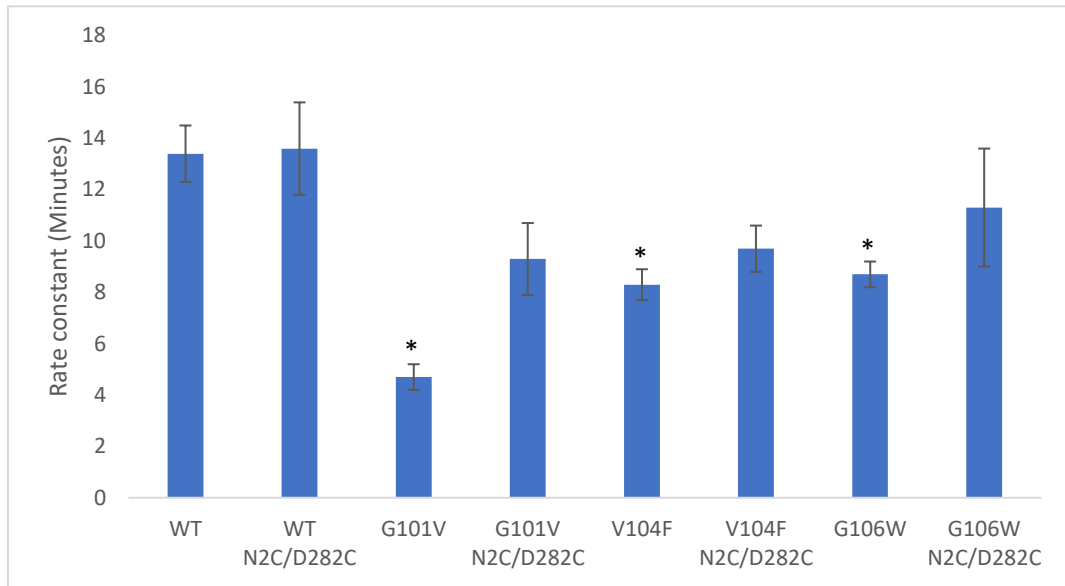


**Figure 3.13- Active State/Meta-II Decay Rate constants.** Half-lives of rhodopsin RP mutants pigments along with their repaired counterparts (N2C/D282C), with WT control for comparison and error bars. \*-  $p < 0.05$  for  $t_{1/2}$  values compared against WT  $t_{1/2}$ .

The data shown in Figure 3.13 highlights that the rhodopsin RP mutant pigments have Meta-II decay half-lives that are significantly different to that of WT rhodopsin. Whereas the repaired RP mutant pigments (and WT N2C/D282C) are not significantly different, with all repaired pigments potentially having a half-life between 10 and 12 minutes.

### 3.4.5 Thermal Stability of Rhodopsin RP mutant pigments

The thermostability of rhodopsin and its mutants can be measured by monitoring the amount of 500 nm pigment at elevated temperatures as a function of time. Measurements are recorded using a spectrophotometer set to measure the sample's absorbance every five minutes for the first hour, before being changed to measure every 30 minutes for the next 24 hours at a temperature of 55 °C (Methods- Rhodopsin Thermal Stability). The absorbance at 500 nm was plotted as a function of time. The data was normalised and fitted with a single component exponential decay function (Figures 3.14 to 3.17). Due to the increased thermostability half-lives of the N2C/D282C variants, theoretical endpoints (shown by the dotted lines in Figures 3.14 and 3.15) have been used to simulate an absorbance of zero. From this endpoint, SigmaPlot has created a curve to fit this using a small data set. However, the results are comparable to published data (Opefi *et al.*, 2013).

WT rhodopsin has a half-life of around 80 minutes at 55 °C under the conditions used (Methods- Thermal Stability). Over time there is a decrease in absorbance at 500 nm and an increase at 380 nm. WT N2C/D282C decays with a longer half-life of 192 minutes (Figure 3.14). For G101V and G101V N2C/D282C, their clear differences in pigment thermostability are evident. G101V has a half-life of three minutes, whereas the G101V N2C/D282C pigment has a half-life of 67 minutes. For G101V rhodopsin there is no pigment remaining after the first ten minutes at 55 °C, yet for G101V N2C/D282C there is pigment remaining after 400 minutes has passed (Figure 3.15). For V104F, half-life of 68 minutes, and V104F N2C/D282C, half-life of 161 minutes, have thermostabilities that are similar to that of WT. However, the half-lives of these pigments do differ with V104F N2C/D282C being much more stable at 55 °C than V104F in the WT rhodopsin background (Figure 3.16). G106W, like G101V, decays rapidly at high temperatures and has a half-life of just one minute (Figure 3.17). The presence of the N2C/D282C disulphide bridge confers enhanced thermal stability in comparison to the same RP mutation in the WT rhodopsin background, increasing half-lives by 22-fold for G101V-G101V N2C/D282C and 2.5-fold for V104F-V104F N2C/D282C.

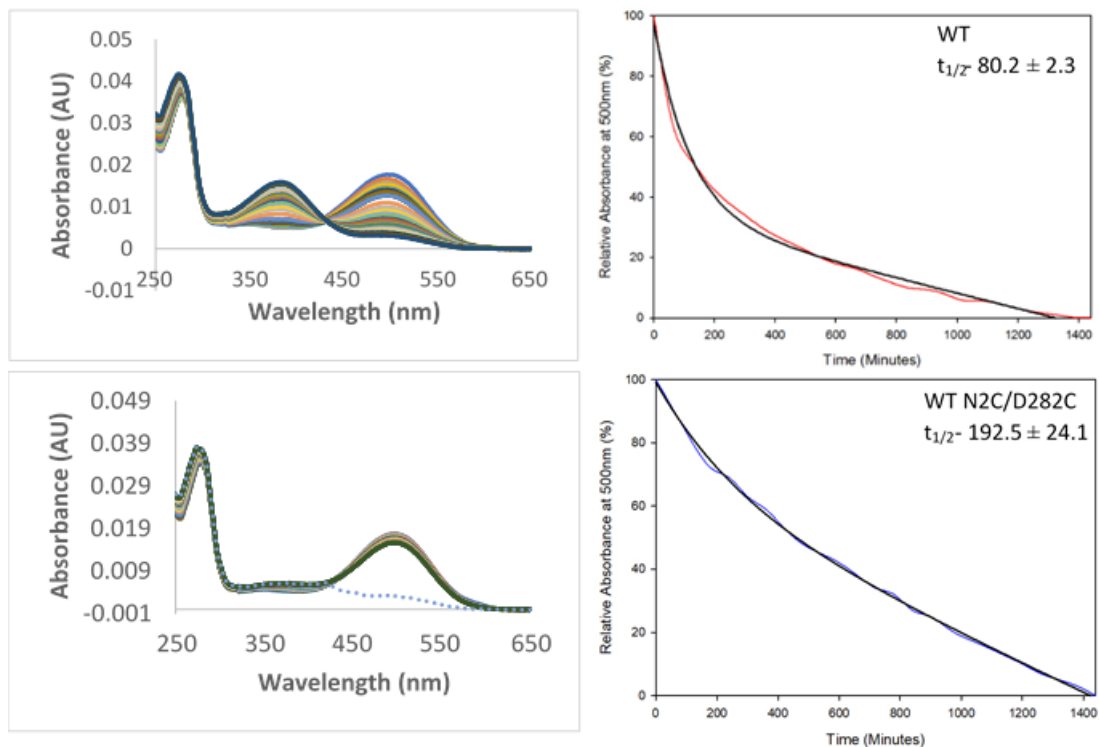


**Figure 3.14- WT Rhodopsin Thermal Decay plots.** Thermal Decay curves measured using a spectrophotometer, set to 55 °C (Methods- Rhodopsin Thermal Stability). Readings were taken every five minutes for the first hour, followed by every 30 minutes for the next 24 hours (n=3, spectrograph colours represent different time points). The data was normalised before being plotted. Decay curves were plotted and fitted using in SigmaPlot. Curve fitted data was used to calculate rhodopsin pigment half-life (minutes) from absorbance at 500 nm (black line).

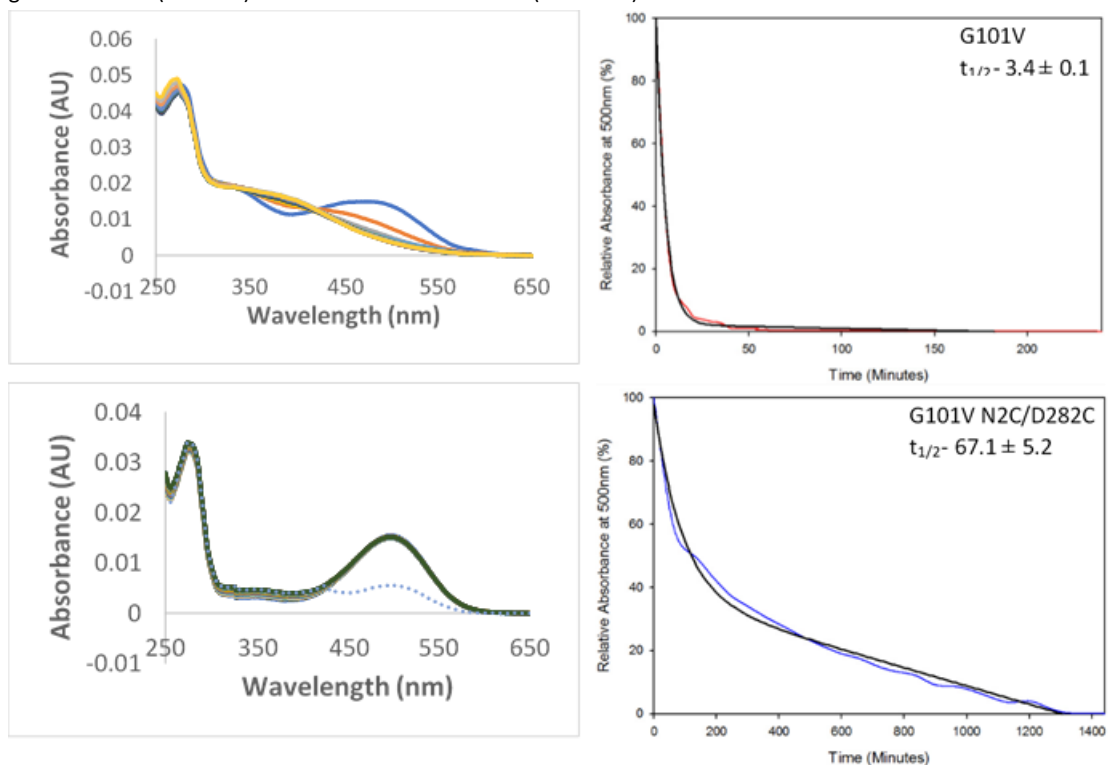


**Figure 3.15- G101V Non-repaired and repaired mutant Rhodopsin Thermal Decay plots.** Thermal Decay curves measured using a spectrophotometer, set to 55 °C (Methods- Rhodopsin Thermal Stability). Readings were taken every five minutes for the first hour, followed by every 30 minutes for the next 24 hours (n=3, spectrograph colours represent different time points). The data was normalised before being plotted. Decay curves were plotted and fitted using in SigmaPlot. Curve fitted data was used to calculate rhodopsin pigment half-life (minutes) from absorbance at 500 nm (black line).

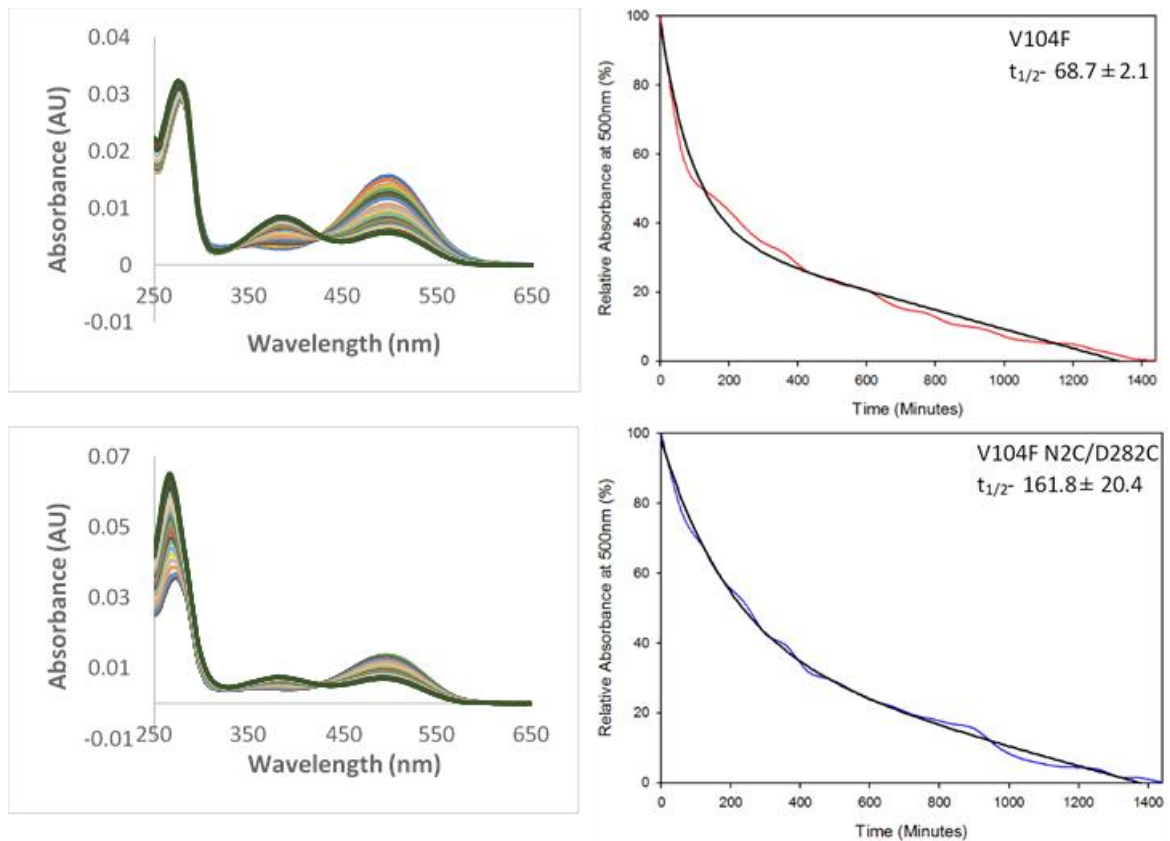


**Figure 3.16- V104F Non-repaired and repaired mutant Rhodopsin Thermal Decay plots.** Thermal Decay curves measured using a spectrophotometer, set to 55 °C (Methods- Thermal Stability). Readings were taken every five minutes for the first hour, followed by every 30 minutes for the next 24 hours (n=3, spectrograph colours represent different time points). The data was normalised before being plotted. Decay curves were plotted and fitted using in SigmaPlot. Curve fitted data was used to calculate rhodopsin pigment half-life (minutes) from absorbance at 500 nm (black line).

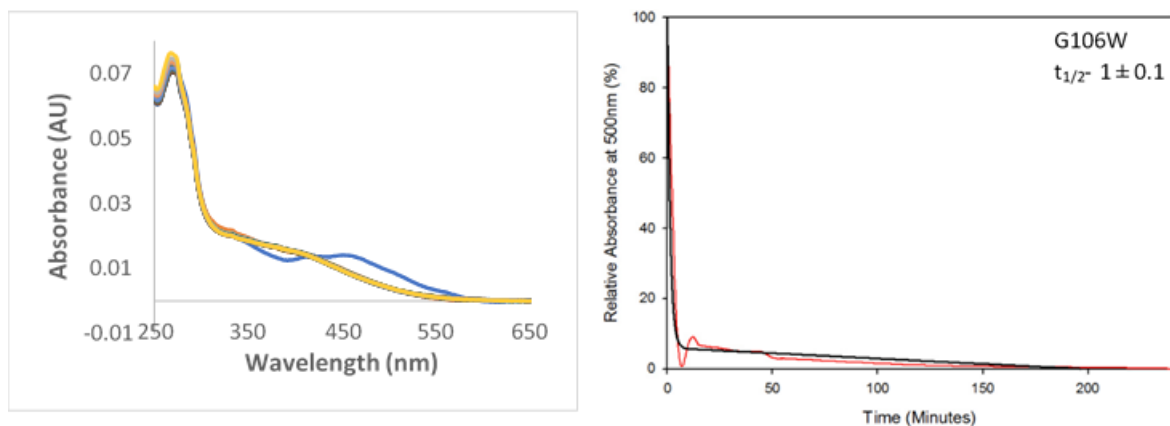


**Figure 3.17- G106W Non-repaired mutant Rhodopsin Thermal Decay plots.** Thermal Decay curves measured using a spectrophotometer, set to 55 °C (Methods- Thermal Stability). Readings were taken every five minutes an hour (n=3, spectrograph colours represent different time points). The data was normalised before being plotted. Decay curves were plotted and fitted using in SigmaPlot. Curve fitted data was used to calculate rhodopsin pigment half-life (minutes) from absorbance at 500 nm (black line).

#### **4. Discussion**

Rhodopsin is a photosensitive GPCR that mediates vision in response to dim light. The rhodopsin gene is a genetic hotspot for the majority of adRP cases (Bravo-Gil *et al.*, 2017). Mutations in rhodopsin are located throughout the length of the receptor and they have been classified into groups (classes 1 to 7) on the basis of phenotype (Mendes *et al.*, 2005).

Three rhodopsin adRP mutants have been the focus of this project: G101V, V104F and G106W. These amino acid residues are located in or near extracellular loop 1 (ECL 1) of rhodopsin. This region is in close contact with the N-terminal cap of rhodopsin, a structure that was previously implicated in the folding, structure and function of rhodopsin (Opefi *et al.*, 2013). The overall aim of this project was to examine the importance of ECL 1 as a docking point for the N-terminal cap. In order to answer this question the recombinant expression, thermal stability, photoactivation and light activated state (Meta-II) stability were measured. These results could provide an insight into the molecular mechanism of pathogenesis and provide clues into the fundamental role of ECL 1 in the receptor folding and stability. Disulphide bridge mediated repair (N2C/D282C) and pharmacological chaperone rescue (9-*cis*-retinal) were used in an attempt to investigate reporter expression/folding and to obtain the mutant rhodopsin pigments for further biophysical characterisation. Similar methods have proved successful in other investigations with other rhodopsin RP mutants; such as V209M (valine to Methionine), F220C (phenylalanine to Cysteine), P23H (Proline to Histidine) and P267L (Proline to Leucine) (Gragg and Park, 2018, Ploier *et al.*, 2016).

For this project, recombinant HEK 293 GnT1<sup>-</sup> cells were transfected with a pMT4 plasmid carrying the mutant rhodopsin genes (see Methods- Transfections). Difference spectra were calculated from UV-visible absorbance spectroscopy data in order to establish relative expression levels of each mutant. These mutant pigments were then purified using Rho-1D4 Sepharose resin for their characterisation.

#### **4.1 Recombinant expression of rhodopsin mutants located in Extracellular Loop 1 (ECL 1)**

Looking back at Figures 3.6 and 3.7 in the results section, we can clearly see that using either 9-*cis*-retinal for pharmacological chaperone rescue or inserting a N2C/D282C bond for disulphide bridge mediated repair gives a significant increase in the pigment expression of two RP mutants; G101V and G106W. Both of these mutants have greater pigment production levels when said methods are used independently but have very little additive effect when used together (at least for G106W). However WT and V104F rhodopsin pigments do not respond positively to either method as their non-rescued and non-repaired pigments have the greatest expression levels. The trends visible in these results tend to show that repaired pigments have higher expression levels than their non-repaired counterparts, rescued pigments have higher expression levels than only non-rescued non-repaired counterparts and there does not seem to be any additive effect from using both methods together. These trends agree with what has been found in previous studies as pharmacological chaperone rescue using 9-*cis*-retinal corrects the folding of a misfolded protein molecule and stabilises it, as well as reducing the misfolded protein's cytotoxic effects (Bernier *et al.*, 2004, Krebs *et al.*, 2010). 9-*cis*-retinal is also thought to help reduce protein aggregation and enhance translocation via the secretory pathway (Mendes and Cheetham, 2008). Whilst disulphide bridge mediated repair has been found to not interfere with protein activation (Standfuss *et al.*, 2008). Disulphide bridge mediated repair has been noted to cause slight reductions in rhodopsin pigment expression levels, most likely because it is still a mutation so will have some effect on pigment production (Reeves *et al.*, 2013). Expression levels from rescued pigments are reduced, possibly due to the severity of the RP mutations or due to the efficiency of pharmacological chaperone rescue, but DMSO has been found to have cytotoxic effects on embryonic cells in particular (HEK cells used for this project) (Pal *et al.*, 2012). This means that fewer cells are able to express the mutant pigments, leading to lower concentrations. However the cytotoxicity effect is overlooked if the pigment is rescued by retinal treatment involving DMSO (Figures 3.6 and 3.7, WT & V104F compared to G101V & G106W).

## 4.2 Thermal stability of rhodopsin mutants in ECL 1

RP rhodopsin mutant pigments have reduced thermal stability properties when compared to WT rhodopsin, yet the presence of the N2C/D282C disulphide bridge has been well recorded to show an increase in rhodopsin pigment thermal stability (Maeda *et al.*, 2014). This trend applies to all of the RP mutant pigments (as well as WT rhodopsin). G101V is very unstable at high temperatures but once repaired has similar stability to WT (Figure 3.15). Little is known about this mutation, with most studies stating that G101V is a class II mutation and causes an RP phenotype (Wan *et al.*, 2019), so this characteristic is a potential new property. V104F is comparable to WT and is stable at high temperatures once repaired (Figure 3.16). Again, not much is known about this mutation, but studies have been conducted about a similar mutation, V104I (Valine to Isoleucine). V104I is classified as a benign mutation and does not result in an RP phenotype (phenotypically silent) (Macke *et al.*, 1993, Wan *et al.*, 2019). However, these results show that V104F might not be completely silent and may result in a mild RP phenotype as stability characteristics are similar (but slightly lower) than WT. When G106W is exposed to high temperatures, the protein falls apart with a very short half-life (Figure 3.17). This result also seems to form a trend as a similar mutation, G106R (Glycine to Arginine), is unstable and causes a severe RP phenotype (Fishman *et al.*, 1992). Possible reasons for this RP mutant's instability could be due to G106W interfering with the binding area for retinal (Tryptophan amino acid protruding into the cleft in between the transmembrane helices) or maybe due to the mutation affecting an essential disulphide bridge (Wan *et al.*, 2019). The disulphide bridge between Cysteine 110 and Cysteine 187 is conserved in vertebrates and if interfered with can result in a defective rhodopsin molecule and unusual "rod dark adaptation kinetics", which can result in a greater amount of retinal damage from light in a shorter period of time (Bareil *et al.*, 1999). From Figures 3.14 to 3.17, there appears to be a trend as the RP mutants in the N2C/D282C background have increased thermal stability half-lives when compared to the non-repaired RP mutants. G101V N2C/D282C mutant pigment has a half-life 22-fold greater than that of the G101V mutant pigment and V104F N2C/D282C & WT N2C/D282C mutant pigments have half-lives 2.5-fold greater than V104F and WT pigments

respectively. These trends agree with results found in previous studies (Xie *et al.*, 2003; Opefi *et al.*, 2013) in the context that a disulphide bridge can increase the rhodopsin pigment thermal stability when a RP mutation is also present. For the thermal decay graphs (Figures 3.14 to 3.16, not 3.17) fixed endpoints were extrapolated from the non-repaired RP mutant (and WT) graphs. This is due to the length of time needed to reach completion. An alternative is to carry out a partial thermal decay followed by photobleaching the pigment sample to reach the end point. However, the 500 nm absorbance peak will not fully reach zero as there is always a retinal shoulder contribution.

#### **4.3 Dark state spectral properties of mutant pigments and their photoconversion to the active state (Metarhodopsin II)**

WT, V104F and their repaired counterparts show very similar spectral properties and photoconversion to the Meta-II active state (Results- Figure 3.11). It can also be noted that their expression levels (Results- Figures 3.6 & 3.7) and thermal stabilities (Results- Figures 3.14 & 3.16) are similar. However, G101V and G106W show somewhat unusual dark state spectral properties, partly due these samples being rescued, and excess 9-*cis*-retinal remaining within the sample solution after the purification process. Yet this over-saturation of retinal did not have any effect on the pigment's photoconversion to the Meta-II state and only shows an increased peak at 360 nm of the dark spectra, as shown in Figure 3.11 for G101V and G106W (Jastrzebska *et al.*, 2009). However the spectra for RP mutants G101V and G106W show some resistance to photobleaching, meaning that the mutant rhodopsin pigments have not been fully converted to the 440 nm species (Kaushal and Khorana, 1994; Krebs *et al.*, 2010). This could be due to rapid photoconversion to the intermediate states (Meta-I and Meta-II rhodopsin) as well as the fast decay of the Meta-II state and release of all-*trans* retinal prior to pigment acidification (Resek *et al.*, 1993; Opefi *et al.*, 2013). The presence of the disulphide bridge did not hinder the repaired WT and V104F RP pigments activation in any way (Standfuss *et al.*, 2008) and corrected the abnormal bleaching spectra for G101V and G106W.

#### **4.4 Stability of the active state of RP mutants located in ECL 1**

WT and WT N2C/D282C show very similar active state stability characteristics in Figure 3.12 and are the most stable rhodopsin pigments in the active state. The RP mutants show a trend as the repaired protein variants are more stable in the active state and possess a longer half-life than their non-repaired versions. V104F and G106W have similar active state stabilities to each other yet G101V has a significantly shorter half-life than the other two RP mutants. Repaired V104F and G106W have slightly longer half-lives but G101V N2C/D282C has a half-life twice as long as non-repaired G101V. Each rhodopsin pigment Meta-II decay functions (WT, RP mutants and RP mutant in N2C/D282C background) are single component. These results agree with those that have been found previously (Xie *et al.*, 2003) and these RP mutants can perform the photoactivation cascade, but have accelerated levels of decay once in the active state (Resek *et al.*, 1993; Heck *et al.*, 2003) perhaps due to an interfered Cys110-Cys187 disulphide bridge (Aguilà *et al.*, 2020; Woods and Pfeffer, 2020). A trend emerges as the half-lives for the repaired rhodopsin pigments are longer than those for their respective non-repaired counterparts, indicating that the presence of the N2C/D282C disulphide bridge improves Meta-II state rhodopsin stability (Figure 3.13) (Opefi *et al.*, 2013).

#### **4.5 Use of PyMol to investigate the basic structural perturbations in these mutants**

Analysing the protein structure should give us a greater depth of knowledge into understanding how the mutant proteins behave. Using the amino acid sequence and the computer software program PyMol, we can visualise the changes that substituting one amino acid for another could have. Starting with the disulphide bridge (N2C/D282C in purple), we can see how replacing the Asparagine and Aspartic Acid residues with Cysteine drastically increases their proximity to each other and forms a disulphide bridge to anchor the amino tail to ECL 3 (represented by dashed lines in Figure 4.1).

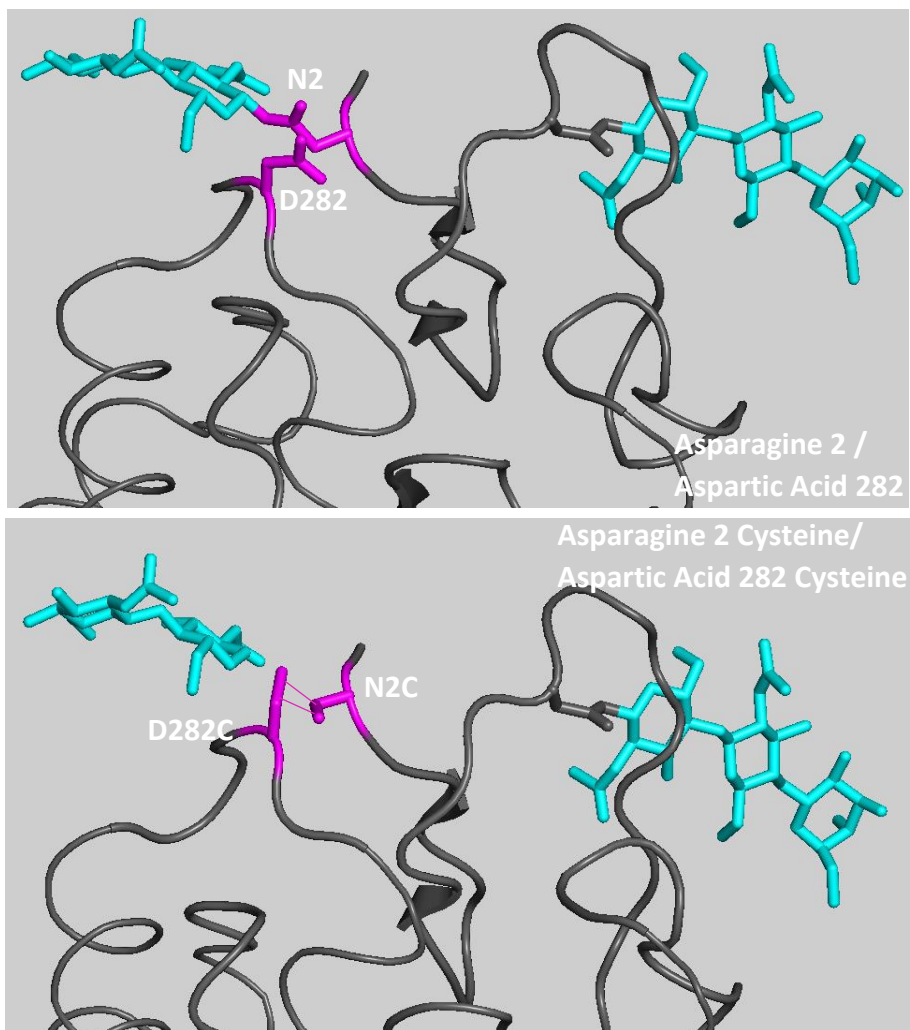


**Figure 4.1- Rhodopsin N2C/D282C protein structure.** PyMol was used to create a three-dimensional rhodopsin protein structure showing both the non-mutated (top) and mutated (bottom) areas in purple with the purple lines representing the disulphide bridge. This disulphide bridge then allows the N-terminus to bind tightly to ECL 3 and increase structural stability. Blue regions are carbohydrates at glycosylation sites. N2C removes a glycosylation sites, therefore the carbohydrate is no longer attached.

The same has been done with G101V, V104F and G106W, although there are several different orientations in which the mutated residues can take. Some of the orientations have fewer interactions than others, these are being deemed the 'best' positions and are used in Figure 4.2 below (all other positions are shown in the Appendix). In G101V, the Glycine residue is simple and does not have any protruding side branches that can interfere with other parts of the protein molecule. However, when this is replaced by Valine, there is likely to be interactions with residues 27 and 29. These interactions show that the mutated residue cannot exist in that location without causing issues for a different part of the protein. In Figure 4.2 G101V is shown in red along with its orbital of interactions, there are

many interactions due to the protruding branches of Valine. V104F (in green) has a larger orbital around Valine but when replaced with Phenylalanine there is an overwhelming number of interactions with surrounding amino acids such as residues 27, 102 and 105. But in a couple of positions Phenylalanine does not interfere with any other residues, however the mutated residue is sticking out of the molecule so may cause issues with protein translocation to the cell surface or when situated in the cell's plasma membrane. G106W (in blue) is very similar to G101V as Glycine has no external branches that could interfere with other protein residues. But when substituted for Tryptophan, there are multiple interactions for each possible position, meaning there is no theoretical unhindered orientation. Most negative interactions seem to be with similar residues as stated before, as well as residues 24 and 107. The Tryptophan residues, no matter the position, always seems to stick into the protein molecule (and potentially the binding cleft for the retinal chromophore). Combining these PyMol observations with the fact that G101V and G106W are the least stable pigments, it is reasonable to presume that the residues somewhat protrude into the retinal binding cleft and interfere with rhodopsin pigment formation. This is backed up by their photobleaching properties and similar effects found in ECL 2 (which acts as a cap above the retinal binding cleft).

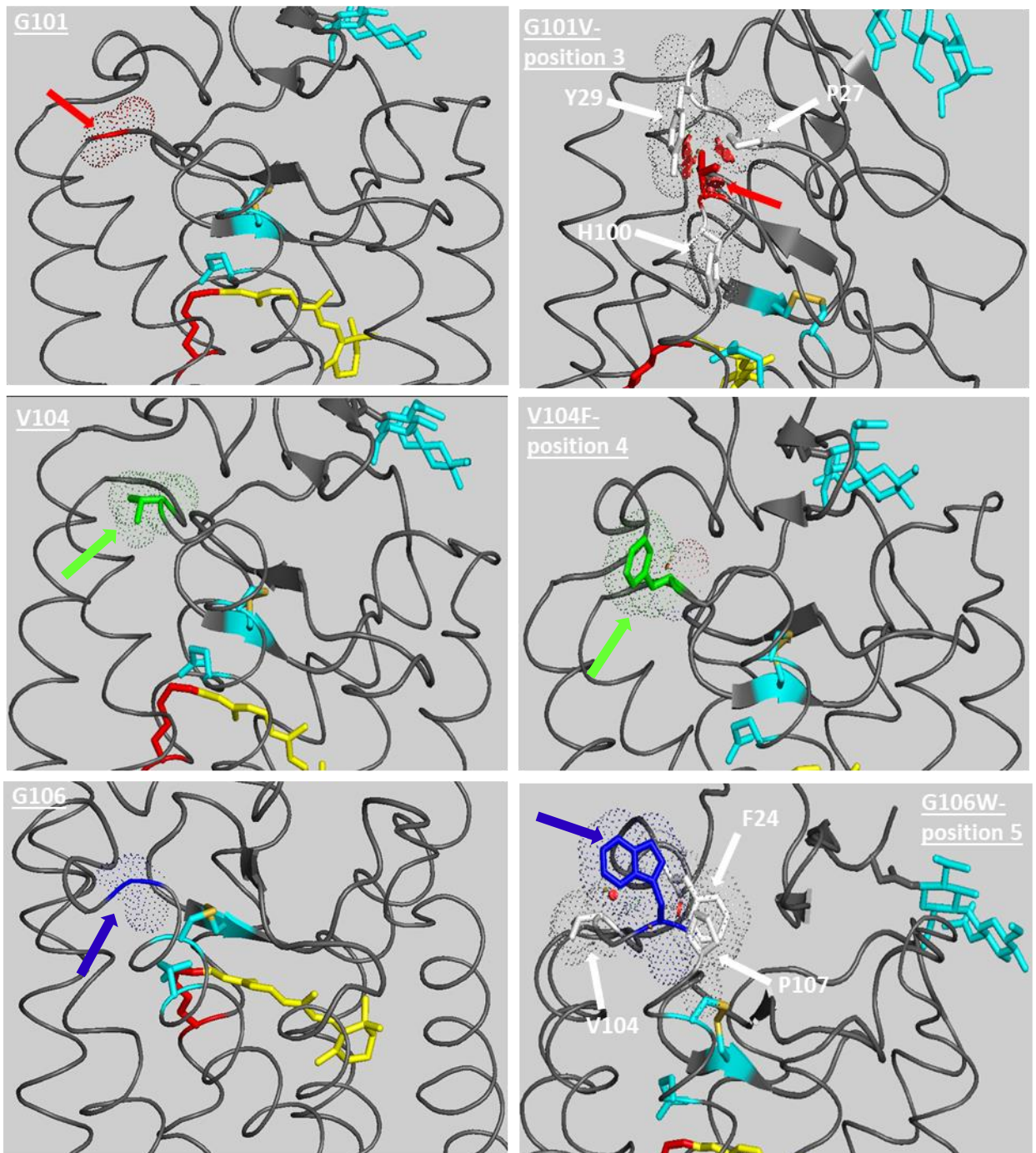


**Figure 4.2- Mutant Rhodopsin protein structures.** PyMol was used to create three-dimensional rhodopsin protein structures containing their normal amino acid sequence (images on the left) and the mutated amino acid residues (images on the right). Images contain the area in which the amino acid can have interactions and any negative interferences with other parts of the protein are highlighted by red circles and interacting residues labelled in white. All images on the right show the 'best' residue positions with the least amount of negative interactions. RP mutations highlighted by coloured arrows: G101 & G101V are red, V104 & V104F are green and G106 & G106W are blue.

Combining these PyMol images with the other results, we can start see why G101V and G106W are much more unstable than V104F, but we can also understand why WT is superior to all of the mutants and how the N2C/D282C disulphide bridge can be formed by close proximity Cysteine residues.

#### 4.6 Explanatory model for the role of ECL 1 in structure and pathology

In terms of the three rhodopsin RP mutations we can conclude that (using these results and other investigations); G101V and G106W pigments, but not V104F pigment, are rescued by the introduction of retinal during the folding process and repaired in the N2C/D282C background. The most logical rationale behind these observations is that the presence of the G101V and G106W RP mutations prevent the N-terminal cap of rhodopsin from correctly docking with ECL 3 and engaging with the ECL 1 loop, resulting in the destabilisation of the rhodopsin helical bundle (Opefi *et al.*, 2013). However, if retinal is present during rhodopsin pigment folding then the helical bundle becomes stabilised upon retinal binding. On the other hand, mutated residue protrusions into the retinal binding pocket can weaken interactions between the rod opsin apoprotein and retinal ligand (Woods and Pfeffer, 2020). In the case of the N2C/D282C background RP mutants, if the N2C/D282C disulphide bridge forms during the folding of the rod opsin apoprotein, the N-terminal cap becomes more tightly associated with the ECL 1 loop (and therefore all of the other ECL loops) to stabilise rhodopsin's helical structure (as ECL 1 coordinates the position of transmembrane helices 2 & 3) (Opefi *et al.*, 2013). Although, these ECL 1 mutations may affect the Cys110-Cys187 disulphide bridge reducing stability, signal transmission and receptor dynamics (Woods and Pfeffer, 2020). We can assume that the extracellular regions of rhodopsin have essentially been free to evolve a compact structure with unique thermostability and activation of rhodopsin in dark conditions. From this, the N-terminal cap is integral but not completely necessary for the formation of the helical bundle (as pharmacological chaperone rescue by retinal can improve pigment stability) (Krebs *et al.*, 2010). Instead, it is likely that the N-terminal cap only adds to the overall stability of the rhodopsin pigment structure. Looking at disulphide bridge mediated repair, the N2C/D282C bond appears to restore pigment folding, indicating that the N-terminal cap stabilises the helical structure and maintains the correct shape of the ligand-binding site. The N2C/D282C bond also improves pigment thermal stability, improves Meta-II decay kinetics and shows photobleaching characteristics similar to WT rhodopsin. This suggests that the N2C/D282C bridge binds the N-terminal cap to ECL 3 (and has interactions with ECL 1 & 2) and

improves stability and photoactivation but is not absolute (in the case of V104F, there is little difference between non-repaired and repaired pigment characteristics except for thermostability) (Opefi *et al.*, 2013). Yet mutations in the ECLs can affect N-terminal cap function by reducing local interactions. This in turn can alter transmembrane helical orientation and reduce pigment stability (Ahuja *et al.*, 2009).

A comparison of both pharmacological chaperone rescue and disulphide bridge mediated repair highlights rhodopsin's N-terminal cap as critical for maintaining stability and function, whilst the RP mutants present in ECL 1 hinder said structural stability. All of the mechanisms are displayed in Figure 4.3.

The Endoplasmic reticulum Associated protein Degradation system (ERAD) is a cellular pathway that targets misfolded proteins in the ER for destruction by the proteasomes (Groisman *et al.*, 2006). The ERAD system begins by identifying misfolded proteins, possibly by hydrophobic protein regions being exposed or unprocessed glycans. If the misfolded proteins cannot be restored to their native conformation, then these proteins are translocated to the cytoplasm for polyubiquitination by E1, 2 and 3 ligase enzymes. The ubiquitination allows the misfolded proteins to be recognised by the 19S proteasome caps, leading to the degradation of the proteins (Olzmann *et al.*, 2013). In rod photoreceptor cells, calnexin is used to identify misfolded or mutated rhodopsin pigments (Kosmaoglou *et al.*, 2009). However the process is more tightly regulated than in other mammalian cells as over-regulation can result in restorable pigment proteins (e.g. those that can be rescued by the binding of retinal) are degraded prematurely and under-regulation leads to misfolded protein aggregation and can inhibit proteasome function (Kosmaoglou *et al.*, 2009).

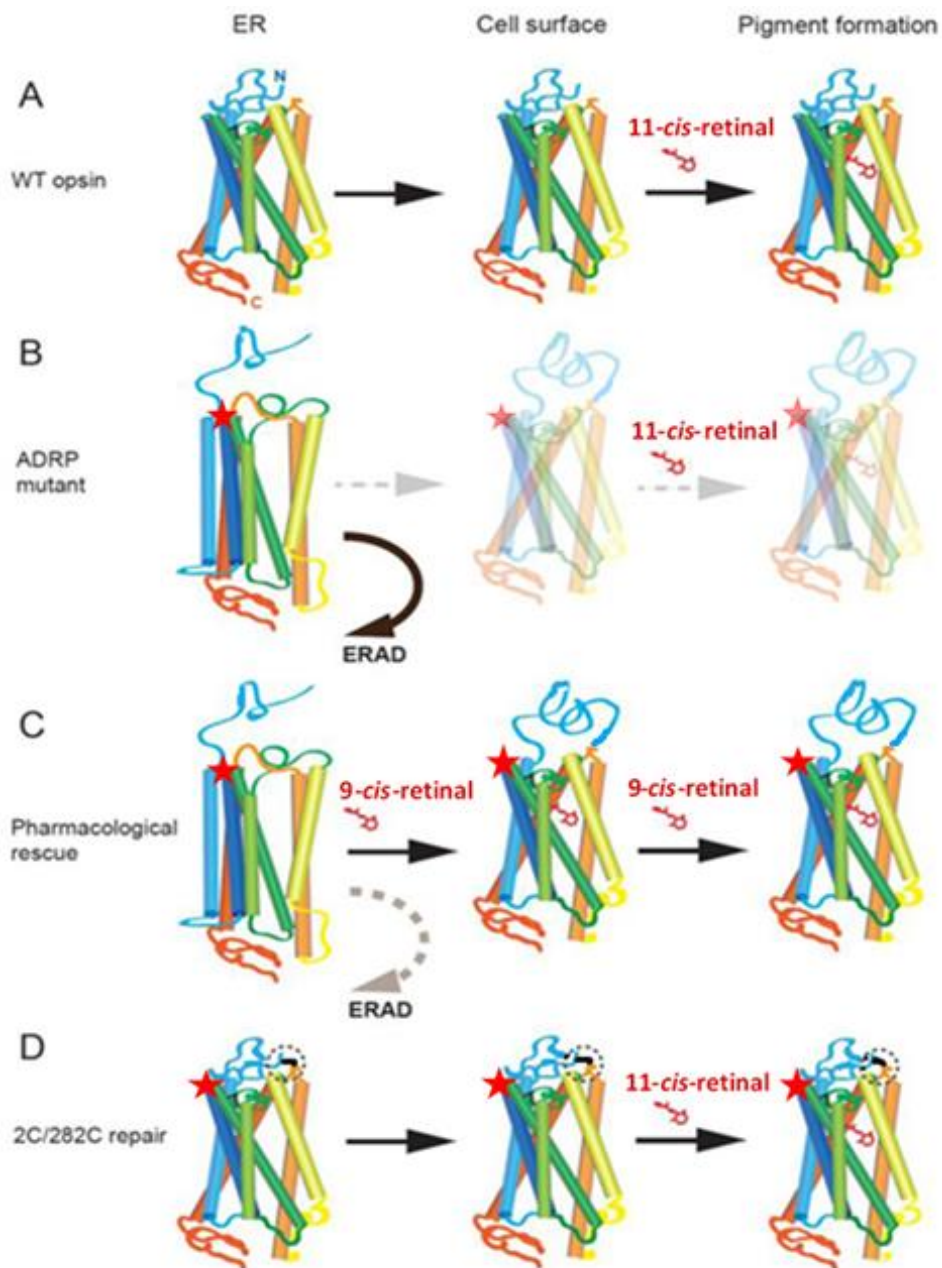


**Figure 4.3- Schematic illustration of pharmacological chaperone rescue and disulphide bridge mediated repair for adRP rhodopsin mutants.** A) WT rod opsin apoprotein folds correctly in the Endoplasmic Reticulum (ER) before translocation to the cell surface and binding with retinal to form rhodopsin. B) adRP mutants fail to fold correctly and N-terminal cap does not bind to extracellular region, resulting in destabilised helical bundle structure and mutant apoprotein is destroyed by ER associated protein degradation (ERAD). C) Pharmacological chaperone rescue with 9-*cis*-retinal corrects folding of RP mutant and translocates to cell surface. Formed pigments still exhibit unstable properties. D) Disulphide bridge mediated repair fixes N-terminal cap in place, restoring correct protein folding and characteristics. RP mutations in ECL 1 indicated by red star. Adapted from Opefi *et al.*, 2013.

As the RP mutant pigments in this study are all less stable than WT rhodopsin, it is not out of the question to assume that they, at least, produce a moderate RP phenotype. Their relation to RP disease progression is especially insightful. The production of defective or misfolded proteins is a normal part of cellular metabolism, however a large accumulation of these RP pigments can lead to ER stress and

cell death (Rao and Bredesen, 2004). Some misfolded pigments may be able to evade the ER degradation systems and escape to the rod outer segments (ROS). The presence of said defective pigments in the ROS is serious as they can begin to aggregate together and lead to mechanical cell breakdown via the destabilisation of the rod cell membrane (Haeri and Knox, 2012). This may be due to the release of retinal following isomerisation from 11-*cis* to the all-*trans* state once photobleached. In individuals without RP, the retinal molecules would be replaced by non-isomerised versions naturally present, but in those affected by RP the mutant pigments may exhibit cytotoxic properties (Galy *et al.*, 2005). G101V, V104F and G106W RP pigments have not been specifically tested to see their relevant retinal degeneration characteristics, but severe RP mutants have (for example P23H). However, in humans it has been observed that retinal degeneration is independent to light exposure (i.e. it still occurs in the dark) and RP progression tends to start in the lower retina as it is exposed to brighter amounts of light (Cideciyan *et al.*, 1998; Tam and Moritz, 2007). It should also be noted that ECL 1 has been found to bind/influence ligands, alter transmembrane helical positioning and partially coordinate activation (Wheatley *et al.*, 2012; Barwell *et al.*, 2012). This could somewhat explain why some mutations (e.g. V104F) are unaffected by pharmacological chaperone rescue.

The main limitations of this study are the number of repeats and time. This study conducted triplicate repeats of each experiment with each protein variant to gain concordant averages, and that can be deemed representative. However a greater number of repeats would be beneficial as more concordant results would give averages that are more representative of what happens in nature.

Additional experiments that could be carried out to further this study include; Transducin Assays, Arrestin binding and alternative chromophores for chaperone rescue. A Transducin Assay can be used to analysis and investigate the rhodopsin protein's activation pathway. This experiment will record the relative increase in Tryptophan fluorescence of transducin, when transducin binds to activated rhodopsin (Metarhodopsin II) in the presence of GTP. Mutant pigment results can be compared to a WT rhodopsin control to see how effective the activation pathway is. Previous studies have found that

some mutations are similar to WT activation levels (E134Q at 98% (Franke *et al.*, 1992)) whereas others have drastically reduced activation levels (T234V at 40% and R153Q at 8%). Along with this, it has been identified that correct protein folding and Meta-II stability are needed for the signal transduction pathway to function properly (Ernst *et al.*, 1995, Franke *et al.*, 1992). In addition to this, the binding properties with arrestin could also be investigated. During the deactivation pathway, arrestin binds to activated rhodopsin in order to dephosphorylate and regenerate the protein (Okawa and Sampath, 2007). However, some RP mutants have been found to activate and remain bound to arrestin after 11-*cis*-retinal has dissociated. This results in rhodopsin being unable to dephosphorylate and therefore cannot regenerate (Bareil *et al.*, 1999, Mendes *et al.*, 2005). A third additional experiment is to replace 9-*cis*-retinal with a different chaperone molecule, 5,8-epoxy-13-*cis* retinoic acid (13-*cis*-5,8-ERA). 13-*cis*-5,8-ERA was virtually screened and discovered to fit the retinal binding pocket relatively well, as well as having a high structural similarity to 11-*cis*-retinal (Ortega and Jastrzebska, 2019). This chaperone has been found to mitigate ER retention whilst also promoting plasma membrane localisation, and has worked well with T17M, P23H and E181K (inserted Lysine creates another salt bridge and increases chaperone-protein stability) (Behnen *et al.*, 2018). Cellular localisation of the mutant proteins could also be looked at by adding a Green Fluorescent Protein (GFP) sequence to the mutant DNA and observe where the expressed protein tends to accumulate within the cell via fluorescent microscopy (Saliba *et al.*, 2002, Sung *et al.*, 1991).

Future studies could be based upon this one but investigate other mutations on different residues located within ECL 1 such as Y102, F103 and F105 or look at different mutations to the residues used in this study, V104K for example. Alternatively, a future study could look at other class II mutations in different parts of the rhodopsin protein. Both of these can then be compared with this study to see if mutations in the same region or mutations of the same class have similar characteristics, stability issues and resulting RP phenotypes. A third future study could revolve around the RP mutant pigment structures, and how the inserted mutations affect the entire protein. This would involve (energy) minimisation, a computational technique used to determine the orientation of atoms, molecules or

ions based on their minimum energy states, according to an algorithm (Jensen, 2017). The process would require the proteins to be solvated (generally in water) and neutralised (e.g. with sodium ions) before being minimised by the steepest decent method to remove amino acid residue clashes. The minimised protein sequences can then be visualised using PyMol. In simplistic terms, this method is used to show which position(s) the amino acid residues are most likely to exist in. Root mean square deviations can also be used to prove these. Software packages such as GROMACS or Amber 9 can be used for this (Ge *et al.*, 2012; Qadah and Jamal, 2019). Ultimately, all of these additional and future studies have one common goal, to better our knowledge about RP and its developmental mechanism(s) and one day result in a treatment that may not cure the disease, but at least slow down the progression of blindness to give the individual a few more years of sight and normality.

In conclusion, this study can say that the presence of an additional disulphide bridge between inserted Cysteines at residues 2 and 282 increases the thermal stability of rhodopsin and that the pharmacological chaperone 9-*cis*-retinal can help rescue misfolded proteins and increase mutant RP pigment expression. In regards to the mutations of this study, G101V and G106W are both thermally unstable yet have good Meta-II stability levels. Whilst V104F has both good thermal stability and Meta-II stability, but all mutants have lower stability and activation levels when compared to WT rhodopsin. The main contributions are the characteristics identified for G101V and V104F as they, at most, have only been mentioned or their properties theorised in other studies but have not been investigated. This study agrees with the hypothesis that the presence of the ECL 1 RP mutations cause the N-terminal cap to fail to associate productively with the docking region in ECL 3. This in turn results in a destabilised rhodopsin pigment with reduced expression levels, thermal instability, altered photobleaching properties and reduced active state kinetics. However more research is needed on the mutations in this study, as well as other mutants that are not yet characterised, in order to understand in greater depth the mechanism(s) of rhodopsin malfunction in Retinitis Pigmentosa (Wan *et al.*, 2019).

## 5. References

- AGUILÀ, M., BELLINGHAM, J., ATHANASIOU, D., BEVILACQUA, D., DURAN, Y., MASWOOD, R., PARFITT, D. A., IWAWAKI, T., SPYROU, G. & SMITH, A. J. 2020. AAV-mediated ERdj5 overexpression protects against P23H rhodopsin toxicity. *Human Molecular Genetics*.
- AHUJA, A. K., DORN, J., CASPI, A., MCMAHON, M., DAGNELIE, G., STANGA, P., HUMAYUN, M., GREENBERG, R. & GROUP, A. I. S. 2011. Blind subjects implanted with the Argus II retinal prosthesis are able to improve performance in a spatial-motor task. *British Journal of Ophthalmology*, 95, 539-543.
- AHUJA, S., HORNAK, V., YAN, E. C., SYRETT, N., GONCALVES, J. A., HIRSHFELD, A., ZILIOX, M., SAKMAR, T. P., SHEVES, M. & REEVES, P. J. 2009. Helix movement is coupled to displacement of the second extracellular loop in rhodopsin activation. *Nature structural & molecular biology*, 16, 168.
- ATHANASIOU, D., AGUILA, M., BELLINGHAM, J., LI, W., MCCULLEY, C., REEVES, P. J. & CHEETHAM, M. E. 2018. The molecular and cellular basis of rhodopsin retinitis pigmentosa reveals potential strategies for therapy. *Progress in retinal and eye research*, 62, 1-23.
- AVERY, R. L., PIERAMICI, D. J., RABENA, M. D., CASTELLARIN, A. A., MA'AN, A. N. & GIUST, M. J. 2006. Intravitreal bevacizumab (Avastin) for neovascular age-related macular degeneration. *Ophthalmology*, 113, 363-372. e5.
- BAILEY, A. J. 1987. Structure, function and ageing of the collagens of the eye. *Eye*, 1, 175-183.
- BAREIL, C., HAMEL, C., PALLARÈS-RUIZ, N., ARNAUD, B., DEMAILLE, J. & CLAUSTRÉS, M. 1999. Molecular analysis of the rhodopsin gene in southern France: identification of the first duplication responsible for retinitis pigmentosa, c. 998^ 999ins4. *Ophthalmic genetics*, 20, 173-182.
- BASSUK, A. G., ZHENG, A., LI, Y., TSANG, S. H. & MAHAJAN, V. B. 2016. Precision medicine: genetic repair of retinitis pigmentosa in patient-derived stem cells. *Scientific reports*, 6, 19969.
- BEHNEN, P., FELLINE, A., COMITATO, A., DI SALVO, M. T., RAIMONDI, F., GULATI, S., KAHREMAN, S., PALCZEWSKI, K., MARIGO, V. & FANELLI, F. 2018. A small chaperone improves folding and routing of rhodopsin mutants linked to inherited blindness. *Iscience*, 4, 1-19.
- BELTRAN, W. A., CIDECIYAN, A. V., LEWIN, A. S., IWABE, S., KHANNA, H., SUMAROKA, A., CHIODO, V. A., FAJARDO, D. S., ROMÁN, A. J. & DENG, W.-T. 2012. Gene therapy rescues photoreceptor blindness in dogs and paves the way for treating human X-linked retinitis pigmentosa. *Proceedings of the National Academy of Sciences*, 109, 2132-2137.
- BERNIER, V., BICHET, D. G. & BOUVIER, M. 2004. Pharmacological chaperone action on G-protein-coupled receptors. *Current opinion in pharmacology*, 4, 528-533.
- BOURNE, R. R., FLAXMAN, S. R., BRAITHWAITE, T., CICINELLI, M. V., DAS, A., JONAS, J. B., KEEFFE, J., KEMPEN, J. H., LEASHER, J. & LIMBURG, H. 2017. Magnitude, temporal trends, and projections of the global prevalence of blindness and distance and near vision impairment: a systematic review and meta-analysis. *The Lancet Global Health*, 5, e888-e897.
- BRAVO-GIL, N., GONZÁLEZ-DEL POZO, M., MARTÍN-SÁNCHEZ, M., MÉNDEZ-VIDAL, C., RODRÍGUEZ-DE LA RÚA, E., BORREGO, S. & ANTIÑOLO, G. 2017. Unravelling the genetic basis of simplex Retinitis Pigmentosa cases. *Scientific reports*, 7, 41937.
- BROWN, C. N., GREEN, B. D., THOMPSON, R. B., DEN HOLLANDER, A. I. & LENGYEL, I. 2019. Metabolomics and age-related macular degeneration. *Metabolites*, 9, 4.
- BURACZYNSKA, M., WU, W., FUJITA, R., BURACZYNSKA, K., PHELPS, E., ANDRÉASSON, S., BENNETT, J., BIRCH, D. G., FISHMAN, G. A. & HOFFMAN, D. R. 1997. Spectrum of mutations in the RPGR gene that are identified in 20% of families with X-linked retinitis pigmentosa. *The American Journal of Human Genetics*, 61, 1287-1292.
- BURKE, J., PETTITT, J. M., HUMPHRIS, D. & GLEESON, P. A. 1994. Medial-Golgi retention of N-acetylglucosaminyltransferase I. Contribution from all domains of the enzyme. *Journal of Biological Chemistry*, 269, 12049-12059.

- CAMPOCHIARO, P. A. & MIR, T. A. 2018. The mechanism of cone cell death in retinitis pigmentosa. *Progress in retinal and eye research*, 62, 24-37.
- CHABRE, M. & DETERRE, P. 1989. Molecular mechanism of visual transduction. *EJB Reviews 1989*. Springer.
- CHEN, Y., CHEN, Y., JASTRZEBSKA, B., GOLCZAK, M., GULATI, S., TANG, H., SEIBEL, W., LI, X., JIN, H. & HAN, Y. 2018. A novel small molecule chaperone of rod opsin and its potential therapy for retinal degeneration. *Nature communications*, 9, 1-18.
- CHEREZOV, V., ROSENBAUM, D. M., HANSON, M. A., RASMUSSEN, S. G., THIAN, F. S., KOBILKA, T. S., CHOI, H.-J., KUHN, P., WEIS, W. I. & KOBILKA, B. K. 2007. High-resolution crystal structure of an engineered human  $\beta$ 2-adrenergic G protein-coupled receptor. *science*, 318, 1258-1265.
- CHOW, A. Y., CHOW, V. Y., PACKO, K. H., POLLACK, J. S., PEYMAN, G. A. & SCHUCHARD, R. 2004. The artificial silicon retina microchip for the treatment of vision loss from retinitis pigmentosa. *Archives of ophthalmology*, 122, 460-469.
- CIDECIYAN, A. V., HOOD, D. C., HUANG, Y., BANIN, E., LI, Z.-Y., STONE, E. M., MILAM, A. H. & JACOBSON, S. G. 1998. Disease sequence from mutant rhodopsin allele to rod and cone photoreceptor degeneration in man. *Proceedings of the National Academy of Sciences*, 95, 7103-7108.
- DAIGER, S., SULLIVAN, L. & BOWNE, S. 2013. Genes and mutations causing retinitis pigmentosa. *Clinical genetics*, 84, 132-141.
- DAIGER, S. P., BOWNE, S. J. & SULLIVAN, L. S. 2007. Perspective on genes and mutations causing retinitis pigmentosa. *Archives of ophthalmology*, 125, 151-158.
- DELAYE, M. & TARDIEU, A. 1983. Short-range order of crystallin proteins accounts for eye lens transparency. *Nature*, 302, 415-417.
- DOBYNS, W. B. 2006. The pattern of inheritance of X-linked traits is not dominant or recessive, just X-linked. *Acta Paediatrica*, 95, 11-15.
- EDWARDS, T. L., COTTRIAL, C. L., XUE, K., SIMUNOVIC, M. P., RAMSDEN, J. D., ZRENNER, E. & MACLAREN, R. E. 2018. Assessment of the electronic retinal implant alpha AMS in restoring vision to blind patients with end-stage retinitis pigmentosa. *Ophthalmology*, 125, 432-443.
- ERNST, O. P., HOFMANN, K. P. & SAKMAR, T. P. 1995. Characterization of Rhodopsin Mutants That Bind Transducin but Fail to Induce GTP Nucleotide Uptake CLASSIFICATION OF MUTANT PIGMENTS BY FLUORESCENCE, NUCLEOTIDE RELEASE, AND FLASH-INDUCED LIGHT-SCATTERING ASSAYS. *Journal of Biological Chemistry*, 270, 10580-10586.
- FEUDA, R., HAMILTON, S. C., MCINERNEY, J. O. & PISANI, D. 2012. Metazoan opsin evolution reveals a simple route to animal vision. *Proceedings of the National Academy of Sciences*, 109, 18868-18872.
- FISHMAN, G. A., STONE, E. M., GILBERT, L. D. & SHEFFIELD, V. C. 1992. Ocular findings associated with a rhodopsin gene codon 106 mutation: glycine-to-arginine change in autosomal dominant retinitis pigmentosa. *Archives of ophthalmology*, 110, 646-653.
- FLAXMAN, S. R., BOURNE, R. R., RESNIKOFF, S., ACKLAND, P., BRAITHWAITE, T., CICINELLI, M. V., DAS, A., JONAS, J. B., KEEFFE, J. & KEMPEN, J. H. 2017. Global causes of blindness and distance vision impairment 1990–2020: a systematic review and meta-analysis. *The Lancet Global Health*, 5, e1221-e1234.
- FRANKE, R., SAKMAR, T., GRAHAM, R. & KHORANA, H. 1992. Structure and function in rhodopsin. Studies of the interaction between the rhodopsin cytoplasmic domain and transducin. *Journal of Biological Chemistry*, 267, 14767-14774.
- FRANKE, R., SAKMAR, T., OPRIAN, D. & KHORANA, H. 1988. A single amino acid substitution in rhodopsin (lysine 248----leucine) prevents activation of transducin. *Journal of Biological Chemistry*, 263, 2119-2122.
- FUNG, A. E., LALWANI, G. A., ROSENFELD, P. J., DUBOVY, S. R., MICHELS, S., FEUER, W. J., PULIAFITO, C. A., DAVIS, J. L., FLYNN JR, H. W. & ESQUIABRO, M. 2007. An optical coherence tomography-guided, variable dosing regimen with intravitreal ranibizumab (Lucentis) for neovascular age-related macular degeneration. *American journal of ophthalmology*, 143, 566-583. e2.

- GALY, A., ROUX, M. J., SAHEL, J. A., LÉVEILLARD, T. & GIANGRANDE, A. 2005. Rhodopsin maturation defects induce photoreceptor death by apoptosis: a fly model for RhodopsinPro23His human retinitis pigmentosa. *Human molecular genetics*, 14, 2547-2557.
- GE, Y., WU, J., XIA, Y., YANG, M., XIAO, J. & YU, J. 2012. Molecular dynamics simulation of the complex PBP-2x with drug cefuroxime to explore the drug resistance mechanism of *Streptococcus suis* R61. *PLoS One*, 7, e35941.
- GENENSKY, S. M. 1971. A functional classification system of the visually impaired to replace the legal definition of blindness. *Optometry and Vision Science*, 48, 631-641.
- GRAGG, M. & PARK, P. S.-H. 2018. Misfolded rhodopsin mutants display variable aggregation properties. *Biochimica et Biophysica Acta (BBA)-Molecular Basis of Disease*, 1864, 2938-2948.
- GRAHAM, F. L., HARRISON, T. & WILLIAMS, J. 1978. Defective transforming capacity of adenovirus type 5 host-range mutants. *Virology*, 86, 10-21.
- GRAHAM, F. L., SMILEY, J., RUSSELL, W. & NAIRN, R. 1977. Characteristics of a human cell line transformed by DNA from human adenovirus type 5. *Journal of general virology*, 36, 59-72.
- GREGORY-EVANS, K. & BHATTACHARYA, S. S. 1998. Genetic blindness: current concepts in the pathogenesis of human outer retinal dystrophies. *Trends in Genetics*, 14, 103-108.
- GROISMAN, B., AVEZOV, E. & LEDERKREMER, G. Z. 2006. The E3 Ubiquitin Ligases HRD1 and SCFFbs2 Recognize the Protein Moiety and Sugar Chains, Respectively, of an ER-Associated Degradation Substrate. *Israel journal of chemistry*, 46, 189-196.
- HAERI, M. & KNOX, B. E. 2012. Rhodopsin mutant P23H destabilizes rod photoreceptor disk membranes. *PLoS One*, 7.
- HARTONG, D. T., BERSON, E. L. & DRYJA, T. P. 2006. Retinitis pigmentosa. *The Lancet*, 368, 1795-1809.
- HOUSDEN, B. E. & PERRIMON, N. 2016. Comparing CRISPR and RNAi-based screening technologies. *Nature biotechnology*, 34, 621.
- JASTRZEBSKA, B., GOLCZAK, M., FOTIADIS, D., ENGEL, A. & PALCZEWSKI, K. 2009. Isolation and functional characterization of a stable complex between photoactivated rhodopsin and the G protein, transducin. *The FASEB journal*, 23, 371-381.
- JENSEN, F. 2017. *Introduction to computational chemistry*, John Wiley & Sons.
- JIN, J., JONES, G. J. & CORNWALL, M. C. 1994. Movement of retinal along cone and rod photoreceptors. *Visual neuroscience*, 11, 389-399.
- JIN, M., YUAN, Q., LI, S. & TRAVIS, G. H. 2007. Role of LRAT on the retinoid isomerase activity and membrane association of Rpe65. *Journal of Biological Chemistry*, 282, 20915-20924.
- JOHN, S. K., SMITH, J. E., AGUIRRE, G. D. & MILAM, A. H. 2000. Loss of cone molecular markers in rhodopsin-mutant human retinas with retinitis pigmentosa. *Molecular Vision*, 6, 204.
- KANWAL, S., NISHAT, S., KHAN, M. I., MALIK, S. I. & AKHTAR, K. 2012. Comparative homology modeling of human rhodopsin with several templates of bovine rhodopsin. *African Journal of Biotechnology*, 11, 466-473.
- KAPLAN, H. J., TEZEL, T. H., BERGER, A. S., WOLF, M. L. & DEL PRIORE, L. V. 1997. Human photoreceptor transplantation in retinitis pigmentosa: a safety study. *Archives of Ophthalmology*, 115, 1168-1172.
- KAUSHAL, S. & KHORANA, H. G. 1994. Structure and function in rhodopsin. 7. Point mutations associated with autosomal dominant retinitis pigmentosa. *Biochemistry*, 33, 6121-6128.
- KHANNA, H. 2015. Photoreceptor sensory cilium: traversing the ciliary gate. *Cells*, 4, 674-686.
- KIVELÄ, T. & UUSITALO, M. 1998. Structure, development and function of cytoskeletal elements in non-neuronal cells of the human eye. *Progress in retinal and eye research*, 17, 385-428.
- KLEIN, R. J., ZEISS, C., CHEW, E. Y., TSAI, J.-Y., SACKLER, R. S., HAYNES, C., HENNING, A. K., SANGIOVANNI, J. P., MANE, S. M. & MAYNE, S. T. 2005. Complement factor H polymorphism in age-related macular degeneration. *Science*, 308, 385-389.
- KOBAYASHI, H. & KOHSHIMA, S. 2001. Unique morphology of the human eye and its adaptive meaning: comparative studies on external morphology of the primate eye. *Journal of human evolution*, 40, 419-435.

- KOSMAOGLU, M., KANUGA, N., AGUILÀ, M., GARRIGA, P. & CHEETHAM, M. E. 2009. A dual role for EDEM1 in the processing of rod opsin. *Journal of cell science*, 122, 4465-4472.
- KREBS, M. P., HOLDEN, D. C., JOSHI, P., CLARK III, C. L., LEE, A. H. & KAUSHAL, S. 2010. Molecular mechanisms of rhodopsin retinitis pigmentosa and the efficacy of pharmacological rescue. *Journal of molecular biology*, 395, 1063-1078.
- LESKOV, I. B., KLENCHIN, V. A., HANDY, J. W., WHITLOCK, G. G., GOVARDOVSKII, V. I., BOWNDS, M. D., LAMB, T. D., PUGH JR, E. N. & ARSHAVSKY, V. Y. 2000. The gain of rod phototransduction: reconciliation of biochemical and electrophysiological measurements. *Neuron*, 27, 525-537.
- LI, T., SANDBERG, M. A., PAWLYK, B. S., ROSNER, B., HAYES, K., DRYJA, T. P. & BERSON, E. L. 1998. Effect of vitamin A supplementation on rhodopsin mutants threonine-17→ methionine and proline-347→ serine in transgenic mice and in cell cultures. *Proceedings of the National Academy of Sciences*, 95, 11933-11938.
- MACKE, J. P., DAVENPORT, C. M., JACOBSON, S. G., HENNESSEY, J. C., GONZALEZ-FERNANDEZ, F., CONWAY, B. P., HECKENLIVELY, J., PALMER, R., MAUMENEE, I. H. & SIEVING, P. 1993. Identification of novel rhodopsin mutations responsible for retinitis pigmentosa: implications for the structure and function of rhodopsin. *American journal of human genetics*, 53, 80.
- MACLAREN, R. E., GROPE, M., BARNARD, A. R., COTTRIAL, C. L., TOLMACHOVA, T., SEYMOUR, L., CLARK, K. R., DURING, M. J., CREMERS, F. P. & BLACK, G. C. 2014. Retinal gene therapy in patients with choroideremia: initial findings from a phase 1/2 clinical trial. *The Lancet*, 383, 1129-1137.
- MAEDA, S., SUN, D., SINGHAL, A., FOGGETTA, M., SCHMID, G., STANDFUSS, J., HENNIG, M., DAWSON, R. J., VEPRINTSEV, D. B. & SCHERTLER, G. F. 2014. Crystallization scale preparation of a stable GPCR signaling complex between constitutively active rhodopsin and G-protein. *PLoS One*, 9.
- MENDES, H. F. & CHEETHAM, M. E. 2008. Pharmacological manipulation of gain-of-function and dominant-negative mechanisms in rhodopsin retinitis pigmentosa. *Human molecular genetics*, 17, 3043-3054.
- MENDES, H. F., VAN DER SPUY, J., CHAPPLE, J. P. & CHEETHAM, M. E. 2005. Mechanisms of cell death in rhodopsin retinitis pigmentosa: implications for therapy. *Trends in molecular medicine*, 11, 177-185.
- MERINO, D., DUNCAN, J. L., TIRUVEEDHULA, P. & ROORDA, A. 2011. Observation of cone and rod photoreceptors in normal subjects and patients using a new generation adaptive optics scanning laser ophthalmoscope. *Biomedical optics express*, 2, 2189-2201.
- MEYER, U. A. 1991. Genotype or phenotype: the definition of a pharmacogenetic polymorphism. *Pharmacogenetics and Genomics*, 1, 66-67.
- MOISEYEV, G., CHEN, Y., TAKAHASHI, Y., WU, B. X. & MA, J.-X. 2005. RPE65 is the isomerohydrolase in the retinoid visual cycle. *Proceedings of the National Academy of Sciences*, 102, 12413-12418.
- MORELLO, J.-P., BOUVIER, M., PETÄJÄ-REPO, U. E. & BICHET, D. G. 2000. Pharmacological chaperones: a new twist on receptor folding. *Trends in pharmacological sciences*, 21, 466-469.
- MURADOV, K. G. & ARTEMYEV, N. O. 2000. Loss of the effector function in a transducin- $\alpha$  mutant associated with Nougaret night blindness. *Journal of Biological Chemistry*, 275, 6969-6974.
- OKAWA, H. & SAMPATH, A. P. 2007. Optimization of single-photon response transmission at the rod-to-rod bipolar synapse. *Physiology*, 22, 279-286.
- OLZMANN, J. A., KOPITO, R. R. & CHRISTIANSON, J. C. 2013. The mammalian endoplasmic reticulum-associated degradation system. *Cold Spring Harbor perspectives in biology*, 5, a013185.
- OPEFI, C. A., SOUTH, K., REYNOLDS, C. A., SMITH, S. O. & REEVES, P. J. 2013. Retinitis pigmentosa mutants provide insight into the role of the N-terminal cap in rhodopsin folding, structure, and function. *Journal of Biological Chemistry*, 288, 33912-33926.
- ORTEGA, J. T. & JASTRZEBSKA, B. 2019. The Retinoid and Non-Retinoid Ligands of the Rod Visual G Protein-Coupled Receptor. *International Journal of Molecular Sciences*, 20, 6218.
- PAL, R., MAMIDI, M. K., DAS, A. K. & BHONDE, R. 2012. Diverse effects of dimethyl sulfoxide (DMSO) on the differentiation potential of human embryonic stem cells. *Archives of toxicology*, 86, 651-661.

- PALCZEWSKI, K., KUMASAKA, T., HORI, T., BEHNKE, C. A., MOTOSHIMA, H., FOX, B. A., LE TRONG, I., TELLER, D. C., OKADA, T. & STENKAMP, R. E. 2000. Crystal structure of rhodopsin: AG protein-coupled receptor. *science*, 289, 739-745.
- PLOIER, B., CARO, L. N., MORIZUMI, T., PANDEY, K., PEARRING, J. N., GOREN, M. A., FINNEMANN, S. C., GRAUMANN, J., ARSHAVSKY, V. Y. & DITTMAN, J. S. 2016. Dimerization deficiency of enigmatic retinitis pigmentosa-linked rhodopsin mutants. *Nature communications*, 7, 1-11.
- QADAH, T. & JAMAL, M. S. 2019. Computational Analysis of Protein Structure Changes as a Result of Nondeletion Insertion Mutations in Human  $\beta$ -Globin Gene Suggests Possible Cause of  $\beta$ -Thalassemia. *BioMed Research International*, 2019.
- QUIGLEY, H. A. 1996. Number of people with glaucoma worldwide. *British journal of ophthalmology*, 80, 389-393.
- RAO, R. V. & BREDESEN, D. E. 2004. Misfolded proteins, endoplasmic reticulum stress and neurodegeneration. *Current opinion in cell biology*, 16, 653-662.
- REEVES, P. J., CALLEWAERT, N., CONTRERAS, R. & KHORANA, H. G. 2002. Structure and function in rhodopsin: high-level expression of rhodopsin with restricted and homogeneous N-glycosylation by a tetracycline-inducible N-acetylglucosaminyltransferase I-negative HEK293S stable mammalian cell line. *Proceedings of the National Academy of Sciences*, 99, 13419-13424.
- REEVES, P. J., REYNOLDS, C. A., SMITH, S. O., OPEFI, C. A. & SOUTH, K. 2013. Retinitis Pigmentosa Mutants Provide.
- ROSENBAUM, D. M., RASMUSSEN, S. G. & KOBILKA, B. K. 2009. The structure and function of G-protein-coupled receptors. *Nature*, 459, 356-363.
- ROSENFELD, P. J., BROWN, D. M., HEIER, J. S., BOYER, D. S., KAISER, P. K., CHUNG, C. Y. & KIM, R. Y. 2006. Ranibizumab for neovascular age-related macular degeneration. *New England Journal of Medicine*, 355, 1419-1431.
- SAKMAR, T. P. 2002. Structure of rhodopsin and the superfamily of seven-helical receptors: the same and not the same. *Current opinion in cell biology*, 14, 189-195.
- SALIBA, R. S., MUNRO, P. M., LUTHER, P. J. & CHEETHAM, M. E. 2002. The cellular fate of mutant rhodopsin: quality control, degradation and aggresome formation. *Journal of cell science*, 115, 2907-2918.
- SANDBERG, M. A., ROSNER, B., WEIGEL-DIFRANCO, C., DRYJA, T. P. & BERSON, E. L. 2007. Disease course of patients with X-linked retinitis pigmentosa due to RPGR gene mutations. *Investigative ophthalmology & visual science*, 48, 1298-1304.
- SCHÖBERER, J., VAVRA, U., STADLMANN, J., HAWES, C., MACH, L., STEINKELLNER, H. & STRASSER, R. 2009. Arginine/lysine residues in the cytoplasmic tail promote ER export of plant glycosylation enzymes. *Traffic*, 10, 101-115.
- SEBAG, J. 2004. Anomalous posterior vitreous detachment: a unifying concept in vitreo-retinal disease. *Graefe's archive for clinical and experimental ophthalmology*, 242, 690-698.
- SEKHARAN, S. & MOROKUMA, K. 2011. Why 11-cis-retinal? Why not 7-cis-, 9-cis-, or 13-cis-retinal in the eye? *Journal of the American Chemical Society*, 133, 19052-19055.
- SHICHIDA, Y. & MATSUYAMA, T. 2009. Evolution of opsins and phototransduction. *Philosophical Transactions of the Royal Society B: Biological Sciences*, 364, 2881-2895.
- SHINTANI, K., SHECHTMAN, D. L. & GURWOOD, A. S. 2009. Review and update: current treatment trends for patients with retinitis pigmentosa. *Optometry-Journal of the American Optometric Association*, 80, 384-401.
- STANDFUSS, J., XIE, G., EDWARDS, P. C., BURGHAMMER, M., OPRIAN, D. D. & SCHERTLER, G. F. 2007. Crystal structure of a thermally stable rhodopsin mutant. *Journal of molecular biology*, 372, 1179-1188.
- STANDFUSS, J., ZAITSEVA, E., MAHALINGAM, M. & VOGEL, R. 2008. Structural impact of the E113Q counterion mutation on the activation and deactivation pathways of the G protein-coupled receptor rhodopsin. *Journal of molecular biology*, 380, 145-157.

- STANLEY, P., TANIGUCHI, N. & AEBI, M. 2017. N-glycans. *Essentials of Glycobiology [Internet]. 3rd edition*. Cold Spring Harbor Laboratory Press.
- SUNG, C.-H., SCHNEIDER, B. G., AGARWAL, N., PAPERMASTER, D. S. & NATHANS, J. 1991. Functional heterogeneity of mutant rhodopsins responsible for autosomal dominant retinitis pigmentosa. *Proceedings of the National Academy of Sciences*, 88, 8840-8844.
- SUNG, C. H., DAVENPORT, C. M. & NATHANS, J. 1993. Rhodopsin mutations responsible for autosomal dominant retinitis pigmentosa. Clustering of functional classes along the polypeptide chain. *Journal of Biological Chemistry*, 268, 26645-26649.
- TAKEDA, S. & HAGA, T. 2005. *G protein-coupled receptors: structure, function, and ligand screening*, CRC Press.
- TAM, B. M. & MORITZ, O. L. 2007. Dark rearing rescues P23H rhodopsin-induced retinal degeneration in a transgenic *Xenopus laevis* model of retinitis pigmentosa: a chromophore-dependent mechanism characterized by production of N-terminally truncated mutant rhodopsin. *Journal of Neuroscience*, 27, 9043-9053.
- THOMAS, P. & SMART, T. G. 2005. HEK293 cell line: a vehicle for the expression of recombinant proteins. *Journal of pharmacological and toxicological methods*, 51, 187-200.
- THYLEFORS, B., NÉGREL, A.-D. & PARARAJASEGARAM, R. 1992. Epidemiologic aspects of global blindness prevention. *Current opinion in ophthalmology*, 3, 824-834.
- WALSH, G. & CHARMAN, W. 1988. The effect of pupil centration and diameter on ocular performance. *Vision Research*, 28, 659-665.
- WAN, A., PLACE, E., PIERCE, E. A. & COMANDER, J. 2019. Characterizing variants of unknown significance in rhodopsin: a functional genomics approach. *Human mutation*, 40, 1127-1144.
- XIE, G., GROSS, A. K. & OPRIAN, D. D. 2003. An opsin mutant with increased thermal stability. *Biochemistry*, 42, 1995-2001.
- ZAKERI, B., FIERER, J. O., CELIK, E., CHITTOCK, E. C., SCHWARZ-LINEK, U., MOY, V. T. & HOWARTH, M. 2012. Peptide tag forming a rapid covalent bond to a protein, through engineering a bacterial adhesin. *Proceedings of the National Academy of Sciences*, 109, E690-E697.
- ZHUKOVSKY, E. A., ROBINSON, P. R. & OPRIAN, D. D. 1991. Transducin activation by rhodopsin without a covalent bond to the 11-cis-retinal chromophore. *Science*, 251, 558-560.



## 6.2 MidiPrep yield and UV absorbance properties of purified samples

MidiPrep DNA concentrations and purity data recorded from Nanodrop 1000 Spectrophotometer for each mutant DNA sample produce by MidiPrep (this data is the first set of MidiPreps completed, these were repeated when necessary to ensure sufficient amounts of DNA were prepared). Glycerol stocks were used along with ampicillin growth plates.

<b>Mutant Sample</b>	<b>DNA Concentration (ng/μl)</b>	<b>260/280 Value</b>	<b>260/230 Value</b>
WT	1098.7	1.91	2.32
WT N2C/D282C	1411	1.91	2.32
G101V	1851.1	1.90	2.31
G101V N2C/D282C	1127.3	1.90	2.30
V104F	437	1.87	2.28
V104F N2C/D282C	212.9	1.92	2.27
G106W	621	1.90	2.28
G106W N2C/D282C	651.6	1.91	2.19
pRSV T-ag	862	NA	NA

### 6.3 Rhodopsin pigment expression levels using disulphide bridge mediated repair or pharmacological chaperone rescue with 9-*cis*-retinal

Amount of protein produced by each RP mutant and RP mutant in N2C/D282C background, with a wild type control. The protein production levels have been based upon the difference between normalised dark and light UV-visible spectrophotometer absorbance values, and then adjusted to coincide with the 0.55 ml sample volume.

Mutant	Run 1	Run 2	Run 3	Averages
WT 1	17.6	25.3	25.9	22.9
WT 2	14.3	28.6	27.0	23.3
WT 3	-	30.8	29.7	30.3
G101V 1	2.2	5.5	3.9	3.9
G101V 2	5.0	5.5	3.9	4.8
G101V 3	2.8	0.6	5.0	2.8
G101V N2C/D282C 1	5.0	9.4	8.3	7.5
G101V N2C/D282C 2	3.9	11.6	10.5	8.6
G101V N2C/D282C 3	-	10.5	11.0	10.7
WT 1	16.5	15.4	21.5	17.8
WT 2	13.8	22.6	20.9	19.1
WT 3	22.0	-	16.5	19.3
V104F 1	17.1	16.5	20.9	18.2
V104F 2	12.7	18.2	17.1	16.0
V104F 3	9.4	14.9	15.4	13.2
V104F N2C/D282C 1	15.4	15.4	16.5	15.8
V104F N2C/D282C 2	12.7	12.1	12.7	12.5
V104F N2C/D282C 3	12.1	16.0	15.4	14.5
WT 1	23.1	27.5	25.5	26.2
WT 2	21.5	16.5	21	20.4
WT 3	-	29.2	20	25.6
G106W 1	0.6	2.2	1.5	1.5
G106W 2	1.1	0.6	1.5	1.1
G106W 3	-	2.8	1.0	1.9
G106W N2C/D282C 1	4.4	12.7	13.5	10.6
G106W N2C/D282C 2	6.1	6.1	10	7.7
G106W N2C/D282C 3	6.6	8.3	8.5	8.1

Amount of protein produced by each RP mutant and RP mutant in N2C/D282C background that have been rescued using 9-*cis*-retinal during transfection, with a wild type control. The protein production levels have been based upon the difference between normalised dark and light UV-visible spectrophotometer absorbance values, and then adjusted to coincide with the 0.55ml sample volume.

Mutant (Rescued)	Run 1	Run 2	Run 3	Averages
WT 1	10.5	-	-	10.5
WT 2	11.0	-	-	11.0
WT 3	9.9	-	-	9.9
G101V 1	6.1	5.0	6.6	5.9
G101V 2	5.5	6.1	6.1	5.9
G101V 3	5.0	7.2	6.1	6.1
G101V N2C/D282C 1	5.5	6.1	5.0	5.5
G101V N2C/D282C 2	5.0	5.5	2.2	4.2
G101V N2C/D282C 3	5.5	6.1	7.2	6.2
WT 1	12.7	-	-	12.7
WT 2	12.1	-	-	12.1
WT 3	14.9	-	-	14.9
V104F 1	13.2	7.7	9.4	10.1
V104F 2	12.1	8.3	7.7	9.4
V104F 3	14.9	8.3	6.6	9.9
V104F N2C/D282C 1	6.6	8.3	8.3	7.7
V104F N2C/D282C 2	16.0	7.2	12.7	11.9
V104F N2C/D282C 3		7.7	2.8	5.2
WT 1	9.4	-	-	9.4
WT 2	9.9	-	-	9.9
WT 3	7.7	-	-	7.7
G106W 1	5.5	7.2	5.0	5.9
G106W 2	6.1	5.0	5.0	5.3
G106W 3	5.5	4.4	5.5	5.1
G106W N2C/D282C 1	8.8	7.7	8.8	8.4
G106W N2C/D282C 2	6.1	6.1	8.8	7.0
G106W N2C/D282C 3	7.7	6.6	8.8	7.7

## 6.4 ANOVA Statistics

ANOVA test of the disulphide bridge repaired rhodopsin RP mutants (Table 6.1), rescued rhodopsin RP mutants (Table 6.2) and rescued-repaired rhodopsin RP mutants (Table 6.3). Statistical ANOVA test carried out to compare the variance both between and within each group to determine whether said groups are significantly different from each other or not. This was then compared with an  $\alpha$ -value of 0.05 to give both a p-value and f-critical value.

Table 6.1- Disulphide bridge repaired rhodopsin RP mutant statistics (RP vs. RP N2C/D282C)

SUMMARY				
<i>Groups</i>	<i>Count</i>	<i>Sum</i>	<i>Average</i>	<i>Variance</i>
WT	9	204.20	22.69	16.67
WT N2C/D282C	3	38.60	12.87	31.76
G101V	9	34.10	3.79	2.83
G101V N2C/D282C	8	69.85	8.73	8.25
V104F	9	141.90	15.77	10.97
V104F N2C/D282C	9	128.15	14.24	3.29
G106W	8	11.55	1.44	0.60
G106W N2C/D282C	9	79.20	8.80	12.02

ANOVA						
<i>Source of Variation</i>	<i>SS</i>	<i>df</i>	<i>MS</i>	<i>F</i>	<i>P-value</i>	<i>F crit</i>
Between Groups	2822.15	7	403.16	45.92	6.18E-21	2.18
Within Groups	491.65	56	8.78			
Total	3313.80	63				

It is clear that the  $p$ -value is well below 0.05 and the variance between and within the mutant sample groups strongly suggests that these groups are significantly different ( $F_{7,56} = 45.92, P < 0.05$ ). From this we can see that there is a large variance between mutant sample groups when looking at the effect of disulphide bridge repair, and when compared with the spectroscopy data (Results- Figure 3.6) this is the case.

Table 6.2- Pharmacological chaperone rescued rhodopsin RP mutant statistics (RP vs. RP rescued)

SUMMARY				
<i>Groups</i>	<i>Count</i>	<i>Sum</i>	<i>Average</i>	<i>Variance</i>
WT	9	204.20	22.69	16.67
WT rescued	9	97.90	10.88	4.37
G101V	9	34.10	3.79	2.83
G101V rescued	9	53.35	5.93	0.51
V104F	9	141.90	15.77	10.97
V104F rescued	9	88.00	9.78	8.30
G106W	8	11.55	1.44	0.59
G106W rescued	9	48.95	5.44	0.64

ANOVA						
<i>Source of Variation</i>	<i>SS</i>	<i>df</i>	<i>MS</i>	<i>F</i>	<i>P-value</i>	<i>F crit</i>
Between Groups	3012.38	7	430.34	75.63	3.21E-28	2.16
Within Groups	358.49	63	5.69			
Total	3370.86	70				

Similar to above, shows a  $p$ -value well below 0.05. The variance between and within the rescued mutant sample groups indicates that said groups are significantly different ( $F_{7,63} = 75.63$ ,  $p < 0.05$ ) than those in Table 6.3. This is also visible in Results- Figure 3.6, as the average amount of protein produced by each rescued sample falls within a range of about 5  $\mu\text{g}$  from most produced (WT at 11  $\mu\text{g}$ ) and least produced (G101V N2C/D282C or G106W at 7  $\mu\text{g}$ ).

Table 6.3- Rescued-repaired rhodopsin RP mutant statistics (RP N2C/D282C vs. rescued RP N2C/D282C)

SUMMARY

<i>Groups</i>	<i>Count</i>	<i>Sum</i>	<i>Average</i>	<i>Variance</i>
WT N2C/D282C	3	38.60	12.87	31.76
WT N2C/D282C Rescued	9	64.25	7.139	0.29
G101V N2C/D282C	8	69.85	8.73	8.25
G101V N2C/D282C Rescued	9	47.85	5.32	1.82
V104F N2C/D282C	9	128.15	14.24	3.29
V104F N2C/D282C Rescued	8	69.30	8.66	15.97
G106W N2C/D282C	9	79.20	8.80	12.02
G106W N2C/D282C Rescued	9	69.30	7.70	1.44

ANOVA

<i>Source of Variation</i>	<i>SS</i>	<i>df</i>	<i>MS</i>	<i>F</i>	<i>P-value</i>	<i>F crit</i>
Between Groups	460.79	7	65.83	9.60	8.82E-08	2.18
Within Groups	383.89	56	6.86			
Total	844.69	63				

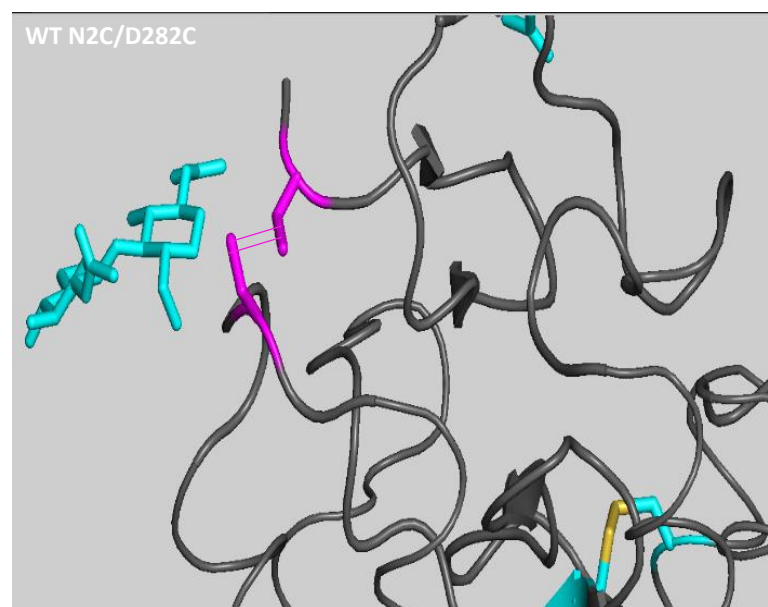
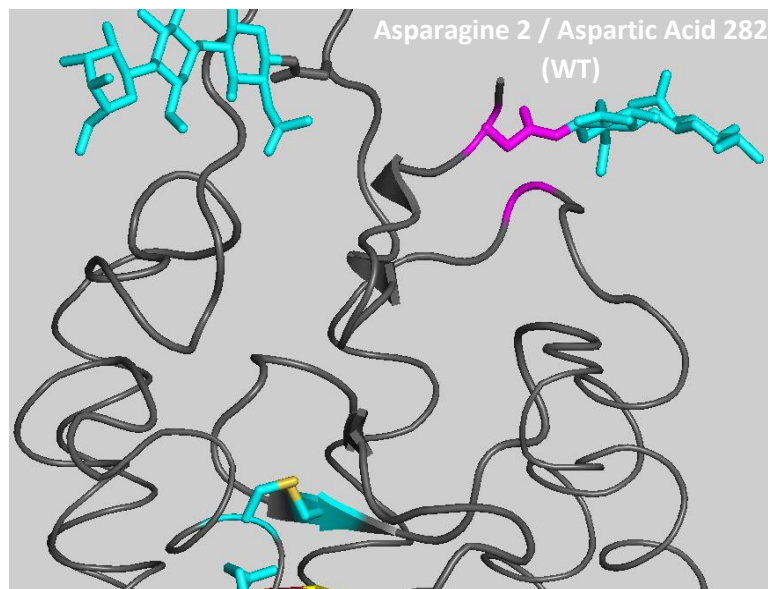
This test indicates that the mutant samples are more significantly similar than those show in the other tables above ( $F_{7,56} = 9.60$ ,  $p < 0.05$ ).

Overall, we can see that pharmacological chaperone rescue seems to have had some influence on the amount of rhodopsin produced by the samples that do not contain the N2C/D282C mutation. V104F does not seem to have responded to the presence of 9-*cis*-retinal, but there is not a significant difference between V104F and V104F N2C/D282C anyway. On the other hand, G101V and G106W have responded to the addition of 9-*cis*-retinal. The rescued G101V and G106W mutant samples have produced a similar amount of rhodopsin as their repaired mutant versions, and significantly more than the non-rescued and non-repaired G101V and G106W mutants. The difference between the rescued and non-rescued samples being approximately 2  $\mu\text{g}$  for G101V and 6  $\mu\text{g}$  for G106W.

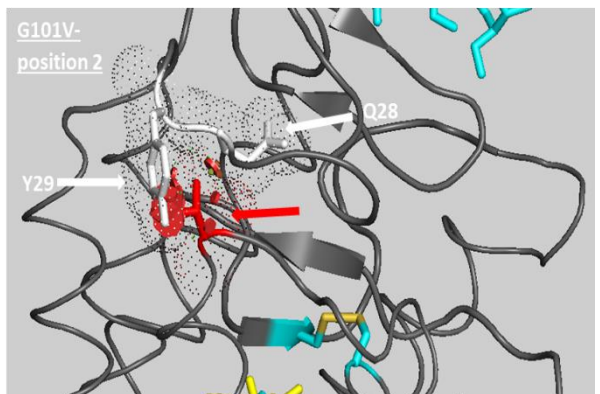
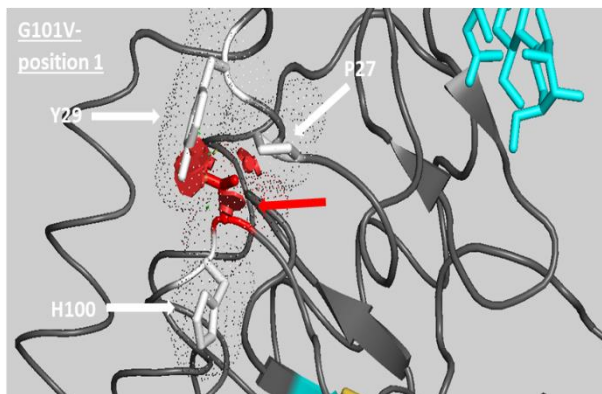
## 6.5 PyMol RP rhodopsin structure perturbations

Rhodopsin structural changes observed using PyMol software to visualise amino acid substitutions for the disulphide bridge (N2C/D282C), G101V, V104F and G106W. Potential amino acid orientations are shown with their appropriate orbitals of interactions (red circles indicate negative interactions with other amino acid residues within the rhodopsin molecule). Best positions, those with the fewest negative interactions, are shown in the Discussion. White arrows show labelled residues with which negative interactions occur.

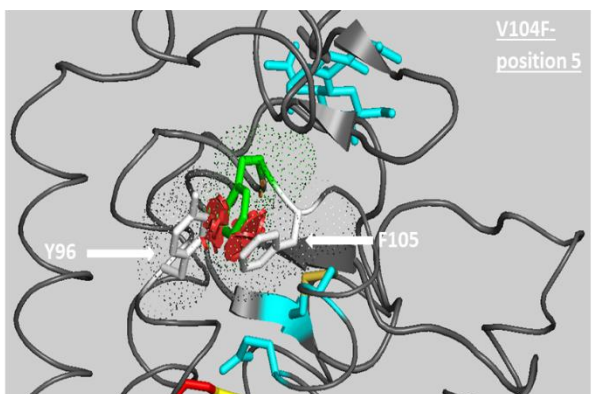
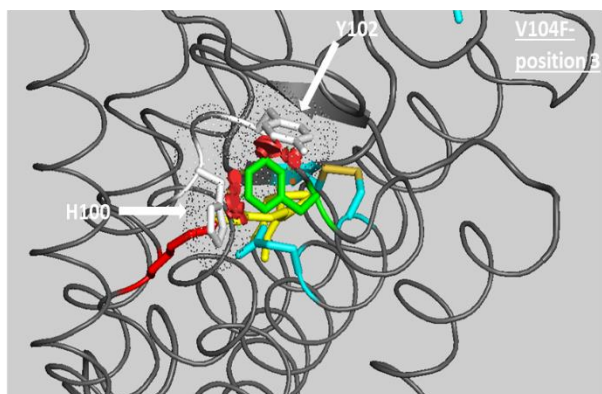
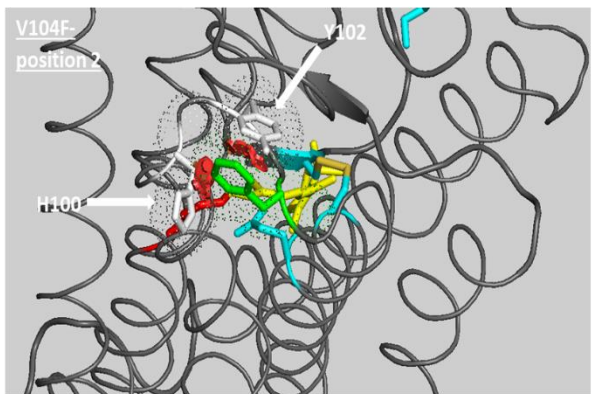
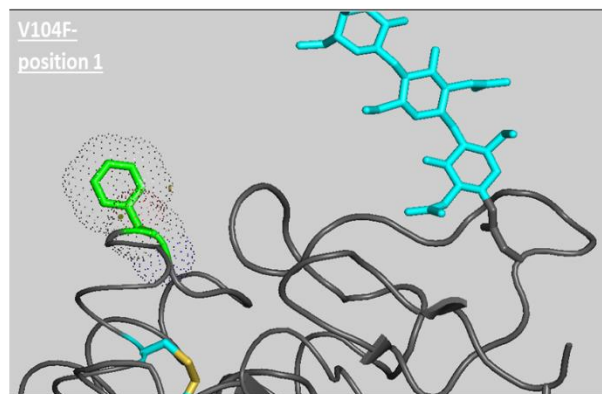
### WT N2C/D282C



### Mutated G101V orientations



### Mutated V104F orientations



## Mutated G106W orientations

